This is to certify that the
dissertation entitled

ELECTRICALLY-ACTIVE POLYANILINE COATED
MAGNETIC NANOPARTICLES: A NOVEL CONCENTRATOR
AND NANOSTRUCTURED TRANSDUCER IN BIOSENSOR
DEVICES

presented by

SUDESHNA PAL

has been accepted towards fulfillment
of the requirements for the

___Ph.D.___   degree in   ___Biosystems Engineering___

ECSlocilja

_____
Major Professor's Signature

9/24/09

_____
Date

PLACE IN RETURN BOX to remove this checkout from your record.
TO AVOID FINES return on or before date due.
MAY BE RECALLED with earlier due date if requested.

DATE DUE	DATE DUE	DATE DUE

5/08 K:/Proj/Acc&Pres/CIRC/DateDue.indd

ELECTRICALLY-ACTIVE POLYANILINE COATED MAGNETIC
NANOPARTICLES: A NOVEL CONCENTRATOR AND
NANOSTRUCTURED TRANSDUCER IN BIOSENSOR DEVICES

By

Sudeshna Pal

A DISSERTATION

Submitted to
Michigan State University
in partial fulfillment of the requirements
for the degree of

DOCTOR OF PHILOSOPHY

Biosystems Engineering

2009

ABSTRACT

ELECTRICALLY-ACTIVE POLYANILINE COATED MAGNETIC NANOPARTICES: A NOVEL CONCENTRATOR AND NANOSTRUCTURED TRANSDUCER IN BIOSENSOR DEVICES

By

Sudeshna Pal

Nanomaterial based biosensors are emerging as sensitive, specific, efficient and rapid diagnostic tools for the detection of pathogenic microorganisms in biodefense and diagnostics. This research demonstrates the novel application of a nanostructured material in the dual function of a magnetic concentrator and a transducer in biosensor devices. The nanostructured materials are synthesized from aniline monomer made electrically active by acid doping coating the surface of gamma iron oxide cores. The synthesized electrically active polyaniline coated magnetic (EAPM) nanoparticles are adapted in antibody based and DNA based biosensors for the detection of *Bacillus anthracis* as a model pathogen. The antibody based detection involves immunomagnetic concentration of targets using biologically modified EAPM nanoparticles followed by their direct application to a charge transfer biosensor. Experimental results indicate that the biosensor is able to detect *B. anthracis* spores at concentrations as low as 4.2×10^2 spores per ml in 16 min. The DNA based detection mechanism encompasses sandwiched hybridization of DNA targets onto probe labeled EAPM nanoparticles which is succeeded by electrochemical detection of the EAPM DNA hybrids on screen printed carbon electrodes. The sensitivity of the DNA biosensor is assessed to be 0.01ng/μl of PCR amplified *B. anthracis pag A* gene fragment in a total detection time of 60 min.

To my parents and my husband, Tuhin

ACKNOWLEDGMENTS

I sincerely thank everyone who contributed to the completion of this research. I express my deepest gratitude to Dr. Evangelyn Alocilja for being more than an advisor to me. I am grateful for her guidance, time, encouragement and appreciation for even the smallest achievements, and her prayers during my graduate program. I am thankful to the members of my Ph.D. guidance committee: Dr. David Tomanek, Dr. Shantanu Chakrabartty, Dr. Daniel Guyer and Dr. Frances Downes for their suggestion and support.

I thank all past and present members of the Biosensors research group (Deng, Edith, Emma, Finny, Maria, Lisa, Michelle, Michael, Shannon, Srini, Yang, Yilun and Zarini) for sharing a pleasant work place. A special thank you to Ms. Edith Torres Chavolla for her guidance in molecular biology and for the help she extended to me. I am also thankful to Ms. Hanna Miller and all the other undergraduate assistants who have worked with me over the past few years.

I owe my gratitude to my parents and my sisters for the unconditional love they have showered upon me throughout the years. Their unceasing support and concern for me will always be my strength.

Last but not the least; I would like to express my heartfelt gratitude to my husband for being my friend, philosopher, and guide in our wonderful journey together. Thank you very much for your love and support!!

Sudeshna Pal

TABLE OF CONTENTS

LIST OF TABLES

LIST OF FIGURES

xiv

CHAPTER 1: INTRODUCTION

In 2001, the anthrax cases associated with the intentional distribution of *Bacillus anthracis* spores through the postal system highlighted the danger posed to global citizens from bioterrorism related attacks. A total of 22 cases of anthrax were identified by the Centers for Disease Control and Prevention (CDC), of which 11 were confirmed to be inhalational and the remaining were determined to be cutaneous (CDC, 2001). Before 2001, smaller incidents of bacteriological criminal assault, such as intentional contamination of salad bars with *Salmonella* in Oregon in 1984, and *Shigella* in muffins and pastries in Texas in 1996 were reported (Chang *et al.*, 2003). A wide range of infectious disease agents have been currently identified that can be intentionally used to cause harm. Diseases caused by these potentially weaponized agents include anthrax, botulism, plague, small pox, tularemia and viral hemorrhagic fevers and have been categorized as 'Category A' agents by the CDC (CDC, 2009).

Bioterrorism related incidents can have huge economic impacts on the society. Researchers have estimated the economic impact of an anthrax scenario on 100,000 people to be as $ 26.2 billon (Kaufmann *et al.*, 1997). Current human and animal diagnostic methods for infectious microbial agents are generally based on conventional microbiological culturing techniques followed by biochemical identification which are time consuming, requiring 2 to 7 days for confirmation (FDA 2000) and include costly and laborious sample preparation. Hence, developing rapid detection devices have become an absolute necessity to strengthen surveillance systems, to provide early identification in timely manner in cases of exposures thus reducing the possibility of developing symptoms, and also to prevent further transmission of the agents.

1

Biosensors are promising, inexpensive, and efficient alternatives for early identification of such infectious pathogens. Biosensor technology is rapidly evolving in the field of pathogen detection with a wide range of detection platforms being explored recently. The emergence of nanotechnology has further allowed the integration of different nanomaterials into these biodetection systems for developing field-ready, low cost, sensitive, and specific devices for pathogen detection.

Different nanostructured materials such as silicon nanowires, carbon nanotubes, gold and magnetic nanoparticles have been employed as transducer materials in biosensor applications. Recently, conductive magnetic nanostructures consisting of a magnetic core and an electrically active conducting polymer shell have been developed. The conducting polymer, polyaniline, is the most exploited in such magnetic nanostructures. These electrically active polyaniline coated magnetic (EAPM) nanostructures have magnetic properties in addition to the electrical properties, electrochemical activity, mechanical strength, and chemical flexibility of the polymer material. Current literature shows that such novel EAPM nanostructures have not been explored in biosensor detection systems till date.

This dissertation describes the development of EAPM nanostructure based detection systems that can utilize the magnetic, electrical, and electrochemical properties of the EAPM nanoparticles for magnetic concentration and biosensor transduction in one system for rapid and specific identification of infectious pathogens. Two different detection approaches have been demonstrated to show the versatility of these novel EAPM nanoparticles in detecting *Bacillus anthracis* as the model target pathogen. In the first approach, an EAPM based immunosensor was developed that coupled

2

immunomagnetic separation with direct electrical detection of the EAPM nanoparticles in a membrane based charge transfer biosensor. In the second approach, an EAPM based DNA biosensor was developed that involved magnetic concentration of DNA targets combined with direct electrochemical detection of EAPM nanoparticles on a screen printed biosensor.

Chapter 2 of this dissertation provides an overview on biosensors and nanotechnology with respect to detection of pathogenic microorganisms and also covers background information on polyaniline and magnetic polyaniline nanostructures. Chapter 3 highlights the novelty and significance of the research conducted and summarizes the research hypothesis and objectives. Chapter 4 walks through the materials and methods involved in synthesizing and characterizing the EAPM nanostructures (Section 4.1), in developing the EAPM based immunosensor and EAPM based DNA biosensor (Sections 4.2 and 4.4), and in implementing the biosensors for detection (Sections 4.3 and 4.5). Chapter 5 presents the results obtained from the objectives set for this research. The first part of this chapter (Section 5.1) discusses the different characterization studies performed on the synthesized EAPM nanostructures. The second part (Sections 5.2 and 5.3) discusses fabrication and performance of the EAPM based immunosensor in pure samples and complex matrices. The final part (Sections 5.4 and 5.5) describes the fabrication and performance of the EAPM based DNA sensor in PCR amplified DNA targets. This is followed by the concluding remarks and future work in Chapter 6. Finally, the appendices give statistical analysis results and data from certain experimental studies.

CHAPTER 2: LITERATURE REVIEW

2.1 *BACILLUS ANTHRACIS* AND ANTHRAX

Bacillus anthracis is a gram-positive, non-motile, aerobic, facultative anaerobic, spore-forming, rod-shaped bacterium and is the etiological agent of anthrax. Anthrax is primarily a zoonotic disease but all mammals, particularly humans, may develop this disease. The spore forms of *Bacillus anthracis* are highly resistant to environmental conditions such as heat, ultraviolet and ionizing radiation, pressure and chemical agents. They are able to survive for long periods of time in contaminated soils and this account for the ecological cycle of the microorganism. However, it is not clear whether the complete life cycle from germination to sporulation occurs outside the host (Mock and Fouet, 2001). The vegetative cells of the bacterium are square ended and capsulated having a size range of 3 to 5 µm while the spores are elliptical with a size range of 1 to 2 µm.

2.1.1 Virulence of Anthrax

The primary virulence factors of *B. anthracis* are toxin production and capsule formation. Virulent strains of the microorganism carry two large plasmids pXO1 and pXO2 which encode these virulence factors. The plasmid pXO1 carries the structural genes for the anthrax toxin proteins *pagA* (protective antigen), *lef* (lethal factor), and *cya* (edema factor); two *trans*-acting regulatory genes *atxA* and *pagR*; a gene encoding type I topoisomerase, *topA*; and a three gene operon, *gerX*, which affects germination. Plasmid pXO2 carries three genes which encode capsule synthesis, *capB*, *capC*, and *capA*; a gene associated with capsule degradation, *dep*; and a trans-acting regulatory gene *acpA*

(Okinaka *et al.*, 1999). Figure 2-1 shows a schematic representation of the *B. anthracis* plasmids and their associated virulence.
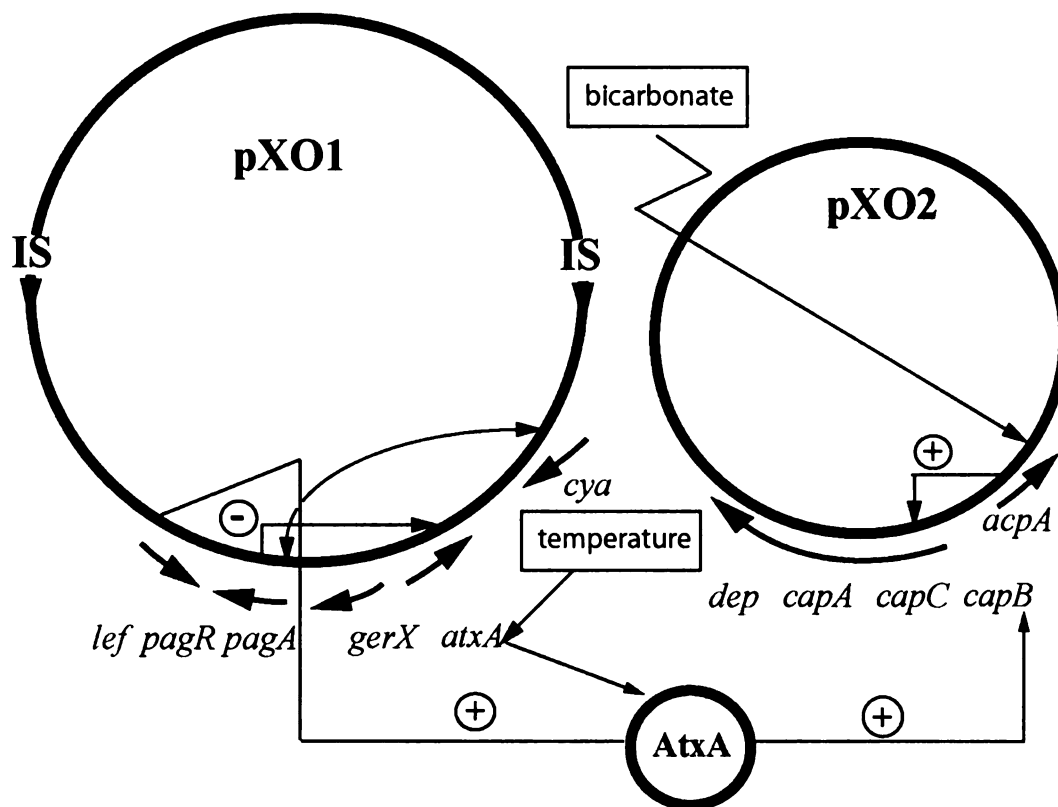
Figure 2-1 Plasmids and genes associated with virulence of *B. anthracis* (adapted from Mock and Fouet, 2001).

B. anthracis toxins are composed of three proteins (Figure 2-2): protective antigen (PA), lethal factor (LF) and edema factor (EF). The mature PA protein, an 83 kDa protein, is made up of 735 amino acids (Petosa *et al.*, 1997). The mature LF (90 kDa) is a protein that contains 776 amino acids (Pannifer *et al.*, 2001). The mature EF protein (89 kDa) is an inactive enzyme that has 767 amino acids (Leppla, 1982). None of the above proteins are toxic separately. Toxicity is associated with the formation of binary

exotoxins. The association of PA and LF results in the formation of lethal toxin (LTx), which provokes lethal shock in animals, while the association of PA and EF forms the edema toxin (ETx), which produces edema in the skin (Collier and Young, 2003).
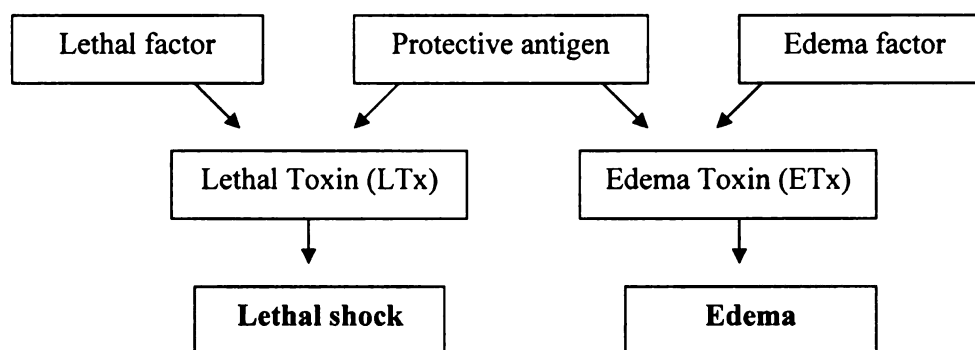
Figure 2-2. Mode of action of *B. anthracis* toxin proteins.

The *Bacillus anthracis* capsule is a polymer of γ-D-glutamic acid. The molecular weight of the polyglutamic chains is in between 20 and 55 kDa in vitro and estimated to be 215 kDa in vivo. The capsule enables the bacteria to evade the host's immune-system and provoke septicemia thus resulting in pathogenicity. However, the capsule by itself is a monotonous linear polymer which is weakly immunogenic and does not favor immune response (Mock and Fouet, 2001).

2.1.2   Routes of Infection

Anthrax is initiated by the entry of the spores into the host body through skin lesions, insect bite, ingestion of contaminated meat or inhalation of airborne spores. Depending on the route of infection, there are three clinical forms of anthrax: cutaneous, gastrointestinal and inhalational (pulmonary). The cutaneous form accounts for 90% of all human cases (Spencer, 2003) and occurs when the spores enter the host body through

a skin lesion and appears at first as a small pimple developing into a painless back eschar within few days. Antibiotic treatment is highly effective in cases of cutaneous anthrax which has a mortality rate of about 20% in untreated cases (CDC, 2001). The gastrointestinal form of anthrax is extremely rare but potentially fatal. It frequently occurs after the ingestion of undercooked meat from infected animals and is characterized by fever, nausea, vomiting, abdominal pain and bloody diarrhea (Mock and Mignot, 2003). Gastrointestinal anthrax has been reported to cause fatalities in 25-60% of cases (CDC, 2001). The inhalational form of anthrax is considered the most dangerous among the three having a mortality rate nearing 100% (CDC, 2001). The inhaled spores reach the alveolus where they are phagocytosed by macrophages and transported to the mediastinal lymph nodes, where spore germination can occur up to 60 days. The disease progresses rapidly following germination resulting in the production of exotoxins that cause edema, necrosis, and hemorrhage (Mock and Fouet, 2001). Diagnosis is difficult in both gastrointestinal and inhalational forms resulting in the disease to become treatment resistant and rapidly fatal.

2.1.3 Anthrax and Biosecurity

The use of microorganisms as biological weapons has long been reported in history. One of the first major attacks that have been reported occurred in the 14th century with *Yersenia pestis* during the siege of Kaffa (Inglesby *et al.*, 2000). The most recent was the deliberate release of *B. anthracis* spores through the postal system in the United States in October 2001, shortly after the September 2001 terrorist attack in New York and Washington resulting in 22 cases of anthrax and 5 deaths (Jernigan *et al.*, 2001). An optimal biological weapon should be highly lethal, easily produced in large quantities,

environmentally stable and have the capability to be readily dispersed into aerosol (i.e. 1 to 10μm particle size) (Peruski and Peruski, 2003). When reviewed for these characteristics, *B. anthracis* is the most likely to be used as a biological weapon since *it* has the ability to form spores which can be easily aerosolized, inhalational anthrax has a high mortality rate nearing 100%, and the spore forms of the bacteria are very stable surviving harsh environmental conditions. It has been estimated that the release of 50 kg of dried anthrax spores for two hours can lead to a complete breakdown in medical resources and civilian infrastructure in a city of 500,000 inhabitants (Spencer, 2003). The Centers for Disease Control and Prevention (CDC) has categorized *B. anthracis* as a category A agent or a high priority agent. Category A agents include agents that can be easily transmitted from person to person, cause high mortality with potential for major public health impact, may cause public panic and social disruption, and require special action for public health preparedness (CDC website).

2.1.4 Traditional Identification Methods

Detection and specific identification of *B. anthracis* require complex techniques and laborious methods because of the genetic similarities among various *Bacillus* species as well as their existence in both spore forms and vegetative state. *B. anthracis* is identified using standard biochemical techniques such as its sensitivity to penicillin, non-motility, non β-hemolytic behavior on sheep or horse blood agar plates and its susceptibility to lysis by gamma phage. It has been reported that identification of *B. anthracis* by initial blood culturing requires 6-24h for growth, which is followed by morphological and biochemical identification that requires additional 12-24h and finally definitive identification that requires an additional 1-2 days (Inglesby, 2000). *B. anthracis* is also

shown to selectively grow on polymyxin-lysozyme EDTA-thallous acetate (PLET) agar which requires 1-2 days for growth followed by further confirmation (Erickson and Kornacki, 2003).

2.2   BIOSENSORS IN PATHOGEN DETECTION

2.2.1   Introduction

A biosensor can be defined as an analytical device that integrates a biological sensing element with an electrical transducer to quantify a biological event (for e.g. an antigen-antibody reaction) into an electrical output. The basic concept of operation of a biosensor has been illustrated in Figure 2-3. The biological sensing elements include enzymes, antibodies, DNA, aptamers, molecularly imprinted polymers, microorganisms and whole cells. Depending on the transducing mechanism used, biosensors can be of many types such as: electrochemical, electrical, optical, mechanical and magnetic biosensors. The different transducing mechanisms and biological sensing elements are discussed in detail in later part of this section.

ANALYTE	BIORECEPTOR	TRANSDUCER	SIGNAL PROCESSING
	Antibodies	Electrochemical	
	Nucleic Acids	Electrical	
	Aptamers	Optical	Amplifier Data Acquisition
	Enzymes	Mechanical	
	Whole Cells	Magnetic	
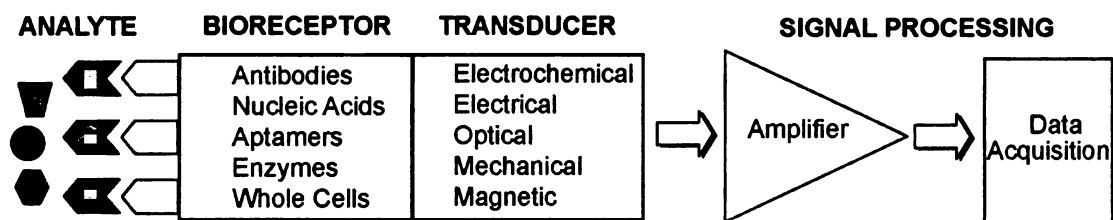
Figure 2-3. Schematic representation of a biosensor.

Biosensor technology is emerging as a promising field for rapid detection of pathogens. Currently, the two most popular methods for detection of pathogens are: microbial culturing followed by biochemical identification, and polymerase chain reaction (PCR) assay. The main disadvantages of the conventional microbial culturing techniques are the time consuming process and the multistep assay procedures for food samples requiring pre-enrichment steps. The PCR technology, although highly sensitive,

has some disadvantages, such as requirement of expensive equipments, skilled personal to perform assays, DNA extraction stages which increase the detection time, and prior information of target DNA sequences. On the other hand, biosensors show high sensitivity and specificity to targets and can be used as simple one-shot measurement tools or as multi-measurement devices. Moreover, biosensors can be designed to be operated on a real-time basis thus eliminating the need of expensive lab-based testing (Terry *et al.*, 2005). The miniaturization ability of biosensors and their compatibility with data processing technologies allow them to be integrated into small portable devices. This versatility in biosensors has prompted worldwide research and commercial exploitation of the technology. Recent trends indicate (Figure 2-4) that biosensors is the fastest growing technology for rapid detection of pathogens (Lazcka *et al.*, 2007).
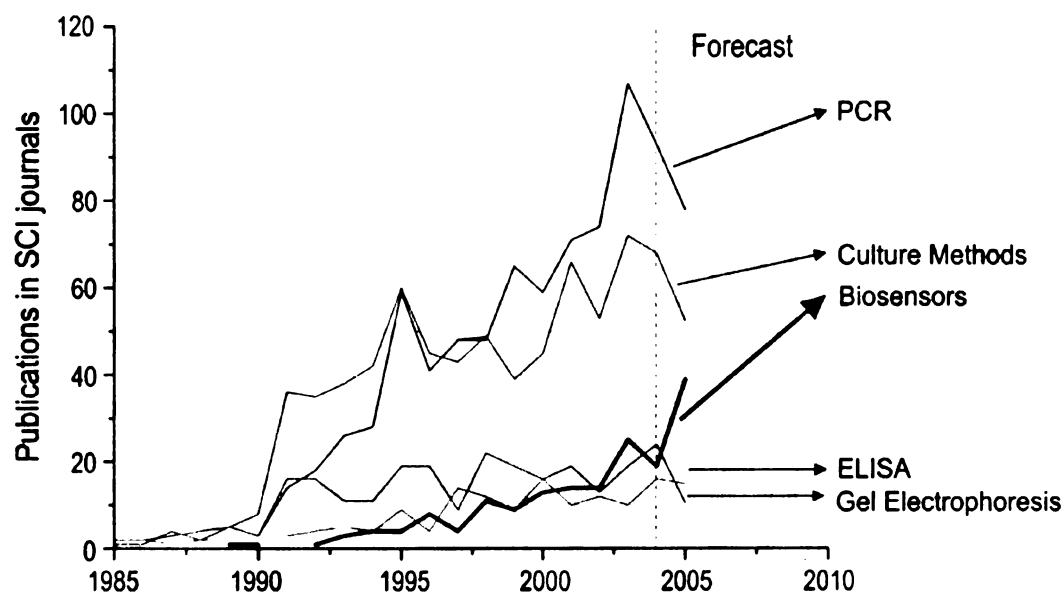
Figure 2-4. Recent trends in pathogen detection (adapted from Lazcka et al., 2007).

2.2.2 Biosensor Transducing Mechanisms

2.2.2.1 Mechanical Biosensors

2.2.2.1.1 Quartz Crystal Microbalance (QCM) Biosensors

Quartz crystal resonators form the basis of QCM sensors. The term "QCM" is used collectively for bulk acoustic wave (BAW), quartz crystal resonance sensors (QCRS) and thickness shear mode (TSM) acoustic sensors (Cooper and Singleton, 2007). QCM sensors comprise of a thin quartz disc with electrodes plated on it. When an oscillating electric field is applied across the disc, an acoustic wave with a certain resonant frequency is induced. The disc can be coated with a sensing layer of biomolecules based on the analyte to be detected. The interaction of the analyte with the biomolecules on the disc surface causes a change in mass and a concurrent change in resonance frequency that can be directly correlated to the biomolecular interactions(O'Sullivan and Guilbault, 1999). The relation between mass and the resonant frequency is given by the Sauerbrey equation:

$$\Delta F = \frac{-2.3 \times 10^6 F_0^2 \Delta m}{A} \tag{2.1}$$

where, ΔF is the change in frequency (Hertz), F_0 is the resonant frequency of the crystal (MHz), Δm is the deposited mass (grams) and A is the coated area (cm^2). The quartz crystals are inexpensive, easily available and robust thus making them suitable for chemical sensors and biosensors. In addition, QCM based sensors provide great flexibility, wide dynamic range of frequency measurements and label free detection (O'Sullivan and Guilbault, 1999).

12

A wide range of non-labeled QCM biosensors have been reported in the literature for the detection of pathogenic bacteria and viruses. QCM sensors based on lectin recognition systems for bacterial identification have been studied by Shen *et al.* and Safina *et al.* (Shen *et al.*, 2007;Safina *et al.*, 2008). Shen et al have used a combination of mannose self-assembled monolayer (SAM) and lectin concanavalin A for the detection of *E. coli* W1485 in a linear range of 7.5 × 10^2 to 7.5 × 10^7 cells/ml. Safina *et al.* utilized lectin reporters to develop a flow injection QCM biosensor for detection of *Campylobacter jejuni* and *Helicobacter pylori*. The authors were able to detect 10^3 to 10^5 cells/ml in 30 min. A SAM based QCM immunosensor was developed for the detection of *E. coli* O157: H7 by Su *et al.* (Su and Li, 2004a). The immunosensor was able to detect the target bacteria in the range of 10^3 to 10^5 CFU/ml in 30-50 min. Detection of *B. subtilis* spores as a surrogate to *B. anthracis* was achieved by Lee *et al.* utilizing a QCM immunosensor to a detection limit of 450 spores/ml (Lee *et al.*, 2005). Furthermore, virus (dengue virus and hepatitis B virus) detection with QCM immuno and nucleic acid based sensors have been reported by Wu *et al.* and Yao *et al.* (Yao *et al.*, 2008;Wu *et al.*, 2005)

QCM biosensors for the detection of DNA sequences have also been developed using nanoparticle labels as amplifiers. Mao *et al.* reported the use of streptavidin conjugated Fe_3O_4 nanoparticles for the detection of *E. coli* O157: H7 *eaeA* gene. The nanoparticles acted as 'mass enhancers' and amplified the change in frequency. The biosensor could attain a sensitivity of 10^{-12} M synthetic oligonucleotides and 2.67 × 10^2 CFU/ml *E. coli* O157: H7 cells (Mao *et al.*, 2006). Similarly, Au nanoparticles were employed by Wang *et al.* for real time bacterial DNA detection in a circulating flow

13

QCM biosensor. The authors reported a sensitivity of 2.0 × 10^3 CFU/ml for *E. coli* O157:

H7 *eaeA* gene (Wang *et al.*, 2008).

Although QCM biosensors are being used widely for pathogen detection, they have

limited potential for scalability since the mass detection capability scales with the QCM

sensor surface.

2.2.2.1.2 *Surface Acoustic Wave (SAW) Biosensors*

SAW sensors are the second class of acoustic wave sensors that have found

applications in biosensor devices. SAW sensors consist of two metal interdigital

transducers (IDT) etched from a thin metal film deposited on a piezo-electric substrate.

The sensing mechanism is based on the changes in SAW velocity or attenuation when

mass is sorbed on the sensor surface. Since the acoustic energy is strongly confined to the

surface, SAW devices are very sensitive to changes in the surface such as mass loading,

viscosity, and conductivity changes (Galipeau *et al.*, 1997). It has been suggested that

SAW based biosensors have greater sensitivities than QCMs because of their higher mass

sensitivities (~ 200 times > QCM) (Galipeau *et al.*, 1997).

SAW biosensors have been successfully applied for the detection of bacteria and

viruses. *E. coli* detection using SAW biosensors have been reported by multiple authors

in the literature (Berkenpas *et al.*, 2006;Deobagkar *et al.*, 2005;Moll *et al.*, 2007;Moll *et al.*, 2008). The biosensors have used antibodies as the biological sensing element with

sensitivities ranging from 10^6 cells/ml to 0.4 cells/μl. Branch and Brozik have developed

a 36° YX cut LiTaO$_3$ based SAW device for the detection of the *Bacillus anthracis*

simulant *Bacillus thuringiensis* spores in aqueous conditions (Branch and Brozik, 2004).

The authors have investigated two waveguide materials polyimide and polystyrene for

creating the Love wave sensors. Detection of *Bacillus thuringiensis* spores at concentrations below the lethal dose of anthrax spores was possible using both waveguide materials. The sensor had a detection limit of a few hundred cells per ml and a response time of < 100 s. Jin *et al.* developed a SAW biosensor for detecting the gene of Staphylococcal Enterotoxin B utilizing ST-cut quartz and SiO_2 guiding layer. The biosensor had a sensitivity of 10 ng/ml and a linear range of 35-200 ng/ml (Jin *et al.*, 2003). Recently, SAW biosensors were used for detecting viral bioagents by Bisoffi *et al.* (Bisoffi *et al.*, 2008). A lithium-tantalate based SAW transducer with SiO_2 waveguide sensor platform was used for Coxsackie virus B4 and Sin Nomber virus detection.

SAW resonators are suitable for use in simple electronic setups because of their low insertion losses and sharp resonance frequencies. As a result, insertion of such devices into oscillator circuits is beneficial as such circuits are commonly used in point-of-care diagnostics. Furthermore, the SAW based biosensors can be prepared from cheap components thus making them suitable for integration into inexpensive sensor arrays (Lange *et al.*, 2008).

2.2.2.1.3 *Microcantilever Based Biosensors*

Microcantilever based biosensors are derived from microfabricated cantilevers used in atomic force microscopy (AFM) and are based on the bending induced in the cantilever when a biomolecular interaction takes place on one of its surface which is translated into nanomechanical motion and is commonly coupled to an optical or piezoelectric readout system (Carrascosa *et al.*, 2006). The cantilevers can be operated in the static deflection mode where analyte binding causes cantilever bending or in the dynamic resonant mode where analyte binding causes change in resonant frequency

(Waggoner and Craighead, 2007). Microcantilever sensors are promising for biosensor applications since they can perform local, high resolution, and label-free molecular recognition measurements (Carrascosa *et al.*, 2006).

Davila *et al.* have demonstrated microcantilever based biosensors in the detection of *B. anthracis* Sterne strain in air and water (Davila *et al.*, 2007). The detection scheme involved measurement of the decrease in resonant frequency driven by thermally induced oscillations as a result of the mass of spores measured by a laser Doppler vibrometer. The authors reported a minimum detection of 2 spores (740 fg) and 50 spores (139 pg) in air and water, respectively, using 20 μm long, 9 μm wide, and 200 nm thick cantilevers. Muthasaran and coworkers have utilized piezoelectric-excited millimeter-sized cantilever sensors for the detection of *B. anthracis* Sterne spores and *E. coli* O157: H7 cells. The sensors consisted of a piezoelectric and a glass layer and were able to detect *B. anthracis* spores at 300 spores/ml and *E. coli* O157: H7 cells in ground beef at 50 to 100 cells/ml. Extremely sensitive microcantilever based biosensors capable of detecting a single pathogen have also been reported in literature(Campbell and Mutharasan, 2006). Illic *et al.* were able to detect a single *E. coli* O157: H7 cell using low stress silicon-nitride cantilever beams in air (Ilic *et al.*, 2001). The mass of a single *E. coli* O157: H7 cell was found by the authors to be 665 fg. Similarly, Johnson *et al.* reported the use of microscale silicon cantilever resonators for vaccinia virus detection in air (Johnson *et al.*, 2006). The authors measured the mass of a single vaccinia virus particle to be 12.4 ±1.3 fg and 7.9 ± 4.6 fg using two different sized cantilever beams.

2.2.2.2 Optical Biosensors

2.2.2.2.1 Surface Plasmon Resonance (SPR) Biosensors

SPR is an optical technique for monitoring biomolecular interactions that occur in the close vicinity of a transducer surface. SPR based biosensing can be subdivided into three categories depending on the mode of SPR detection: angular SPR biosensing, spectral SPR biosensing, and local SPR biosensing. Angular SPR biosensing is the most common form of SPR biosensing and involves attenuated total reflection approach using Kretschmann geometry (Erickson *et al.*, 2008). Spectral SPR biosensing is conducted at a fixed incident angle and utilizes the wavelength dependence of the dielectric constant of the metal film to interrogate the surface plasmon coupling conditions. Local SPR (LSPR) biosensing or nanoparticle based SPR involve coupling of surface immobilized metallic nanoparticles or nanostructures into a plasmon mode which results in a decrease in the transmitted power at a specific resonant wavelength dependant on environmental dielectric conditions (Erickson *et al.*, 2008).

SPR biosensors provide several advantages over conventional transduction techniques, such as, capability of label-free detection, ability to produce continuous real-time responses, regeneration of the active sensor surface, feasibility for miniaturization, sensitive detection of small molecules, and multiplexing ability ((Shankaran *et al.*, 2007). Particularly, multiplex detection, or detection of different targets on the same platform, is an important characteristic in these biosensors since it adapts to screening of unknown samples.

SPR based immunosensors have been developed for the detection of *E. coli* O157: H7 by Irudayaraj and coworkers. The authors have demonstrated a sensitivity of 10^3

CFU/ml for the pathogen using a SAM based SPR biosensor and the commercially available Spreeta SPR biosensor (Waswa *et al.*, 2007;Subramanian *et al.*, 2006). Detection of *Salmonella* Typhimurium in chicken carcasses was achieved using an antibody based SPR biosensor by Lan *et al.* (Lan *et al.*, 2008). The SPR biosensor had a lowest detection limit of 1×10^6 CFU/ml. Highly sensitive detection of *Salmonella* Enteritidis was attained by Waswa *et al.* using the commercial Biacore™ SPR biosensor (Waswa *et al.*, 2006). The limit of detection (LOD) of the biosensor as reported by the authors was 23 CFU/ml for *Salmonella*. Chen *et al.* have demonstrated an immunomagnetic separation based SPR detection method for the foodborne pathogen *Staphylococcus aureus* (Chen *et al.*, 2007). The detection system involved an initial immunomagnetic bead based separation step of 30 min and had a sensitivity of 10^6 CFU/ml in a total assay time of 2 h. A SAM based SPR immunosensor was developed by Jyoung *et al.* for the detection of *Vibrio cholerae* O1 with a detection range of 10^5 to 10^9 cells/ml (Jyoung *et al.*, 2006). Detection of viruses using SPR based biosensors have been reported by Chung *et al.* and Vaisocherova *et al.* (Chung *et al.*, 2005;Vaisocherova *et al.*, 2007). Vaisocherova and coworkers developed a SPR biosensor for detecting antibodies against Epstein-Barr virus. The antibody detection was performed using an immunoreaction between the antibody and a synthetic peptide for the virus. The sensor had a sensitivity of 0.2 ng/ml (~ 1pM). Furthermore, multiplex detection of four foodborne bacterial pathogens (*E. coli* O157: H7, *Salmonella* Typhimurium, *Listeria monocytogenes* & *Campylobacter jejuni*) was demonstrated by Taylor *et al.* using an eight-channel SPR biosensor (Taylor *et al.*, 2006). The LOD for each of the four species of bacteria was in the range of 3.4×10^3 and 1.2×10^5 CFU/ml.

Several detailed review articles are available in literature that focus on different SPR based detection techniques and their applications (Shankaran *et al.*, 2007;Homola, 2008;Hoa *et al.*, 2007).

2.2.2.2.2 Fluorescence Based Biosensors

Fluorescence is the radiative deexcitation of a molecule following the absorption of a photon. Generally, the emitted photon is of lower energy than the absorbed photon, and the fluorescence emission peak of a species is at longer wavelength than the absorption peak, the wavelength separation being referred as Stoke's shift. Fluorescence based detection systems have gained popularity in biosensors due to their high sensitivity and are mostly based on the detection of the fluorescent signal generated by fluorophores used to label the biomolecules.

Fluorescence detection techniques can be performed in the high-throughput mode in combination with platforms such as microarrays. Microarrays offer the advantage of using a two-dimensional layout of recognition elements for simultaneous detection and quantification. Taitt *et al.* have demonstrated a fluorescence based microarray immunosensor for the simultaneous detection of nine targets comprising of *B. anthracis* Sterne, *B. globigii*, *Francisella tularensis*, *Yersenia pestis*, *S.* Typhimurim, Staphylococcal enterotoxin B, ricin, cholera toxin and MS2 coliphage (Taitt *et al.*, 2002). Li et al. have developed DNA-based fluorescence nanobarcodes to integrate with DNA-microarrays for the simultaneous detection of four targets (*B. anthracis*, *Francisella tularensis*, Ebola virus and SARS coronavirus) (Li *et al.*, 2005). The feasibility study involved confocal microscopy, dot blotting and flow cytometry which resulted in attomolar sensitivity.

Fluorescence resonance energy transfer (FRET) based detection involves non-radiative energy transfer between a donor fluorophore and an acceptor fluorophore when they are in close proximity (Epstein *et al.*, 2002). A fiber optic portable biosensor utilizing the principle of FRET was developed by Ko and Grant for rapid detection of *S.* Typhimurium in ground pork samples (Ko and Grant, 2006). The biosensor had a sensitivity of 10^5 CFU/ml in a response time of 5 min. Kim *et al.* reported a molecular beacon DNA microarray system for fast detection of *E. coli* O157: H7 based on FRET (Kim *et al.*, 2007a). In this system, unlike conventional fluorophore-quencher beacon design, two fluorescence molecules allowed active visualization of both hybridized and unhybridized states of the beacon. The target gene detection limit for the system was 1ng/µl.

Fluorescence based tapered fiber optic biosensors have also been employed in pathogen detection. A fluorescence based fiber optic biosensor for detecting *E. coli* O157: H7 in ground beef samples was developed by Geng *et al.* (Geng *et al.*, 2006). The authors reported sensitivity of 10^3 CFU/ml in pure cultures and of 1 CFU/ml in artificially contaminated ground beef samples after 4 h enrichment using a sandwich immunoassay. Nanduri *et al.* developed an automated fiber optic based immunosensor called RAPTOR^{TM} for the detection of *Lysteria monocytogenes* in food samples. The LOD of the system was 5×10^5 CFU/ml in food samples and 1×10^3 CFU/ml in PBS (Nanduri *et al.*, 2006).

Inspite of the enhanced sensitivity, all fluorescence based biosensors suffer from disadvantages attributed mainly to the characteristics of the fluorescent probe such as

stability and efficiency of labeling. The expensive fluorescent labels are also a drawback of this technology.

2.2.2.3 Electrochemical Biosensors

Electrochemical biosensors are based on the detection of electrochemical signal generated by consumption or production of electrons from biological interactions occurring at the sensor surface. Advantages such as low cost, high sensitivity, miniaturization ability, low power requirements, and simple instrumentation make the electrochemical biosensors well suited for clinical and environmental analysis. Electrochemical biosensors are generally classified as amperometric, potentiometric, conductometric and impedimetric.

2.2.2.3.1 Amperometric Biosensors

Amperometric biosensors are based on the measurement of current changes resulting from oxidation or reduction of an electroactive species in a biochemical reaction. The current is typically measured at a fixed potential (amperometry) or during controlled variations of the potential (voltammetry).

Theegala *et al.* reported an oxygen-electrode based amperometric biosensor for the qualitative detection of *E. coli* O157: H7 in water (Theegala *et al.*, 2008). The biosensor detected changes in oxygen concentration due to decrease in enzymatic activity upon binding of bacterial cells. The biosensor could detect as low as 50 cells/ml in 20 minutes. A renewable amperometric immunosensor for the detection of *S.* Typhi was reported by Singh *et al.* (Singh *et al.*, 2005). The detection technique involved a sandwich ELISA system with a LOD of 10^5 cells/ml in 90 minutes. Amperometric detection of antibodies against *Bacillus anthracis* protective antigen was also achieved by Aguilar *et al.* (Aguilar

and Sirisena, 2007). The antibodies were captured and detected using microcavities with a LOD of 10 fg in a 200 nL sample. A disposable amperometric immunosensor based on screen printed electrode (SPE) coated with agarose/nano-Au membrane and horseradish peroxidase labeled antibody for specific detection of the foodborne pathogen *Vibrio parahaemolyticus* was developed by Zhao et al. (Zhao et al., 2007). The immunosensor showed a sensitivity of 7×10^4 CFU/ml for the pathogen and its accuracy was in good agreement (97.5%) with ELISA results.

Lermo *et al.* described a genomagnetic assay for the electrochemical detection of *Salmonella* spp. based on *in situ* DNA amplification and magnetic primers (Lermo *et al.*, 2007). Detection was achieved by sandwich hybridization of the target on magnetic beads which were then separated by a magneto electrode based on graphite-epoxy composite followed by electrochemical detection using an enzyme marker anti-digoxigenin horseradish peroxidase. The authors achieved a sensitivity of 2.8 fmol with PCR amplicons. Multianalyte detection using electrochemical genosensors have also been studied by Farabullini *et al.* and Elsholz *et al.* (Elsholz *et al.*, 2006;Farabullini *et al.*, 2007). Farabullini *et al.* achieved nanomolar detection limits for the pathogenic bacteria, *Salmonella* sp., *E. coli* O157:H7, *L. monocytogenes* and *S. aureus* using differential pulse voltammetry to detect α-napthol signal in less than 1 h.

2.2.2.3.2 *Potentiometric Biosensors*

Potentiometric devices are based on the measurement of accumulation of charge potential at the working electrode of an electrochemical cell in comparison to the reference electrode with zero or negligible current flow between the electrodes. The

measured potential is related to the concentration of the analyte through the Nersnt equation:

$$E = E_0 \pm (RT / nF) \ln Q \qquad (2.2)$$

where, E is the cell potential at zero current, E_0 is the standard potential, R is the universal gas constant, T is the absolute temperature, F is the Faraday constant, n is the total number of charges of ion, Q is the ratio of ion concentration at the anode to that at the cathode (Diamond, 1998;Eggins, 2002).

Among electrochemical transducing methods, potentiometric methods are the least exploited in pathogen detection due to their high detection limits and poor selectivity, the main advantage of these devices being wide detectable concentration range and continuous measurement capability (Palchetti and Mascini, 2008). Another approach involves ion selective field effect transistors (ISFETs) that employ semiconductor field-effect to detect biorecognition events. However, the application of these devices in biosensors has been limited by production problems related to immobilization, fabrication and packaging, poor detection limits and device stability (Lazcka *et al.*, 2007). An advancement that has evolved from the ISFET is the light addressable potentiometric sensor (LAPS) which combines potentiometry with optical detection (Hafeman *et al.*, 1988;Lazcka *et al.*, 2007). Ercole *et al.* reported an antibody based LAPS biosensor for determination of *E. coli* in food (Ercole *et al.*, 2003). The biosensor detected variations in pH due to ammonia production by urease-*E. coli* antibody conjugates in commercial lettuce, sliced carrot, and rucola samples. The sensor was able to reach a sensitivity of 10 cells per ml in an assay time of 1.5 h.

2.2.2.3.3 Conductometric Biosensors

Conductometric biosensors utilize the electrical conductivity of a sample to determine the components and their concentration (Rahman *et al.*, 2008). Muhammad Tahir and Alocilja (Muhammad-Tahir and Alocilja, 2003a;Muhammad-Tahir *et al.*, 2005) have developed a conductometric biosensor for the detection of pathogenic bacteria and viruses. The biosensor was fabricated using conducting polyaniline as an electronic label in a sandwich immunoassay scheme and the authors demonstrated that polyaniline improved the sensitivity of the biosensor by forming a conductive molecular bridge between silver electrodes. The authors reported a sensitivity of 8.3×10^1 CFU/ml for *Salmonella*, 7.9×10^1 CFU/ml for *E. coli* O157:H7, 7.5×10^1 CFU/ml for *E. coli* and 10^3 CCID/ml for BVDV virus in a detection time of 10 min with the conductometric biosensor. A conductometric immunosensor based on magnetic nanoparticles has been recently developed for the detection of *E. coli* by Hnaiein *et al.* (Hnaiein *et al.*, 2008). The immunosensor was composed of streptavidin modified magnetic nanoparticle layer immobilized on a conductometric transducer consisting of interdigitated gold electrodes. Conductivity measurements allowed detection of 0.5 CFU/ml of *E. coli* without the need for amplification.

2.2.2.3.4 Impedimetric Biosensors

Impedance spectroscopy involves applying small amplitude perturbing sinusoidal voltage signal to an electrochemical cell and measuring the resulting current response. The complex impedance, sum of real and imaginary impedance components, can be calculated as a function of the excitation frequency of the applied potential by varying it over a range of frequencies (Katz and Willner, 2003). Impedimetric detection techniques

provide advantages of high sensitivity, linearized current-potential characteristics, measurement over wide time or frequency range and label free sensing (Rahman *et al.*, 2008;Lazcka *et al.*, 2007)

Radke and Alocilja had developed a microimpedance biosensor for the detection of *E. coli* (Radke and Alocilja, 2005). The sensor detected changes in impedance caused by the presence of bacteria immobilized on interdigitated gold electrode arrays fabricated from silicon. The biosensor was able to discriminate between different cellular concentrations of the bacteria (10^5 to 10^7 CFU/ml) in 5 min. Nandakumar *et al.* have demonstrated the detection of *S.* Typhimurium using electrochemical impedance spectroscopy based on Bayesian decision theory (Nandakumar *et al.*, 2008). The technique detected the pathogen in 6 min at a lowest concentration of 500 CFU/ml. An impedance biosensor based on interdigitated array microelectrode coupled with magnetic nanoparticle-antibody conjugates was developed for rapid and specific detection of *E. coli* O157:H7 in ground beef samples by Varshney *et al.* (Varshney and Li, 2007). Magnitude of impedance and phase angle was measured in a frequency range of 10 Hz to 1 MHz in the presence of 0.1 M mannitol solution. The lowest detection limit of the biosensor for *E. coli* O157:H7 was 7.4×10^4 CFU/ml in pure cultures and 8.0×10^5 CFU/ml in ground beef samples, the total detection time being 35 min.

2.2.2.4 Magnetic Biosensors

Devices based on the detection of magnetic labels are emerging as a promising new approach in the field of biosensing. Magnetic labels have gained popularity in biosensing because they are physically and chemically stable, are relatively inexpensive, and can be easily made biocompatible. Several approaches have been developed in the past few

years for both direct and indirect detection of magnetic labels. Direct detection includes approaches for measuring magnetic parameters such as magnetic permeability, magnetic remanence, magnetoresistance, and Hall Effect. The indirect detection methods are based on micro-cantilever based force amplified sensors and magnetic relaxation switches (Tamanaha *et al.*, 2008). However, the applications of these magnetic devices for detection of actual targets such as pathogenic microorganisms remain limited and require further research.

Edelstein *et al.* had developed a multi-analyte BARC (Bead Array Counter) biosensor using giant magnetoresistive (GMR) sensors to detect and identify biological warfare agents (Edelstein *et al.*, 2000). The prototype designed by the authors consisted of a microfabricated chip with GMR sensor arrays, an electronic chip-carrier board, a fluidics cell and an electromagnet. DNA probes were patterned onto the GMR sensor chips and hybridized with complementary PCR products. Micron sized magnetic beads were then bound to the DNA sample by streptavidin biotin interactions and the unbound beads were removed by applying a magnetic field. The bound magnetic beads were then detected by the GMR sensors. The authors were able to demonstrate the detection of *B. anthracis* lethal factor and *C. botulinum* neurotoxin A using the BARC biosensor.

A mass-sensitive magnetoelastic immunosensor for the detection of *E. coli* O157:H7 was reported by Ruan *et al.* (Ruan *et al.*, 2003). The detection was based on the immobilization of alkaline phosphatase labeled antibodies on the surface of a micrometer-scale magnetoelastic cantilever and amplification of the mass change associated with antigen-antibody binding reaction by biocatalytic precipitation of bromo-

26

4-chloro-3-indolyl phosphate. The minimum detectable level of the immunosensor was 6 $\times 10^2$ cells/ml.

A high efficiency Hall effect micro-biosensor platform has recently been developed for the detection of magnetically labeled biomolecules by Sandhu *et al.* (Sandhu *et al.*, 2007). In this system, the integration of Hall-effect structures with micro-current lines allowed manipulation of the magnetic beads position via field gradients. The authors studied the hybridization of fully-complementary DNA strands of 20-25 bases using Dynabeads as magnetic labels with this platform. Although, the sensitivity of the sensor was not reported, the authors were able to demonstrate a quantitative relationship between the number of magnetic labels and the output signal.

2.2.3   Biological Sensing Elements

The main classes of biological sensing elements that are currently used in biosensors for pathogen detection are: (i) enzymes, (ii) antibodies, (iii) nucleic acids, (iv) aptamers and (v) molecularly imprinted polymers.

Enzymes are large complex macromolecules consisting mainly of protein, and containing a prosthetic group, that often include one or more metal atoms. Enzymes act as biocatalysts in biochemical reactions. Enzymes are mostly used for labeling other biomolecules such as antibodies and DNA in pathogen biosensing similar to assays such as ELISA (Lazcka *et al.*, 2007).

Antibodies are molecules consisting of polypeptide chains and can be classified as polyclonal, monoclonal and recombinant antibodies. Antibodies have been extensively applied in biosensors for the following advantages: they are very selective for a particular antigen, they are ultra-sensitive, and can bind very strongly with the corresponding

antigen. Antibodies can also be easily labeled with different molecules such as enzymes, radioisotopes, fluorescent probes, chemiluminescent probes or metal tags (Eggins, 2002). Most antibody based biosensors (immunosensors) are based on a competitive or sandwich assay when applied to detection of low and high molecular weight molecules, respectively (Marquette and Blum, 2006).

Nucleic acid (DNA & RNA) hybridization is a thermodynamically favored process which is triggered by highly specific interactions between the base-pairs where each nucleotide base strongly binds to its complementary base through multiple hydrogen bonds. This property makes nucleic acids an excellent choice for use as bio-recognition elements in biosensors. The nucleic acid based biosensors reported in literature can be classified based on optical, mass sensitive or electrochemical detection platforms (Diamond, 1998). Of these, DNA-based electrochemical sensors which rely on the conversion of DNA base-pair recognition event into useful electrical signal have been exploited the most. Such DNA based electrochemical devices have the advantages of high sensitivity, selectivity, low-cost, miniaturization ability and minimal power requirements (Wang, 2002). Numerous approaches for electrochemical detection of DNA have been developed which include direct electrochemistry of DNA, electrochemistry at polymer-modified electrodes, electrochemistry of DNA-specific redox reporters, electrochemical amplification with nanoparticles and devices based on DNA-mediated charge transport chemistry (Drummond *et al.*, 2003).

Aptamers are synthetic folded DNA or RNA oligonucleotide sequences specifically generated complementary to diverse target molecules. Aptamers offer multiple advantages as bio-recognition elements in biosensors in comparison to natural receptors

such as antibodies and enzymes. These include: high selectivity for targets (similar to monoclonal antibodies), smaller size, high reproducibility with minimum batch to batch variations, cost-effectiveness, chemical stability, greater flexibility for biosensor design and synthesizing ability for any given target (Song *et al.*, 2008;Mairal *et al.*, 2008).

Molecular imprinting is a template-induced process for the formation of specific recognition sites in a polymeric material, where the template directs the positioning and orientation of the material's structural components by a self-assembling mechanism. Molecularly imprinted polymers (MIPs) have several advantages over natural biomolecules such as antibodies and receptors. These include their unique stability in harsh environmental conditions, high affinity and selectivity similar to that of natural receptors, and their simplicity of preparation and ease of adaptation to practical applications (Ye and Haupt, 2004;Piletsky *et al.*, 2006). MIPs have been generated for a broad range of molecules from small molecules such as drugs to large proteins and cells, the best results being obtained for molecular weights in the range of 200-1200 Da (Piletsky *et al.*, 2006).

2.3   NANOBIOSENSORS & NANOSTRUCTURED TRANSDUCERS

Nanotechnology is defined as the creation of functional materials, devices and systems through the control of matter at the 1-100 nm scale (Wang, 2005). Recent advances in nanotechnology have led to the development of a variety of nanomaterials, e.g., nanowires, nanotubes, nanoparticles, nanospheres and nanorods. Due to their extremely small size, these nanomaterials exhibit unique properties such as physical strength, chemical reactivity, electrical conductivity, magnetism and optical characteristics. Such characteristics of the nanomaterials offer enormous prospects in designing novel methods of signal transduction and in integrating them into biosensing devices. Nanomaterials and nanoelectrodes are an important component of nanobiosensors. This section describes different nanostructured transducer materials and their current applications in biosensors with special emphasis on the detection of pathogenic microorganisms.

2.3.1   Nanowire Based Biosensors

Recently, nanowires have been explored as biosensor transducers for the following reasons: Firstly, the high aspect ratios of the nanowires make them extremely sensitive to biological interactions. Secondly, the electronically switchable properties of semiconducting nanowires allow direct and label-free electrical detection. Thirdly, the size-tunability of the nanowires to sub-100 nm allows high density device fabrication (Wang *et al.*, 2007a). Semiconducting nanowires including silicon nanowires, and conducting polymer nanowires, as well as metallic nanowires are the most studied ones in biosensor architectures. Laser-assisted metal-catalyzed growth (LCG), Vapor-liquid-solid growth (VLS), Vapor-solid-solid growth (VSS), chemical-solution based growth and

template-assisted growth are some techniques employed in the synthesis of nanowires (Spanier, 2006).

2.3.1.1 Silicon Nanowires

Semiconductor nanowire based detectors that show a change in conductivity with respect to variations in electric potential are referred to as field-effect transistors (FET). FETs have been widely used as transducers in detection devices because of the high surface to volume ratio and high sensitivity of the carrier mobility to variations in electric field at the semiconductor nanowire surfaces. Silicon (Si) nanowire based FETs are particularly attractive for electrical based sensing because of their superior electrical performance characteristics, high reproducibility and controllability during growth, and their high-performance switching characteristics that affect sensitivity (Cui *et al.*, 2003;Eggins, 2002;Patolsky *et al.*, 2006).

In a recent study, Mishra and coworkers have developed a nanowire field effect transistor (nano-FET) for detecting the enterotoxins released by the food borne pathogen *Staphylococcus aureus* (*S. aureus* Enterotoxin B, SEB) (Mishra *et al.*, 2008). The nano-FETs were fabricated using 50 nm doped polysilicon nanowires that were attached to small gold terminals separated by a gap of 150 nm using e beam lithography with controlled reactive ion etching using chlorine plasma. The authors reported a very low sensitivity of 10 fM of pure SEB using electrochemical impedance spectroscopy. Detection of single influenza A viruses was achieved by Patolsky *et al.* with antibody modified Si nanowire arrays (Patolsky *et al.*, 2006). The detection was based on the change of conductance of the nanowire device from a baseline value upon binding of the

virus particle followed by simultaneous return of the nanowire conductance to the baseline value upon unbinding of the viruses

Si nanowires have also been applied for the detection of DNA sequences. A two-terminal Si nanowire based electronic device for ultrasensitive DNA detection have been described by Hahm *et al.* (Hahm and Lieber, 2004). The device was modified by the authors with peptide nucleic acid (PNA) receptors that could distinguish between the wild type and and $\Delta F508$ mutation site in the cystic fibrosis trans membrane receptor gene. The time dependant conductance change due to PNA-DNA hybridization demonstrated that the device could selectively detect DNA concentrations as low as 10 fM. The detection limit of the device as suggested by the authors were better than other real-time measurement systems such as nanoparticle enhanced surface plasmon resonance (SPR) sensors and quartz crystal microbalance. More recently, arrays of highly ordered n-type silicon nanowires were fabricated using complementary metal-oxide semiconductor (CMOS) technology by Gao *et al.* (Gao *et al.*, 2007). The Si nanowire arrays enabled real time linear detection of DNA hybridization to its complementary target over a large dynamic range of 25 fM to 5 pM with a detection limit of 10 tm.

2.3.1.2 Conducting Polymer Nanowires

Conducting polymer (CP) nanowires or 'organic' nanowires are another class of nanowires that are used as transducer materials in biosensors. Simple synthetic procedures, controllable electrical properties, flexible chemical structures, compatability with biomolecules and efficient charge transfer in biochemical reactions are some of the properties which make CP nanowires attractive candidates for biosensing. Polyaniline and polypyrrole are the two most studied CPs in biosensor applications.

Pal *et al*. have described a polyaniline nanowire based direct-charge transfer biosensor for the detection of *Bacillus* species (Figure 2-5) (Pal *et al.*, 2008). The biosensor used two sets of antibodies (secondary and capture antibodies) for detection of the food borne pathogen, *Bacillus cereus*. The detection principle involved an immunoreaction coupled with direct electron charge flow by polyaniline nanowires across silver electrodes. The biosensor could attain sensitivity as low as 10^1 CFU/ml in 6 min through a reagentless process. The biosensor showed little or no cross-reactivity with other non-target bacteria and was also able to detect the presence of the target in a mixed culture of five different microorganisms.
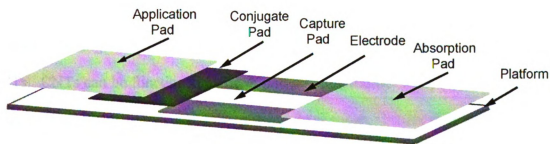
Figure 2-5. Schematic of the polyaniline nanowire biosensor for *Bacillus cereus* detection (Pal *et al.*, 2008).

Fan *et al*. have reported a nanogapped microelectrode-based biosensor array for detection of microRNAs (miRNAs) utilizing polyaniline nanowires (Fan *et al.*, 2007). PNA capture probes were immobilized in nanogaps of the microelectrodes and hybridized with their complementary miRNA. Conductance of the enzymatically catalyzed polyaniline nanowires, deposited on hybridized target miRNA, corresponded to the hybridized target concentration. The detection limit of the biosensor as reported by the authors was 5.0fM. Ramanathan *et al.* demonstrated DNA detection using avidin

functionalized polypyrrole nanowires that were electrodeposited in nanometer sized channels on the surface of silicon wafers and the resistance change of the avidin modified polypyrrole nanowires were used as indicator of the binding event of biotin-DNA (Ramanathan *et al.*, 2005). Resistance change for biotin-DNA concentration as low as 1 nM could be detected with an increasing resistance for increasing concentration till 100 nM.

2.3.2 Nanotube Based Biosensors

2.3.2.1 Carbon Nanotubes

In recent years, carbon nanotubes (CNT) have found broad applications in biosensors for detecting biomolecules and biological agents. This can be attributed to a number of factors such as unique electrical and electrochemical properties, high mechanical strength, and high aspect ratio for adsorption and immobilization of biomolecules on CNTs. CNTs can be functionalized in different configurations as covalent/non-covalent, defect, sidewall and endohedral, thus, making them compatible for different applications and can also be grown as single-walled nanotubes (SWNT) and multi-walled nanotubes (MWNT) (Figure 2-6) with diameters ranging from 0.4 to 3 nm for SWNT, and from 2 to 100 nm for MWNT respectively (Erickson *et al.*, 2008;Kim *et al.*, 2007b;Vaseashta and mova-Malinovska, 2005). CNTs have two distinct advantages over Si nanowires in their higher electron mobilities and their diameters in sub nanometer range and were first used in FET based devices for chemical sensing by Kong *et al.* (Kong *et al.*, 2000).
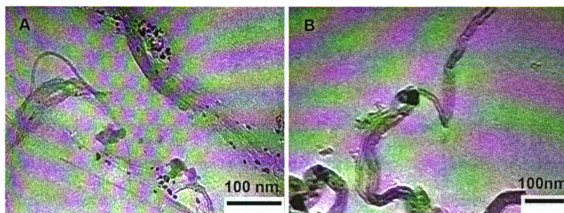
Figure 2-6. TEM images of (A) single-walled carbon nanotubes and (B) multi-walled carbon nanotubes.

A SWNT based FET device was developed by Villamizar *et al.* for the detection of the foodborne pathogen *Salmonella* Infantis (Villamizar *et al.*, 2008). The device used anti-*Salmonella* antibodies adsorbed onto the CNTs as the biological sensing element and was able to detect 100 CFU/ml of the pathogen in 1h. The device was selective and showed no cross-reactivity with antigens such as *S. pyogenes* and *S. sonnei*. So *et al.* reported an aptamer (So *et al.*, 2008) based SWNT FET array as a screening tool for *E. coli* DHα5 using the most probable number method. The sensor applied RNA based *E. coli* aptamers as the molecular recognition element and was able to complete the detection process in 20 min. Zhou *et al.* had utilized the high polarizability and dielectric mobility of SWNTs to capture, concentrate, and detect low numbers of bacteria in small sample volumes using microelectrode arrays (Zhou *et al.*, 2006). AC impedance spectra measurements yielded a detection threshold of 10^4 bacteria/ml with this technique. SWNT based FET devices functionalized with PNA were also used to detect an RNA sequence of the Hepatitis C virus at concentrations as low as fractional pM range by Dastagir *et al.* (Dastagir *et al.*, 2007). Dong *et al.* have shown a label-free detection

method for DNA sequences using resistors prepared from double-walled carbon nanotube networks (Dong *et al.*, 2008). The device was able to detect DNA concentrations in the range of 50 and 500 nM and has potential for handheld applications.

CNTs have also been extensively applied in the electrochemical detection of biomolecules. CNT based electrochemical biosensors usually employ electrodes modified with CNTs, or hybrid materials, such as CNT-conducting polymer composites, CNT-metal nanoparticles, and other CNT based composites as their detection platforms. Direct electron transfer promoted by the nanotubes between enzymes and the CNT modified electrodes has enabled the widespread application of CNTs in enzyme based electrochemical biosensors (Zhu *et al.*, 2007). CNT based electrochemical immunosensors and genosensors have also been reported in the literature (Yun *et al.*, 2007;Chang *et al.*, 2008).

2.3.2.2 Conducting Polymer Nanotubes

Conducting polymer nanotubes are the new class of one-dimensional nanostructures that have found applications as biosensor transducers. Unlike CNT based sensors, conducting polymer nanotube based sensors have the potential of achieving high sensitivity without involving complicated reaction steps, purification or end open processing (Chang *et al.*, 2007b).

A polyaniline nanotube array based electrochemical biosensor reported by Chang *et al.* enabled ultrasensitive detection of nucleic acids (Chang *et al.*, 2007b). The authors demonstrated a sensitivity of 1.0 fM target DNA for the biosensor and selectivity of one-nucleotide mismatch at concentrations as low as 37.59 fM. Label-free DNA detection using polypyrrole nanotubes has been shown by Ko *et al.* with a biosensor sensitivity of

1.0 nM target DNA (Ko and Jang, 2008). An aptamer conjugated amine-functionalized polypyrrole nanotube based FET device has been developed by Yoon *et al.* (Yoon *et al.*, 2008) for the detection of the protein, human-α-thrombin. The device could detect 166 nM thrombin in blood serum samples.

2.3.3 Nanoparticle Based Biosensors

Nanoparticles have unique physical, chemical, optical, and electronic properties that have made them appropriate for numerous applications in electrochemical sensors and biosensors. Immobilization and labeling of different biomolecules such as enzymes, antibodies, and DNA; acting as electrochemical catalysts and electron transfer agents; and performing the function of reactants and magnetic concentrators are the basic functions performed by these nanoparticles in sensing systems (Luo *et al.*, 2006). Discussed below are current developments in biosensors based on magnetic nanoparticles, metal nanoparticles including gold and silver, and semiconductor nanocrystalline particles (quantum dots).

2.3.3.1 Magnetic Nanoparticles

Magnetic nanoparticles (mostly superparamagnetic) have the ability to quickly agglomerate and resuspend in response to changes in external magnetic field. These unique properties of magnetic nanoparticles have led to their exploitation in various separation processes and detection devices such as biosensors. Magnetic separation techniques are widely used in bioengineering and biomedical applications such as magnetic resonance imaging, gene delivery, drug delivery, diagnostics, immunoassays and biosensors (Xu and Sun, 2007;Ludwig *et al.*, 2006;Lee *et al.*, 2006). In biosensor detection, magnetic separation techniques can provide a number of advantages, such as,

elimination of nonspecific adsorption of interfering biomolecules by modifying surface chemistries, elimination of sample pretreatment by centrifugation or chromatography thus reducing analysis time, and exclusion of centrifugation steps thus reducing stress-induced damages to biomolecules.

Varshney *et al.* have developed an impedance biosensor based on interdigitated array microelectrode coupled with magnetic nanoparticle antibody conjugates for detection of *E. coli* O157: H7 in ground beef samples (Varshney and Li, 2007). The biosensor provided rapid and specific detection of the pathogen with a sensitivity of 7.4 × 10^4 CFU/ml in pure cultures and 8.0 × 10^5 CFU/ml in ground beef samples in a detection time of 35 min.

Magnetic nanoparticles have also been employed for concentrating and electrochemical sensing of DNA targets in the literature. Zhu *et al.* have developed a method for detecting DNA hybridization using magnetic nanoparticle modified pyrolitic graphite electrode and the common electrochemical redox couple $K_3[Fe(CN)_6]/K_4[Fe(CN)_6]$ (Zhu *et al.*, 2006b). Magnetoswitchable controlled DNA hybridization was performed on DNA probe modified electrodes with subsequent electrochemical detection of the redox indicator. The detection limit for the sensor was 2 nM target DNA. In a separate study, DNA hybridization at magnetic nanoparticles coupled with electrochemical stripping detection of zinc sulfide nanoparticle tags on glassy carbon electrode was used by Zhu *et al.* (Zhu *et al.*, 2004).The authors were able to attain sensitivity as high as 0.2 pmol /L with the described methods.

Lately, several sensing devices have been developed that perform the detection process by measuring the magnetic properties of the magnetic nanoparticle tags. Kaittanis

et al. have reported a magnetic nanosensor for detecting *Mycobacterium avium* sp. *paratuberculosis* (MAP) in blood and milk samples using magnetic relaxation switches (MRS) (Kaittanis *et al.*, 2007).The detection mechanism involved switching of superparamagnetic iron oxide nanoparticles between a dispersed and clustered state upon target interaction and measurement of the resultant change in spin-spin relaxation time of the protons in water solution. The authors were able to quantify MAP from 15.5 to 775 CFUs in milk samples using these magnetic nanosensors. A magnetic microarray was developed by Wang *et al.* utilizing magnetic tunnel junction (MTJ) detectors which was aimed at detecting single molecules of DNA on individual magnetic nanoparticle tags (Wang *et al.*, 2005). Wang and coworkers have also recently prototyped magneto-nano chips using 8 × 8 array of 64 giant magnetoresistance (GMR) spin valve (SV) sensors (Wang and Li, 2008). The authors were also able to successfully detect Human Papillomavirus (HPV) DNA sequences using these GMR DNA chips at concentration levels of 10 pM. A magnetic permeability meter (MPM-100) was developed by Abrahamsson *et al* for DNA detection (Abrahamsson *et al.*, 2004). The limit of detection of the MPM sensor was 12 μg/ml in buffered solutions.

2.3.3.2 Gold Nanoparticles

In the last few years, intensive research has been carried out in the field of gold (Au) nanoparticle based biosensing devices. Au nanoparticles have a unique physical property of localized surface plasmon resonance i.e. the change in color that arises in the nanoparticles during aggregation (red-to-purple) or redispersion of aggregates (purple-to-red) from interparticle plasmon coupling. The above principle has been applied in Au nanoparticle based colorimetric biosensors for detection of different targets including

nucleic acids, proteins, saccharides, metal ions, small molecules and cells. A detailed review on colorimetric biosensing assays has been provided by Zhao *et al.* (Zhao *et al.*, 2008).The ability of Au nanoparticles to provide a suitable microenvironment for the immobilization of biomolecules retaining their bioactivity is a major advantage in biosensor fabrication. In addition, Au nanoparticles facilitate direct electron transfer between immobilized biomolecules and electrode surfaces without the use of electron transfer mediators, thus making them appropriate for electrochemical biosensing (Pingarron *et al.*, 2008).

Panda *et al.* have developed an optical detection method for the rapid quantification of bacterial cells using fluorescent Au nanoparticle-polymer composites (Panda *et al.*, 2008). The method is based on the loss of fluorescence intensity of positively charged Au nanoparticle-polythiophene composites in the presence of bacterial cells. The detection limit of the system was 1000 bacterial cells for both Gram-positive and Gram-negative bacteria. A highly sensitive electrochemical immunosensor for the detection of *S typhi* has been reported by Dungchai *et al.* using copper enhanced gold nanoparticles (Dungchai *et al.*, 2008). The presence of bacteria was detected by measuring the concentration of released copper ions from copper deposited on the colloidal Au nanotags using a copper enhancer solution by anodic stripping voltammetry. The authors reported a detection limit of 98.9 CFU/ml using the electrochemical immunosensor. Wang *et al.* have described a Quartz Crystal Microbalance (QCM) biosensor based on Au nanoparticles for the real-time detection of *E. coli* O157: H7 DNA in a circulating flow system (Wang *et al.*, 2007c). The sensor was able to detect the target DNA corresponding

to 2.0×10^3 CFU/ml of *E. coli* O157: H7 cells based on mass change and concomitant frequency shifts of the QCM.

Au nanoparticle based biobarcode assays allow highly sensitive detection of DNA sequences and are emerging as promising alternatives to polymerase chain reaction (PCR) for DNA detection. Au nanoparticles heavily functionalized with oligonucleotide probes are the building blocks of biobarcode assays. Hill *et al.* have reported a biobarcode assay for the detection of *B. subtilis* genomic DNA (Hill *et al.*, 2007). The biobarcodes were detected by scanometric methods. The assay demonstrated a sensitivity of 2.5 fM for double stranded genomic DNA. A fluorescent bio barcode assay for the detection of the foodborne pathogen *Salmonella* Enteritidis has been reported by Zhang *et al.* (Zhang *et al.*, 2009a). Au nanoparticles were first coated with target specific DNA probes and fluorescent labeled DNA barcodes. The DNA target was then sandwiched between the Au nanoparticles and magnetic nanoparticle coated with second DNA probes and separated by applying a magnetic field. The barcode DNA was released from the Au nanoparticles and quantified by fluorescence measurements. The authors reported a sensitivity of 1 ng/ml with the assay.
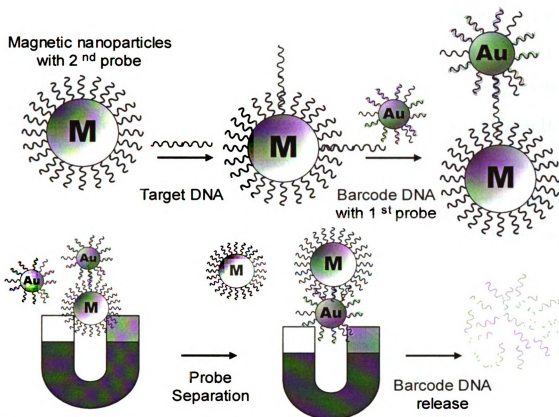
Figure 2-7. Schematic representation of Au nanoparticle based bio barcode assay (Zhang *et al.*, 2009a).

2.3.3.3 Semiconductor Nanoparticles (Quantum Dots)

Quantum dots (QDs) are luminescent nanocrystalline semiconductor particles that are roughly spherical in nature with particle diameters ranging from 1 to 12 nm. QDs have higher fluorescence quantum yields, better photoluminescence stability, and less toxicity than organic fluorophores along with their size tunable fluorescent properties. QDs are also resistant to photobleaching, denaturation of biomolecules and to variations in pH and temperature. Multi color QD nanocrystals have the potential for multiplexed and high-throughput analysis. These properties have made QDs suitable for application in optical detection systems (Costa-Fernandez, 2006;Sapsford *et al.*, 2006;Pileni, 2001). QD based optical biosensors can be roughly divided into luminescence-based and absorption-

based sensors depending on the changes of emission and absorption intensity (Comparelli *et al.*, 2007).

Recently, Liu *et al.* have used multi-layers of quantum dots for rapid magnetic bead based detection of *E. coli* O157: H7 *eae t*arget DNA (Liu *et al.*, 2008). The target DNA was first captured on magnetic beads by probe hybridization and the signal was amplified by using multi-layers of QDs. Fluorescence intensity measurements yielded a sensitivity of 250 zM within 40-60 min using this method. Su *et al.* reported an antibody based rapid, sensitive, and specific detection method for *E. coli* O157: H7 using cadmium selenide- zinc sulfide (CdSe-ZnS) QDs (Su and Li, 2004b). Magnetic beads coated with anti- *E. coli* O157: H7 antibodies were used to capture the target bacteria and were labeled with QDs by streptavidin-biotin conjugation. Fluorescence intensity measurements were proportional to *E. coli* O157: H7 concentrations in the range of 10^3 to 10^7 CFU/ml with the total detection time being less than 2h. The detection system was also selective against *E. coli* K12 and *S.* Typhimurium. Goldman *et al.* have utilized CdSe-ZnS QDs conjugated with antibodies to perform multiplex fluoroimmunoassays for the detection of cholera toxin, ricin, shiga-like toxin 1 and Staphylococcal enterotoxin B (Goldman *et al.*, 2004).

QDs have also found suitable applications in fluorescence resonance energy transfer (FRET) biosensors. The FRET technique relies on distance-dependant transfer of energy from a donor fluorophore to an acceptor fluorophore. The narrow emission spectra and the broad absorption spectra of QDs combined with their donor-acceptor separation distance of 1-10 nm result in improved performance of QDs in FRET assays over organic fluorophores. Zhang *et al.* reported an ultrasensitive DNA nanosensor based on FRET

using single QDs (Zhang *et al.*, 2005a). The system used QDs conjugated with DNA probes to capture DNA targets bound to dye-labelled reporter strands which formed a donor-acceptor ensemble. The QDs acted as a target concentrator and signal amplifier in the nanoscale domain. The nanosensor was capable of generating a strong FRET signal when bound to 50 copies of DNA or less. Recently, a FRET biosensor based on Au nanoparticles and QDs was developed by Stringer *et al.* for the detection of Porcine Reproductive and Respiratory Syndrome Virus (PRRSV) (Stringer *et al.*, 2008). The biosensor consisted of two architectures; a PRRSV- specific capture antibody labeled with a fluorescent dye bound to a QD labeled protein and a PRRSV- specific capture antibody labeled with a fluorescent dye bound to a Au nanoparticle labeled protein. The detection limit of the sensor was 3 particles /μl.

The metal components of the semiconductor nanoparticles in the QDs (CdS, PbS, and ZnS) have intrinsic redox properties susceptible to sensitive electrochemical stripping analysis thus making them suited for electrochemical biosensors. QD based electrochemical biosensors have been reported in literature for detection of different protein molecules and DNA but have not been applied in the detection of pathogenic microorganisms (Thurer *et al.*, 2007;Hansen *et al.*, 2006). Pumera *et al.* have developed a protocol for the detection of DNA hybridization based on magnetically triggered electrochemical detection of Au_{67} QD tracers (Pumera *et al.*, 2005). The authors reported a detection limit of 12nM target DNA with this system.

2.3.3.4 Silica Nanoparticles

Literature reveals that silica (Si) nanoparticles have been successfully used as nanotransducers in electrochemical and fluorescence based biosensors and bioassays.

Zhao *et al.* have reported a rapid bioassay for the detection of a single bacterial cell of *E. coli* O157: H7 using fluorescent-bioconjugated silica nanoparticles (Zhao *et al.*, 2004). The authors were able to detect a single *E. coli* O157: H7 bacterium within 20 min in spiked ground beef samples with this bioassay. Multicolored FRET Si nanoparticles were used by Wang *et al.* for multiplex monitoring of bacterial pathogens (Wang *et al.*, 2007b). Each dye doped Si nanoparticle encapsulated about 10,000 dye molecules in a 60 nm silica sphere which provided an extremely strong fluorescent signal for bioanalysis. The authors reported simultaneous detection of *E. coli*, *S.* Typhimurium and *S. aureus* with this assay in 30 min.

Ping *et al.* have developed a PCR based detection system for the detection of a SARS Coronavirus gene using Si coated superparamagnetic nanoparticles and Si coated fluorescent nanoparticles (Gong *et al.*, 2008). PCR amplified targets were concentrated using Si coated magnetic nanoparticles and then hybridized with the Si coated fluorescent nanoparticles in a sandwiched hybridization format. The limit of detection of the assay was 2.0×10^3 copies in a total detection time of less than 6h. A sensitive electrogenerated chemiluminescence (ECL) detection of DNA hybridization based on $Ru(bpy)_3^{2+}$ doped Si nanoparticles was developed by Chang *et al.* (Chang *et al.*, 2006). The $Ru(bpy)_3^{2+}$ doped Si nanoparticles labeled DNA probes were first hybridized with DNA targets immobilized on the surface of polypyrrole modified platinum electrodes. The hybridization events were then detected by ECL signals. Using the ECL signals, the authors were able to detect the target DNA at levels as low as 1.0×10^{-13} mol/l with selectivity of a three base mismatch sequence and a non-complementary sequence.

2.3.4 Nanoporous Material Based Biosensors

Novel nanoporous materials such as porous silicon, porous carbon, and porous alumina have recently found effective applications as biosensor transducers. Nanoporous silicon, characterized by its high surface to volume ratio and photoluminescence properties, has been employed in more than one biosensor transduction mechanisms. Mathew and Alocilja developed a pathogen biosensor for the detection of *E. coli* exploiting the optical properties of nanoporous silicon (Mathew and Alocilja, 2005). The reaction of β-galactosidase enzyme from *E. coli* with a dioxetane-polymyxinB mixture functionalized on porous silicon chips generated light at 530 nm. Light emission measurements from the porous silicon biosensor demonstrated a sensitivity of 10^1-10^2 CFU/ml for the pathogen. Electrochemical detection of targets using nanoporous silicon platforms has been reported by Zhang *et al.* (Zhang and Alocilja, 2008). The authors fabricated nanoporous silicon with P-type silicon wafers by electrochemical etching and applied them in the detection of DNA targets for the foodborne pathogen *Salmonella* Enteritidis. The sensitivity of the biosensor based on the electrical properties of DNA, redox indicators, and cyclic voltammetry was 1 ng/ml. The extremely high surface area of nanoporous silicon films have also been used for sensitive detection of the bacteriophage virus MS2 by Rossi *et al.* (Rossi *et al.*, 2007). Porous silicon films were used to selectively capture dye-labeled MS2 viruses from solution and a sensitivity of 2 × 10^7 plaque-forming units per ml (PFU/ml) were reported by the authors by measuring fluorescence from the exposed porous silicon film.

Bothara *et al.* (Bothara *et al.*, 2008) have developed an electrical immunoassay based on nanoporous alumina membranes for the sensitive detection of proteins. The detection

principle involves the formation of electrical double layer and the perturbations caused by proteins trapped in a nanoporous alumina membrane over a microelectrode array platform. Label-free electrical detection of protein biomarkers for cardiovascular diseases, C-reactive protein and (CRP) and myeloperoxidase (MPO) were achieved through this assay. The lower detection limits for CRP and MPO were 200 pg/ml and 500 pg/ml respectively.

Porous conductive carbon has been shown to be a good matrix for biosensor construction. The high conductivity of carbon is suitable for electrochemical transduction and in combination with its porosity makes it ideal for adsorption of biomolecules. Nanoporous carbon has been successfully used for the construction of acetylcholine esterase biosensor by Sotiropoulou and Chaniotakis (Sotiropoulou *et al.*, 2005).

2.3.5 Nanorod and Nanosphere Based Biosensors

Gold nanorods have been successfully employed in optical biosensors. Marinakos *et al.* have developed a label-free chip-based localized surface plasmon resonance (LSPR) biosensor using gold nanorods (Marinakos *et al.*, 2007). The biosensor monitored streptavidin binding to biotin by studying the LSPR peak shifts at the gold nanorod surface. The biosensor sensitivity was 94 pM in phosphate buffered saline and 19 nM in serum. Multiplex detection of three different IgG molecules was also achieved on gold nanorods of different aspect ratios fabricated by a seed-mediated growth by Yu and Irudayaraj (Yu and Irudayaraj, 2007). A gold/silicon hetero nanorod biosensor was developed by Fu *et al.* for detection of the foodborne pathogen *Salmonella* Typhmurium (Fu *et al.*, 2008). The hetero nanorods were functionalized with anti-Salmonella

antibodies and detection was accomplished through fluorescence signaling mediated by multiple Alexa488 dye molecules bound on the nanorods.
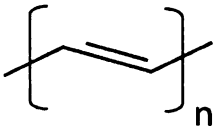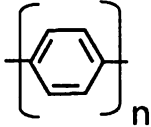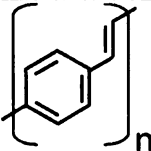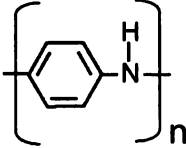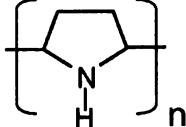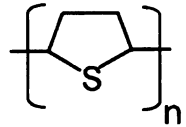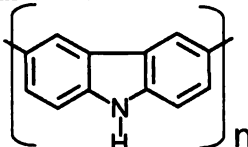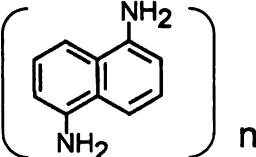
Different nanospheres viz. silica, nickel oxide (NiO), cadmium sulfide (CdS), and magnetic gold are being currently utilized as biosensor transducers in literature. NiO hollow nanospheres have been used for glucose biosensing by Li *et al.* (Li *et al.*, 2008). A novel nitrite biosensor based on direct electron transfer of hemoglobin (Hb) immobilized on CdS hollow nanosphere modified glassy carbon electrode has been reported by Dai *et al.* (Dai *et al.*, 2008). Thionine doped magnetic gold nanospheres synthesized by reverse micelle method have enabled ultrasensitive electrochemical immunosensing of carcinoembroyonic antigen protein by Tang *et al.* (Tang *et al.*, 2008). The use of fluorescent silica nanospheres as luminescent signal amplifiers in detecting the breast cancer marker HER2/neu in a simple glass slide based assay has been reported by Rossi *et al.* (Rossi *et al.*, 2006).

2.4 POLYANILINE – A CONDUCTING POLYMER

2.4.1 Introduction

Polymers containing loosely held electrons in their backbones are referred to as conjugated polymers or conducting polymers and have attracted considerable interest for the past two decades. Research on conducting polymers intensified after the rediscovery of polyacetylene in 1977 by McDiarmid and Heeger. They were able to enhance the electrical conductivity of polyacetylene by many orders of magnitude by simple doping with oxidizing and reducing agents (Gerard *et al.*, 2002). The presences of π-electron backbones in the conducting polymers result in their unusual electronic properties, such as high electrical conductivity, low ionization potential, and high electron affinity. They are also known as 'intrinsically conducting polymers' due to the presence of partially filled molecular orbitals which allow free movement of electrons throughout the polymer lattice and overlapping molecular orbitals which allow the formation of delocalized molecular wave functions. These types of polymers have also attracted interest for their nonlinear optical properties, since the electrons in these delocalized systems are easily polarized by an external electric field. These polymers have been considered to be as "molecular wires" for nanotechnology (Gorman and Grubbs, 1991). As a result of such unusual properties, conducting polymers have a number of practical applications, such as in electronic displays, telecommunication, electrochemical storing systems, and molecular electronics and sensors (Hohnholz *et al.*, 2005;Kaneto *et al.*, 2007;Ramanavicius *et al.*, 2006). Table 2-1 shows the chemical structures and conductivity of some common conducting polymers.

49

Table 2-1. Chemical structure and conductivity of typical conducting polymers (adapted and modified from Rahman et al., 2008).

Conducting Polymer	Structure	Conductivity (S/cm)
Polyacetylene		~ 1000
Polyparaphenylene		100 ~ 500
Polyparaphenylene vinylene		~3
Polyazulene		~0.1
Polyaniline		1~ 100
Polypyrrole		40 ~ 100
Polythiophene		10 ~ 100
Polycarbazole		10 ~ 100
Polydiaminonapthalene		10^{-3}

2.4.2 Structure and Electrical Properties

Among all conducting polymers, polyaniline is intensely investigated particularly due to its excellent stability in different solutions, good electronic properties, and strong biomolecular interactions (Feast *et al.*, 1996;Ryder *et al.*, 1997). Polyaniline is synthesized from its monomer form, aniline. There are two basic methods of polyaniline synthesis: chemical synthesis and electrochemical synthesis. The chemical synthesis involves step-growth polymerization of an aqueous solution of the monomer in the presence of an oxidizing agent and a protonating acid. In the aqueous acidic media, aniline cation radicals are the first product of the oxidation. The aniline cation radicals then recombine into benzidine and N-phenyl-p-phenylenediamine, or, participate in the growth of polyaniline chains in the pernigraniline form. The oxidative polymerization reaction continues according to equations 2-3 and 2-4 until all the pernigraniline is converted into emeraldine by equations 2-5 and 2-6 (Stejskal and Gilbert, 2002).

$$\langle \bigcirc \rangle \text{—NH}_3^+ \rightleftharpoons \langle \bigcirc \rangle \text{—}\overset{+ \cdot}{\text{NH}}_2 + \text{H}^+ + \text{e}$$

(2-3)

$$\text{R—}\langle \bigcirc \rangle \text{—}\overset{+ \cdot}{\text{NH}}_2 + \langle \bigcirc \rangle \text{—}\overset{+ \cdot}{\text{NH}}_2 \rightleftharpoons$$

$$\text{R—}\langle \bigcirc \rangle \text{—}\overset{+ \cdot}{\text{NH}}\text{—}\langle \bigcirc \rangle \text{—}\overset{+ \cdot}{\text{NH}}_2 + 2\text{H}^+ + 2\text{e}$$

(2-4)

51

$$S_2O_8^{2-} + 2e \rightleftharpoons 2SO_4^{2-} \qquad (2\text{-}5)$$

$$(2\text{-}6)$$
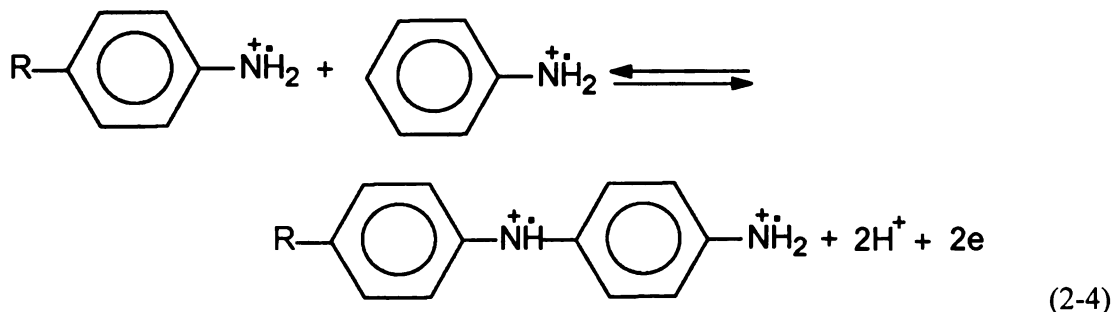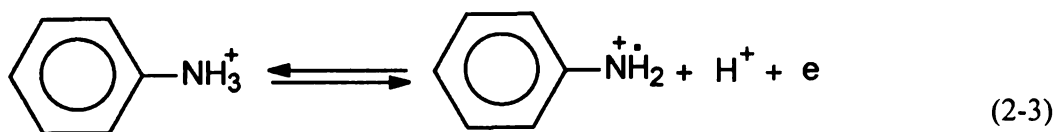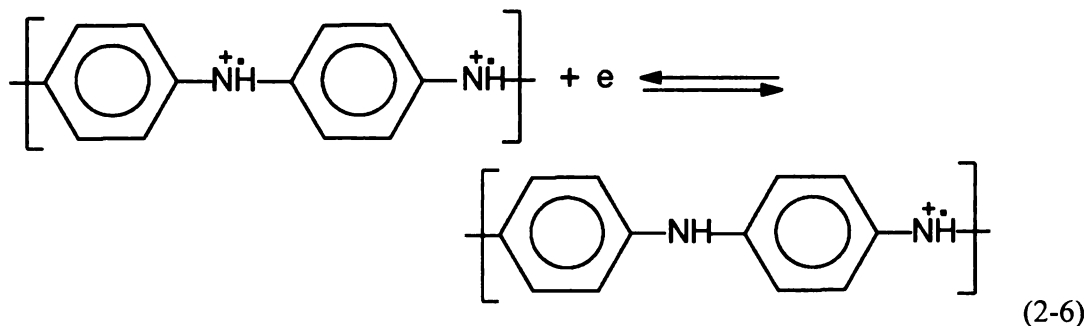
The electrochemical synthesis of polyaniline is carried out in a typical electrochemical bath by adopting a standard three-electrode configuration. The standard three-electrode system usually comprises of a working electrode, a counter electrode and the reference electrode. The electrochemical polymerization generally employs a constant current or galvanostatic, constant potential or potentiostatic or potential scanning/cycling methods (Ahuja *et al.*, 2007). The commonly used working electrodes are chromium, nickel, gold, platinum, palladium and glass coated with tin oxide or indium tin oxide.

2.4.2.1 Oxidation States

The conducting polymer, polyaniline, exists in a variety of forms differing in electrical conductivity and color. The general chemical structure of polyaniline has been

shown in Figure 6, where, indicate the reduced repeat units, and

 indicate the oxidized repeat units of the polymer.
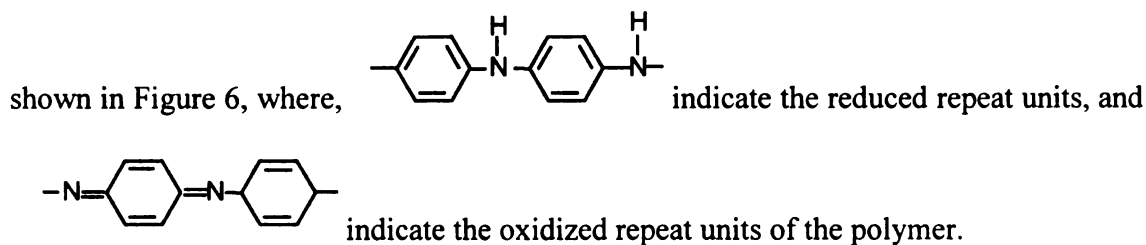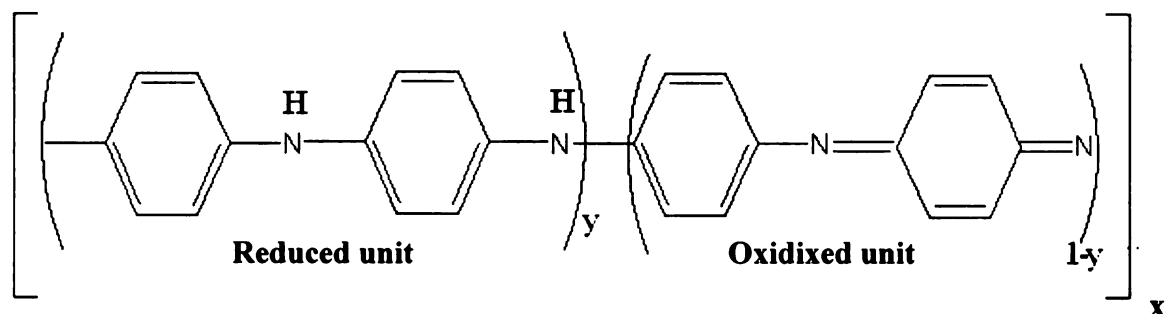
Figure 2-8. Structure of polyaniline, x = degree of polymerization, [y + (1-y)] = 1. (Ray *et al.*, 1989)

There are three distinct oxidation states of the polymer, namely, "leucoemeraldine", "emeraldine" and "pernigraniline". The fully reduced form of polyaniline is "leucoemeraldine" (1-y = 0, y =1), while "pernigraniline" (1-y = 1, y = 0) is the fully oxidized form of polyaniline and "emeraldine" (y = 1-y = 0.5) is the 50% oxidized form of polyaniline (Ray *et al.*, 1989). Each oxidation state of the polymer can exist in its base form or its protonated form (salt) by treatment of the base with acid.

Interconversion between the different forms of polyaniline occurs during the oxidative polymerization of aniline which imparts electrical conductivity and color to the different forms. The most important and stable form of polyaniline is protonated emeraldine which is green in color and electrically conductive. It is produced directly by the oxidative polymerization of aniline. When stronger oxidizing conditions are employed, it converts to protonated pernigraniline which is blue and is expected to be conducting. Further treatment with alkali results in pernigraniline base which is violet and non-conducting. The acid-base transition occurs at pH 0-1. Emeraldine can also be reduced to the colorless, non-conducting, leucoemeraldine form (Stejskal *et al.*, 1996).

2.4.2.2 Electronic Conduction

It is well known that the electrical conduction properties of elemental semiconductors, such as Si, can be rigorously controlled by addition of small quantities of foreign atoms into the semiconductor lattice. The semiconductors can be made n type or p type depending on the nature of the dopant atoms, i.e. whether it has an excess or deficit of electrons. The electrical conduction in conjugated or conducting polymers can also be explained by a similar terminology. However, the doping mechanism in conducting polymers is considerably different from the conventional semiconductors. Firstly, the doping levels are significant in conjugated polymers (as large as 10 mole percent) and secondly, there is charge transfer between the incorporated dopant atom and the polymer chain, hence the later is partially oxidized or reduced (Lyons, 1994). The partial oxidation of the polymer chain is termed as p-doping while partial reduction is termed as n-doping.

Electrical conductivity results (σ) from the existence of charge carriers and the ability of those carriers to move. It is expressed as,

$$\sigma = ne\mu \qquad (2\text{-}7)$$

where, n is the number of charge carriers per unit volume, e is the electronic charge and μ is the carrier mobililty. Hence, doped conjugated polymers or conducting polymers are good conductors for two reasons; firstly, doping introduces charge carriers into the π-electron system of the polymer and since every monomer is a potential redox site, they can be heavily doped, and secondly, the π- bonding leads to π- electron delocalization along the polymer chains thereby leading to charge carrier mobility which is extended

into three dimensional transport by interchain electron transfer interactions (Heeger and Smith, 1991).

The half-oxidized form of polyaniline (i.e. emeraldine) is the most studied and the most stable form of polyaniline. The emeraldine base form of polyaniline has been found to be different from other polymers in several aspects. First, it is not charge conjugation symmetric in contrast to polymers such as polyacetylene and polythiophene. Second, both the carbon rings and the nitrogen atoms in polyaniline are within the conjugation path forming a generalized "A-B" polymer. Third, the C_6 benzenoid rings of polyaniline can rotate or flip thus significantly altering the electronic structure (Pouget *et al.*, 1991).

It has been shown that the emeraldine base form of polyaniline can be reversibly varied from an insulator ($\sigma < 10^{-10}$ ohm^{-1}cm^{-1}) to a conductor ($\sigma \sim 10$ ohm^{-1}cm^{-1}) through protonation (Epstein *et al.*, 1987). The doping of emeraldine base with a non-oxidizing protonic acid such as HCl involves a new concept. Unlike the doping of all other conducting polymers, the number of electrons in the polymer backbone remains unchanged (Macdiarmid *et al.*, 1987). Unlike other doped conducting polymers which are polycarbonium ions or polycarbanions, the emeraldine salt polymer is based on a "nitrogenonium" ion polymer in which the positive charge resides chiefly on the nitrogen (Macdiarmid *et al.*, 1987).

The conductivity of polyaniline is believed to be due to the analogous protonation of emeraldine base which leads to the formation of a polysemiquinone radical cation (polaron) and gives rise to a polaron conduction band by coulombic repulsion leading to a metallic state (Macdiarmid *et al.*, 1987).
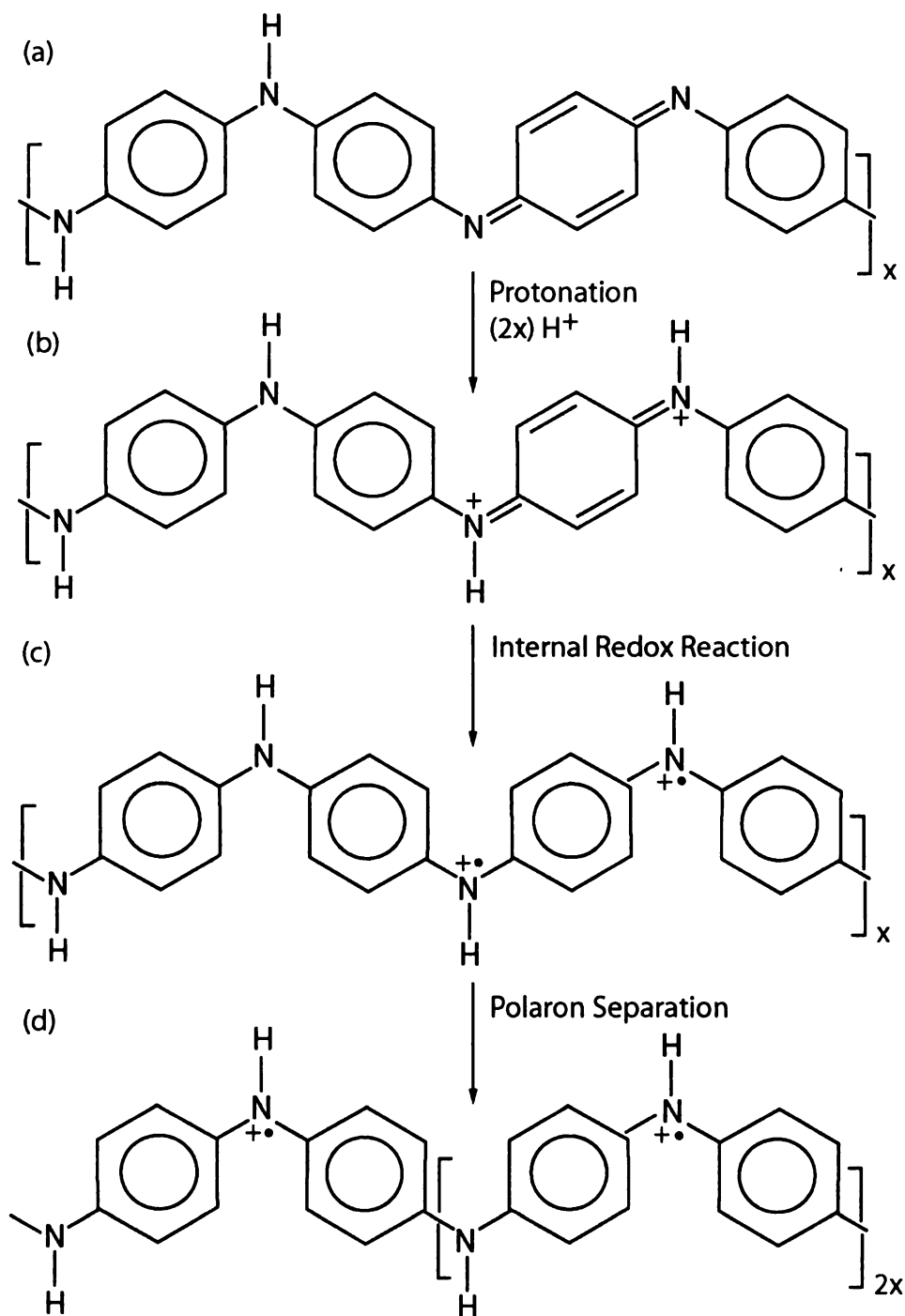
Figure 2-9. Structure of emeraldine (polyaniline), (a) before protonation and (b) -
(d) after protonation, (b) formation of bipolarons, (c) formation of polarons, and (d)
the separate polarons which result in a polaron lattice (adapted from Stafstrom *et
al.*, 1987).

A model based on two-step transition from isolated, doubly charged spinless, bipolarons to a polaronic metal has been suggested by Stafstrom et al (Stafstrom et al., 1987). The first step relates to instability of a bipolaron on a polyemeraldine chain which results in the formation of two polarons, and the second step involves the separation of the polarons to yield a polaron lattice (Stafstrom et al., 1987). Figure 2-9 shows the changes in the structure of polyaniline as suggested in the above model.

Figure 2-10 shows the band structure of a conjugated polymer as a function of doping level which illustrates the polaronic and bipolaronic states in the band gap. A neutral polymer acts as an insulator and has a full valence band and an empty conduction band which is separated by a band gap. Removal of an electron by doping results in the generation of a polaron level at the midgap. Further oxidation results in the removal of a second electron to generate a bipolaron.
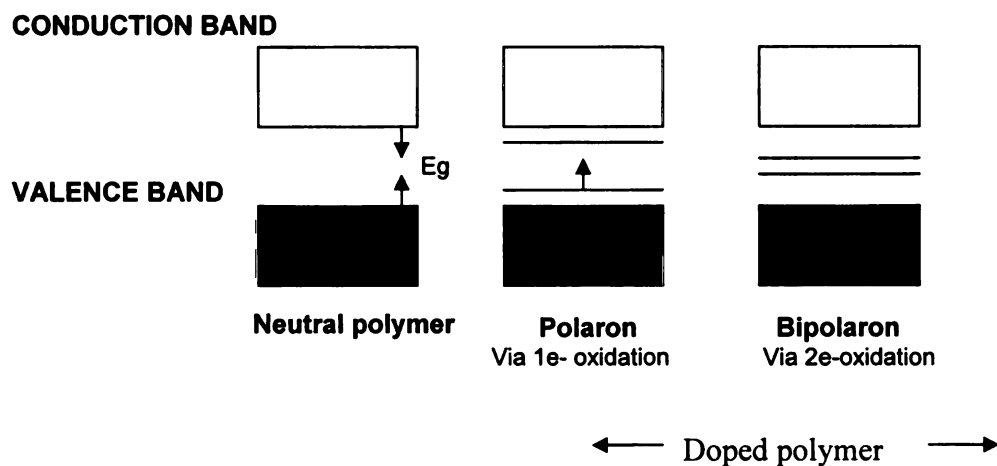
Figure 2-10. Band structure of conjugated polymers showing polaronic and bipolaronic states.

2.4.3 Electrochemistry and Redox Switching

The electrochemical preparation of polyaniline has typically been carried out in aqueous electrolytes galavanostatically, potentiostatically or through cycling of the potential of the substrate anode. Several electrolytes have been successfully used for the synthesis of polyaniline such as hydrochloric acid, perchloric acid, sulfuric acid, nitric acid, trifluoroacetic acid and fluoroboric acid (Delvaux *et al.*, 2000;Duic *et al.*, 1994;Duic *et al.*, 1995;Pan *et al.*, 2006;Wei and Ivaska, 2006)with the polymer being deposited on diverse substrates such as platinum, gold, indium tin oxide, carbon and stainless steel (Bereket *et al.*, 2005;Mazur *et al.*, 2002;Tang *et al.*, 1996;Wei *et al.*, 2008;Zhang *et al.*, 2009b). Investigation of the electrochemical properties (redox switching) of polyaniline is considered to be the key factor in understanding the physical and chemical properties of polyaniline.

The redox switching process of polyaniline has been studied for many years using various kinds of voltammetry. The concomitant processes that occur during the redox switching of polyaniline are as follows: (a) cyclic voltammetry reveals that two peaks are associated with the switching of polyaniline from the fully reduced leucoemeraldine state to the conducting emeraldine state and from the emeraldine state to the fully oxidized pernigraniline state; (b) the conducting emeraldine state of polyaniline exits in a potential window instead of a fixed potential; (c) the redox switching property of polyaniline depends mainly on the pH of the medium and in neutral or alkaline medium, the polymer loses its electrochemical activity; (d) the redox behaviour of polyaniline is fundamentally asymmetric; and (e) the oxidation transition occurs at a lower rate than that of the

reduction transition (Gospodinova *et al.*, 1996;Grzeszczuk and Szostak, 2003;Hong and Park, 2005).

The redox transition of polyaniline usually occurs in the potential range of -200 to 400mV (saturated calomel electrode) and is accompanied by proton ejection or injection. There is a proton ejection during the oxidation of a fully relaxed polymer from the leucoemeraldine form to emeraldine form and from it to fully oxidized form, while the reduction of the polymer is accompanied by proton injection which is incomplete because of the slow proton equilibration process (Ybarra *et al.*, 2000;Lyons, 1994). The redox switching in polyaniline is also accompanied by a small increase in volume of the polymer. Several factors such as water and ion exchange with the electrolyte, coulombic repulsion between charged sites in the polymer backbone, anion-polymer interactions, and a structural change of the polymer backbone govern the swelling of the polymer during the switching process (Lizarraga *et al.*, 2004).

The effect of pH on the electrochemical activity of polyaniline has been studied by authors (Prakash, 2002). Cyclic voltammograms (CVs) of polyaniline films on a Pt working electrode and Ag/AgCl reference electrode were recorded in HCl solutions in the pH range of 1-4 by the author (Figure 2-11). At pH 1.0, three reversible anodic peaks and their corresponding reduction peaks, were observed. As the pH was increased, a shift in one redox peak toward lower potential values which merged into a single broad peak at pH 4.0 occurred This peak was associated with the involvement of protons in the redox reaction which made the peak pH dependant, whereas, the other peaks only involved transfer of electrons (Prakash, 2002).
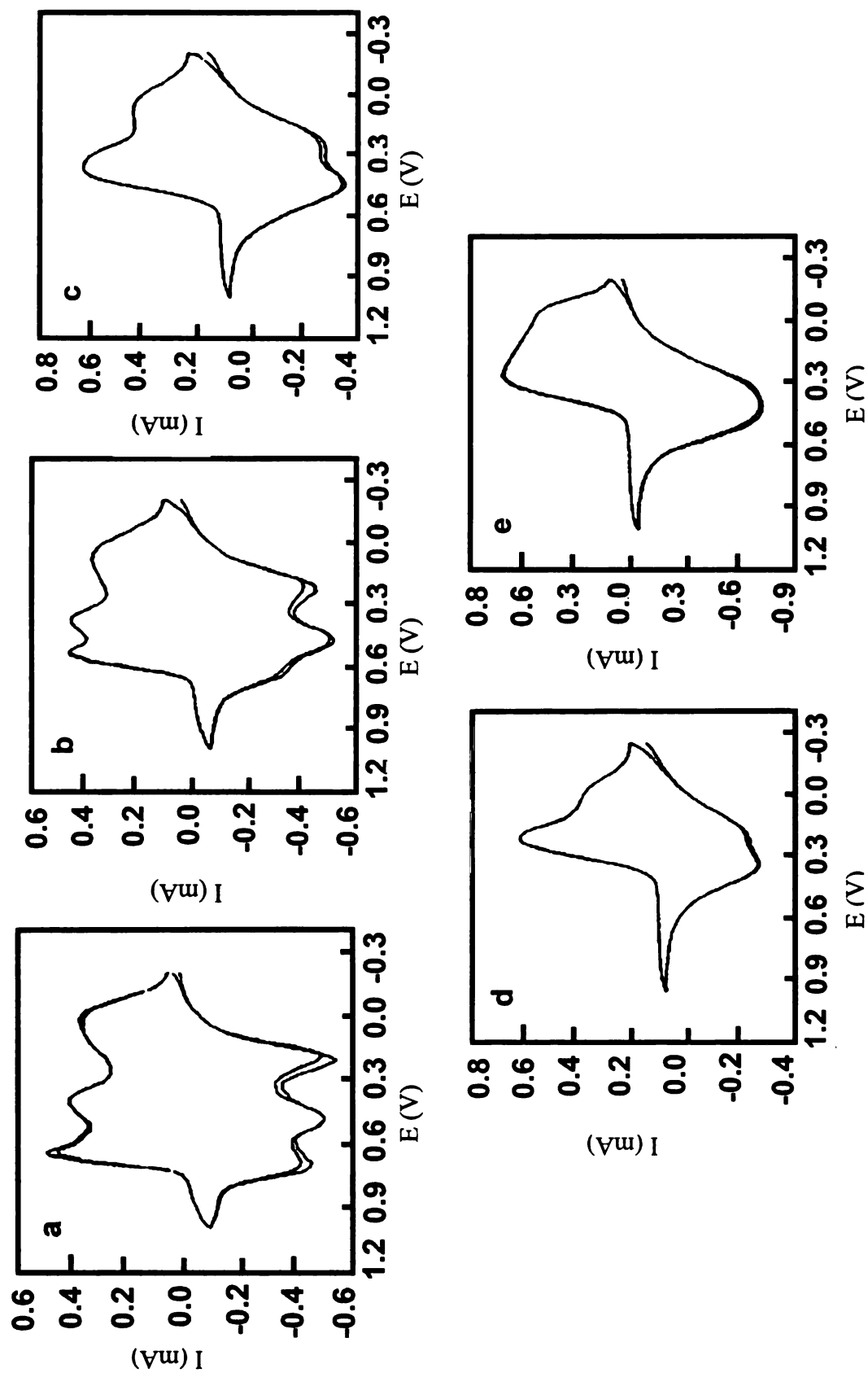
Figure 2-11. CVs of polyaniline films recorded at pH values of (a) 1.0, (b) 2.0, (c) 2.5, (d) 3.0 and (e) 4.0 (Prakash, 2002).

2.4.3.1 Cyclic Voltammetry

Cyclic voltammetry is a form of linear sweep voltammetry in electrochemistry where the potential applied to the working electrode of a three electrode electrochemical cell is ramped linearly versus time between an initial potential (E_1) and a final potential (E_2). When the potential reaches E_2, it is ramped back to the initial potential of E_1. This ramping of the potential is known as the scan rate and is usually expressed in V/s or mV/s. For a reversible redox system, the resulting current (I) measured while scanning the potential is represented with respect to the potential (E) in a typical cyclic voltammogram. Figure 2-12 shows a typical I-E curve (cyclic voltammogram) for a redox system. The voltammogram is characterized by a peak potential E_p, a potential corresponding to the point where the measured current reaches its maximum value I_p. In Figure 2-12, I_{pa} and I_{pc} indicate the anodic and cathodic peak currents and E_{pa} and E_{pc} indicate the anodic and cathodic peak potentials, respectively. Two parameters that are of interest in the I -E curves are the ratio of the peak currents I_{pa}/I_{pc}, and the separation peak potentials, $E_{pa} - E_{pc}$.

For a reversible system, the peak current, I_p, is given by the equation

$$I_p = 0.4463 \left(\frac{F^3}{RT} \right)^{1/2} n^{3/2} A D_0^{1/2} C_0^* v^{1/2} \tag{2-8}$$

where, F = Faraday's constant (Q mol^{-1}), R = universal gas constant (J mol^{-1}K^{-1}), T = temperature (K), n = no. of electrons exchanged in the reaction, A = area of the electrode surface (cm^2), D_0 = diffusion coefficient of the electroactive species (cm^2/s), C_0^* =

concentration of the electroactive species (mol/cm^3), and v = scan rate (V/s) (Bard and

Faulkner, 2001).

Similarly, the peak potential, E_p, for a reversible system is given by the equation

$$E_p = E_{1/2} - 1.109 \frac{RT}{nF}$$
(2-9)

For systems with stable product (reversible reactions), the following two conditions

should be satisfied: the anodic peak current should be equal to the cathodic peak current,

i.e., I_{pa}/I_{pc} = 1 and the separation of the anodic and cathodic peak potentials should obey

the following equation:

$$\left| \Delta E_p \right| = \left| E_{pa} - E_{pc} \right| = 0.059/n$$
(2-10)

For totally irreversible redox systems, E_p is a function of scan rate, shifting (for

reduction) in a negative direction by an amount of about 0.03V ten fold increase in v

whereas in quasi-reversible systems, I_p is not proportional to v (Bard and Faulkner,

2001).
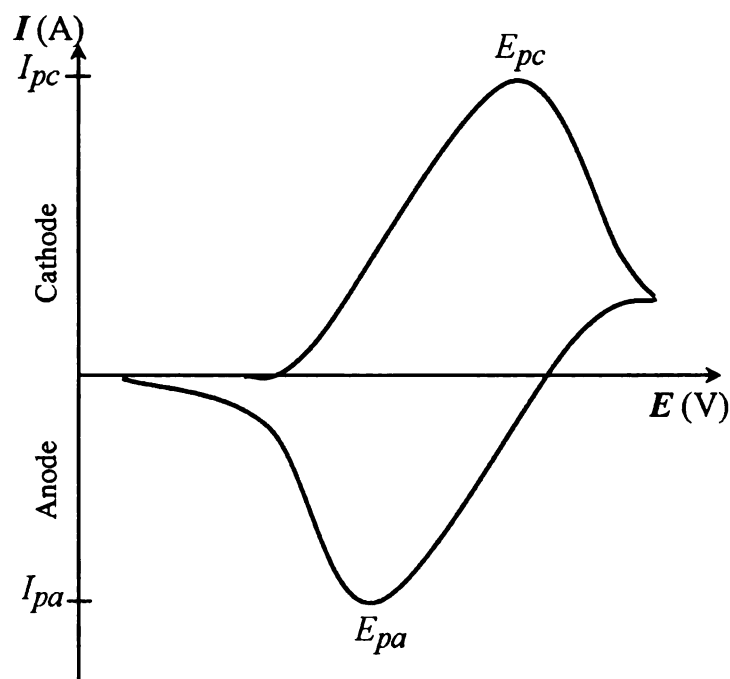
Figure 2-12. Typical cyclic voltammogram (*I-E* curve) for a redox system.

Cyclic voltammtery is a very powerful tool for electrochemical studies of new systems and provides useful information on complicated electrode reactions. The current research will investigate the diagnostic strength of cyclic voltammetry in evaluating the concentration of an electrically active species from peak current heights.

2.4.4 Electrically-Active Magnetic Polyaniline

Magnetic polymer nanostructures are a new class of materials where magnetic nanoparticles are embedded in polymer matrices. Such nanostructures have attracted considerable interest in recent years due to their immense potential for applications in electromagnetic devices, drug targeting, cell separation, enzyme immunoassays and electromagnetic interface shielding (Asmatulu *et al.*, 2005;Boissiere *et al.*, 2006;El-Tantawy *et al.*, 2004). Multi component systems containing conducting polymers and nanoparticles of metal oxides have the advantages of non-corrosiveness, light weight,

mechanical strength and dielectric tunability along with novel magnetic and optical properties (Poddar *et al.*, 2004b). Polyaniline is the most studied conducting polymer in such multi component systems due to its unique properties such as controllable electrical and chemical properties, excellent environmental stability and simple and low cost synthesis (Ray *et al.*, 1989).

The general approach for the synthesis of such magnetic polyaniline nanocomposites or nanoparticles is polymerization of the monomer aniline around a magnetic core or template nanoparticle as represented in Figure 2-13.
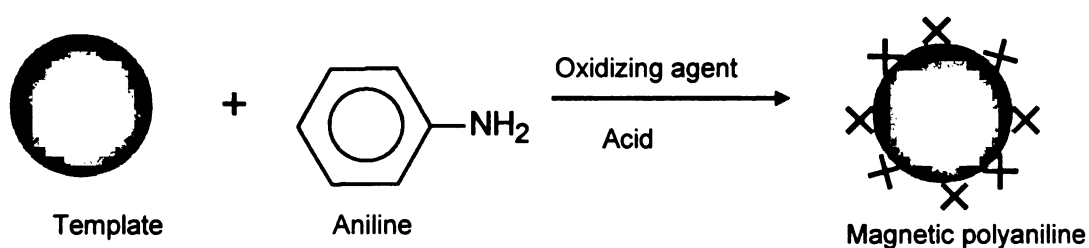
Figure 2-13. Synthesis of electrically-active magnetic polyaniline (Li *et al.*, 2007b).

Till date, the most common magnetic nanomaterials that are used in the synthesis of magnetic polymer composites are iron oxides and ferrofluids. A review of the magnetic properties of iron oxides has been provided by Kryszewski *et al* (Kryszewski and Jeszka, 1998). Some of the most important properties as mentioned by them are: (a) electrostatic exchange dominates for Fe ions at adjacent sites, (b) the specific saturation magnetization of iron oxide nanoparticles decrease with increase in specific surface of the nanoparticle and is also influenced by the particle morphology, (c) surface hydroxyl groups by adsorption of water make iron oxide nanoparticles amphoteric so that they can react both with acids and bases, and (d) the acidity and reactivity of differently coordinated iron

changes. According to Kryszewski *et al.* the incorporation of iron oxide nanoparticles into polymer matrices involves specific interactions with ligands which replace the surface hydroxyl groups as represented in Figure 2-14.
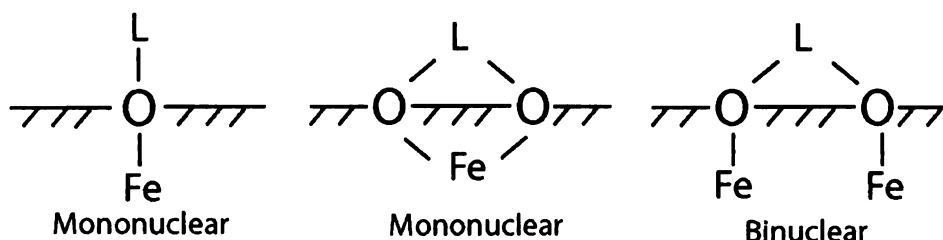
Figure 2-14. Polymer ligand interactions to iron oxide particle surfaces (L = ligand) (Kryszewski and Jeszka, 1998).

Under ideal circumstances, nanoparticles can exhibit novel magnetic properties when they exist as isolated particles. A critical obstacle in maintaining a nanoscale magnetic material is its tendency to agglomerate (Kryszewski and Jeszka, 1998). For practical applications, a collection or aggregate of nanoparticles or nanopowders are more prevalent. The dispersion of the nanoparticles in the polymer matrix is also a critical issue and needs extensive research. The competition between polymer-polymer and polymer-particle needs to be balanced in order to achieve good dispersion and avoid clustering of particles in the polymer composites (Alam *et al.*, 2007).

Recent literatures suggest that different kinds of magnetic nanoparticles are being used as a core or template for the synthesis of electrically active magnetic polyaniline nanostructures. Table 2-2 shows a brief review of electrically active magnetic polyaniline nanostructures available in the literature. The size range of the synthesized nanostructures varies from 30 nm to 5 μm and their magnetization values are in between 0.76 and 181 emug^{-1}.

Table 2-2. Review of electrically-active magnetic polyaniline nanostructures.

Dopant	Core/Template	Dimension (nm)	Magnetization (emu/g)	Reference
β-NSA	Hydroxyl iron (FeOH)	500-5000	180.4	(Li et al., 2007b)
HCl	Iron (II, III) oxide (Fe_3O_4)	70-100	4.22-48.4	(Deng et al., 2003)
Toluene	Iron (III) oxide (γ-Fe_2O_3)	~	50.0-60.0	(Dallas et al., 2006)
H_3PO_4	γ-Fe_2O_3, Fe_3O_4	Dia: 40-80, Length: 500-600	6.0-16.0	(Zhang et al., 2005b)
DBSA	Iron nanoparticles (Fe)	~	32.0-78.0	(Xue et al., 2006)
HCl	NiZnFerrite ($Ni_{0.5}Zn_{0.5}Fe_2O_4$)	30-50	0.76-5.71	(Li et al., 2006)
HCl	LiNiFerrite($LiNi_{0.5}La_{0.02}Fe_{1.98}O_4$)	Core: 30-50, Shell: 10-20	~	(Jiang et al., 2006)
$FeCl_3$	CoFerrite ($CoFe_2O_4$)	Dia: 15, Core: 100-200	10.0-50.0	(Ding et al., 2008)
HCl	Silica@Fe_3O_4	Core: 10, Shell: 2-4	1.0-4.0	(Park and Chang, 2007)
HCl	Bismuth Ferrite ($BiFeO_3$)	~	0.44	(Prabhakaran and Hemalatha, 2008)
Sulfate	Fe_3O_4	~	2.87-8.19	(Reddy et al., 2007)
KOH	Fe_3O_4	~	10.0	(Wan and Li, 1998)

(NSA = Naphthalene sulfonic acid, HCl = Hydrochloric acid, H_3PO_4 = Phosphoric acid, DBSA = Dodecylbenzylsulfonic acid, $FeCl_3$ = Iron (III) chloride, KOH = Potassium hydroxide)

2.4.5 Polyaniline in Biosensor Applications

Conducting polymers such as polyaniline have gained popularity in biosensor applications due to the following reasons:

- Flexible chemical structure that allows modulation of the required electronic and mechanical properties of the polymer.

- Suitable immobilization matrix for biomolecules providing suitable environment for the immobilization.

- Associated with efficient transfer of electric charge produced by biochemical reaction to electronic circuits.

- Can be deposited onto electrode surfaces which provide them with the versatility of being used in diverse biosensor platforms.

- Control over parameters such as polymer layer thickness, electrical properties and bio-reagent loading.

Langer *et al.* have developed an enzyme based biosensor for detection of the amino alcohol, choline, using nanostructured polyaniline layers of controlled porosity and micrometer or nanometer thickness (Langer *et al.*, 2004). The enzyme choline oxidase was immobilized in the nanoporous polyaniline layers which were useful in trapping the enzymes due to coulombic interactions between the positively charged polyaniline and negatively charged polar groups in the enzyme molecules. The authors were able to enhance the electrical response of the biosensor by continuous charging and discharging of the polyaniline molecules in presence of the enzyme. The sensitivity of the sensor as reported by the authors was 5 μA mmol/L in the amperometric mode and 10 mV mmol/L

in the potentiometric mode, with the detection limit being 20 mmol/L for choline in the potentiometric mode.

An antibody based polyaniline biosensor was developed by Muhammad-Tahir *et al.* for detection of the bovine viral diarrhea virus using indium tin oxide (ITO) as the platform (Tahir *et al.*, 2007). The ITO glass was spin coated with self-doped polyaniline which served as a matrix for immobilization of antibodies specific to the virus. The antibody modified electrodes were then treated with 1 ml of the viral culture for 30 min. The detection process involved measurement of the amperometric response of the antibody modified polyaniline spin coated ITO electrodes before and after treatment with the viral culture in a three electrode electrochemical cell.

Malhotra and coworkers have reported polyaniline based nucleic acid sensors for detection of *E. coli* and *Mycobacterium tuberculosis* genomic DNA. Avidin modified polyaniline was electrochemically deposited on a Pt disk electrode and immobilized with biotin labeled *E. coli* probes (Prabhakar *et al.*, 2008;Arora *et al.*, 2007). Direct detection of *E. coli* was performed using differential pulse voltammetric technique in the presence of methylene blue as DNA hybridization indicator. The authors were able to detect 0.01 ng/μL of *E. coli* genomic DNA and 11 *E. coli* cells/mL within 60s to 14 min. Detection of *M. tuberculosis* genomic DNA was achieved by the same authors using polyaniline modified gold electrodes and PNA as the bio-recognition element. The authors reported a detection limit of 0.125×10^{-18}M in a 5 min sonicated *M. tuberculosis* genomic DNA within 1 min of hybridization time.

Polyaniline has been used in numerous biosensing applications, viz, amperometric, potentiometric, conductometric, optical, calorimetric and piezoelectric biosensors.

Different biomolecules ranging from enzymes, microorganisms, and antibodies to nucleic acids have been employed in the polyaniline based biosensors. Detailed information on the different polyaniline and conducting polymer based biosensors can be found in review articles by Wei *et al.*, Malhotra *et al.*, and Gerard *et al.* (Wei and Ivaska, 2006;Malhotra *et al.*, 2006;Gerard *et al.*, 2002).

CHAPTER 3: RESEARCH HIGHLIGHTS

3.1 RESEARCH NOVELTY

The innovativeness of this research lies in exploring the prospect of a novel nanostructured material (electrically active magnetic polyaniline, EAPM, nanoparticles) in the dual function of a magnetic concentrator as well as a biosensor transducer. The dual potential of this novel nanomaterial was exploited in the development of a nano-biosensor for food safety and biodefense. The versatility of the nanomaterial was demonstrated in both antibody based and DNA based biosensor detection systems. The nanobiosensor described in this study is novel in terms of design and application. Current literature shows a considerable amount of research on polyaniline and magnetic polyaniline synthesis. A sizeable number of applications can be found in the use of polyaniline transducers in biosensors as well. Extensive literature is also available in magnetic concentration procedures using different micro- and nano- magnetic particles. However, till date no literature has been reported that employ EAPM nanoparticles in an integrated design of biosensor transduction and magnetic concentration in one system. Table 3-1 demonstrates the novelty of this research in contrast to existing literature. The shaded regions indicate the absence of any current literature in these areas and the contribution of this research to the knowledge base at this point of time.

Table 3-1. Novelty of research as compared to existing literature

Parameters	Current literature	Comments
Polyaniline synthesis	(Li *et al.*, 2007a)	One dimensional nanostructures, vanadic acid oxidant, size-10/50 nm
Polyaniline based antibody biosensor	(Sai *et al.*, 2006)	Piezoelectric immunosensor, IgG detection
Polyaniline based DNA biosensor	(Chang *et al.*, 2007a)	Alumina electrode, electrochemical detection of synthetic oligos
Electrically active magnetic polyaniline (EAPM) synthesis	(Li *et al.*, 2007b)	Polyaniline-hydroxyl iron, diameter: 0.5-5 µm
EAPM based antibody biosensor		
EAPM based DNA biosensor		
EAPM nanoparticles as redox indicators in DNA detection		
Magnetic particles as cell concentrator in biosensor	(Yang and Li, 2006)	Impedance detection of *Salmonella*, Dynabeads®, diameter-2.8 µm
Magnetic particles as DNA concentrator in biosensor	(Yeung and Hsing, 2006)	Electrochemical detection of *E. coli*, commercial beads, diameter-3 µm
EAPM as cell concentrator		
EAPM as DNA concentrator		

3.2   RESEARCH SIGNIFICANCE

Electrically active polyaniline coated magnetic (EAPM) nanoparticles couple the flexibility of the conducting polymer, in terms of its chemical, electrical and mechanical properties, with the magnetic properties of the core material, iron oxide. EAPM nanoparticles when adopted in biosensors are expected to provide several advantages in detection. The nanoscale dimensions of the EAPMs will impart an increased surface to volume ratio for biological events to occur. Appropriate biological surface modification of the EAPMs can bring them in close proximity to targets for achieving fast assay kinetics, e.g., rapid antigen-antibody interactions. In addition, magnetic manipulation of the EAPMs can minimize matrix interference due to improved separation thus avoiding pre-enrichment and pre-treatment procedures commonly practiced in food and environmental samples. Hence, magnetic manipulation will be advantageous in reducing sample processing time and background signal in detection devices. Furthermore, the electrical, electrochemical, and magnetic properties of the EAPMs will present multiple options in designing biosensor platforms. The compatibility of the polymer surfaces in EAPMs with biomodification procedures will add to the versatility of these biosensor platforms.

As described above, EAPM nanoparticles hold great promise in future biosensing applications. The current research developed an antibody based and a DNA based EAPM biosensor with high sensitivity and specificity and rapid detection time. Two different biosensor platforms involving different transducing mechanisms were examined.

72

3.3 HYPOTHESIS

This research was based on the following hypothesis:

- Electrically-active polyaniline coated magnetic (EAPM) nanoparticles can be synthesized and modified with different biological detecting elements such as antibodies and DNA.

- The magnetic properties of the EAPM nanoparticles will concentrate biological targets such as whole cells and DNA.

- The electrical properties of the EAPM nanoparticles can be exploited in different biosensor transducing mechanisms to report a biodetection event.

- The dual function of the EAPM nanoparticles can be demonstrated using *B. anthracis* as the model pathogen

3.4 RESEARCH OBJECTIVES

The specific objectives of this research are as follows:

<u>Objective 1</u>: Synthesis and characterization of EAPM nanoparticles.

<u>Objective 2</u>: Design and fabrication of an EAPM based immunosensor for detection of *B. anthracis* spores.

<u>Objective 3</u>: Evaluation of sensitivity and specificity of the EAPM based immunosensor and determination of EAPM immunomagnetic capture efficiency

<u>Objective 4</u>: Fabrication of an EAPM based electrochemical DNA biosensor for detection of *B. anthracis*.

<u>Objective 5</u>: DNA hybridization on EAPM NPs and sensitivity and specificity evaluation of the EAPM based electrochemical DNA biosensor.

CHAPTER 4: RESEARCH MATERIALS & METHODS

4.1 OBJECTIVE 1

Synthesis and characterization of electrically active polyaniline coated magnetic (EAPM) nanoparticles (NPs)

This objective was aimed at synthesizing the EAPM NPs following a chemical synthesis procedure and performing magnetic, electrical, and structural characterization studies of the NPs for assessing their suitability and applicability prior to developing the biosensors.

4.1.1 EAPM Nanoparticle Synthesis

The EAPM NPs were synthesized from aniline monomer made electrically active by acid doping and gamma iron (III) oxide (γ-Fe_2O_3) NPs (Sharma *et al.*, 2005). The γ-Fe_2O_3 NPs were obtained from a commercial source (Sigma-Aldrich, MO). These NPs were dispersed in a mixture of 50 ml 1M HCl, 10 ml de-ionized water and 0.4ml of aniline by sonication for 1h at 0°C to disintegrate the agglomerated nanoparticles. This was followed by a slow drop-wise addition of the oxidant, ammonium persulfate, at a rate of 0.1 ml/min with continuous stirring of the above solution mixture which resulted in coating of polyaniline on the smaller γ-Fe_2O_3 NPs. The above reaction was continued for an additional 4 h in an ice bath and the final product was filtered followed by subsequent washings with 1M HCl, methanol and diethyl ether. The product obtained was dried for 48 h at room temperature. Four different weight ratios of γ-Fe_2O_3: aniline monomer (1:0.1, 1:0.4, 1:0.6, and 1:0.8) was maintained in the synthesis procedure (from literature) with increasing concentrations of the monomer.
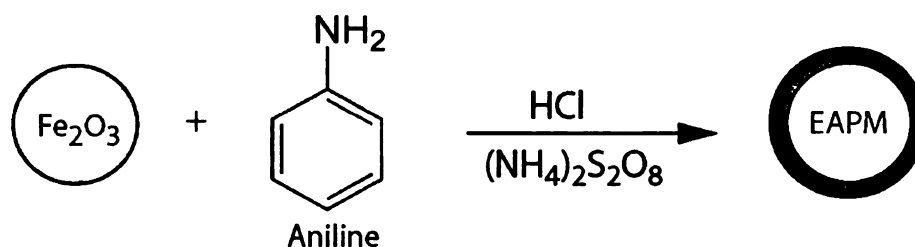
Figure 4-1. Schematic representation of polyaniline coating of gamma-iron oxide nanoparticles.

4.1.2 EAPM Nanoparticle Characterization

4.1.2.1 Magnetic Characterization

A superconducting quantum interference device (Quantum Design MPMS SQUID) was used for magnetic characterization and room temperature hysteresis measurements of the synthesized EAPM NPs. The M-H hysteresis loop measurements for the four different EAPM samples (1:0.1, 1:0.4, 1:0.6, and 1:0.8) were performed at a constant temperature of 300K with the magnetic field cycling between + 20 kOe and -20kOe. The saturation magnetization (M_S) values of the EAPM NPs were determined in emu/gm and were compared with that of bare γ-Fe$_2$O$_3$ NPs. The coercivity (H_C) and retentivity (M_R) of the NPs were also determined from the hysteresis loop measurements in order to study the presence of super paramagnetic behavior in these samples. Zero field cooled-field cooled (ZFC-FC) measurements were performed for the 1:0.6 EAPM NPs for a temperature range of 5K to 300K at an applied magnetic field of 100 Oe in order to determine the blocking temperatures of the EAPM NPs.

4.1.2.2 Electrical Characterization

The electrical conductivity of the four different EAPM samples (1:0.1, 1:0.4, 1:0.6, and 1:0.8) was evaluated in the solid form. Approximately, 0.25 gm of each sample was

compressed into pellets of 1.5 to 2 mm thickness using a hydraulic press (Fisher Scientific, NJ) and applying a pressure of about 10,000 psi. Room temperature electrical conductivity of the compressed pellets was then measured using a Four Point Probe (Lucas/Signaton Corporation, Pro4, CA).

4.1.2.3 Structural Characterization

The structural morphology of the four types of EAPM NPs were analyzed using both transmission electron microscope (TEM, Japan Electron Optics Laboratories, JEOL 100CX II) and scanning electron microscope (SEM, JEOL 6400V). The crystalline nature of the EAPM NPs was studied by selected area electron diffraction using the 200kV JEOL 2200 field emission TEM. In order to confirm the presence of the polymer, elemental analysis of the EAPM NPs was performed by X-ray energy dispersive spectroscopy using the JEOL 6400 SEM at an accelerating voltage of 20 kV and a working distance of 15 mm.

4.1.2.4 Spectral Analysis

The UV-visible spectra of the four different EAPM samples were obtained using a UV-VIS-NIR Scanning spectrophotometer (UV-3101PC, Shimadzu, Kyoto, Japan). The EAPM NPs were at first dispersed in de-ionized water at a concentration of 1 mg/ml by sonication for 10 min. 1 ml of the nanoparticle suspension was transferred into a quartz cuvet (10 mm path length) and the absorbance was measured by the scanning the sample for a wavelength range of 300 to 1000 nm using a step size of 1 nm.

4.2 OBJECTIVE 2

Design and fabrication of an EAPM NP based immunosensor for the detection of *B. anthracis* spores.

This objective was aimed at designing and constructing an antibody based biosensor detection system using EAPM NPs as magnetic concentrator and biosensor transducer for the rapid detection of *B. anthracis* (Sterne) spores as a model pathogen.

4.2.1 Biosensor Design and Data Collection

The biosensor was comprised of three distinct membrane pads: sample application pad, capture pad, and absorption pad. The dimensions of the overall as well as different biosensor zones are presented in Table 4-1. The membrane pads were arranged on a polystyrene adhesive backing with silver electrodes fabricated 0.5 mm apart on the capture membrane. The application and the absorption pads were made of cellulose membranes with a flow rate 180 ml/min and the capture pad was made of nitrocellulose membrane with a flow rate of flow rate 135 sec/4cm according to the manufacturer's specification (Millipore, Bedford, MA). For data collection, the fabricated biosensor unit was attached to an etched copper printed circuit board (PCB) and connected to a portable multimeter [BK Precision, Model 390A, range: 400Ω - $40M\Omega$, resolution: 0.1Ω – 10k Ω, accuracy: ± (0.5 to 1.5% rdg + 4 digits), sampling rate: 2 measurements per second] with RS-232 interface to a computer. The biosensor architecture and the data collection system are shown in Figure 4-2 along with a picture of the setup.
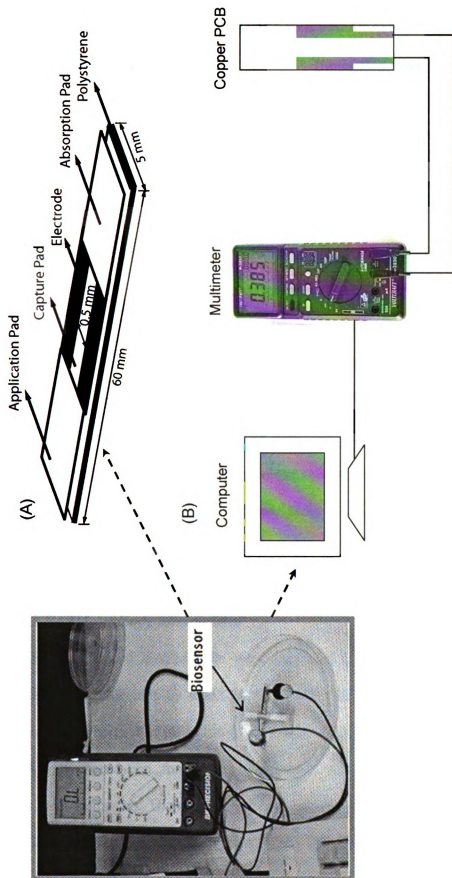
Figure 4-2. Schematic of (A) EAPM based immunosensor architecture and (B) data collection system for detection of *B. anthracis* spores.

Table 4-1. Dimensions of the EAPM based immunosensor.

Biosensor Zone	Dimension (mm)
Application	20 × 5
Capture	23 × 5
Absorption	17 × 5
Overall	60 × 5

4.2.2 EAPM Based Immunosensor Fabrication

4.2.2.1 Chemicals and Reagents

Tris-HCl buffer, glutaraldehyde, polysorbate 20 (Tween 20), peptone water, and sodium phosphate (dibasic and monobasic) were purchased from Sigma-Aldrich (St. Louis, MO). Mouse monoclonal anti-anthrax IgG (clone 2C3) and polyclonal goat anti-anthrax combo IgG molecules were obtained from Chemicon International (Millipore, CA) whereas anti-goat IgG-FITC (whole molecule) was obtained from Sigma- Aldrich (St. Louis, MO). Nitrocellulose and cellulose acetate membrane pads for the biosensor were purchased from Millipore (Bedford, MA). Conductive micro tip pen used for dispensing silver electrodes were procured from Chemtronics (Kennesaw, GA). De-ionized water from Millipore Direct-Q system was used for preparing all reagents.

4.2.2.2 EAPM Antibody Modification

The synthesized EAPM NPs were conjugated with mouse monoclonal anti-*B. anthracis* IgG molecules by direct physical adsorption of the antibodies onto the NPs (Figure 4-3). The EAPM NPs (100 mg/ml) were dispersed in 100 mM phosphate buffer (pH-7.4) by sonication for 10 to 20 min and mixed with anti- *B. anthracis* IgG (150μg/ml) antibodies. The reaction mixture was incubated for 1 h at 25°C in a rotational hybridization oven (Amerex Instruments Inc., CA). After incubation, the IgG labeled

NPs (immuno-EAPMs) were magnetically separated to remove the supernatant using a magnetic separator (Spherotech, IL). The resulting immuno-EAPMs were washed three times with a blocking buffer consisting of 100 mM Tris-HCl buffer (pH-7.6) and 0.1% (w/v) casein. Finally, the immuno-EAPMs were suspended in 100 mM phosphate buffer (ph-7.4) and stored at 4°C.
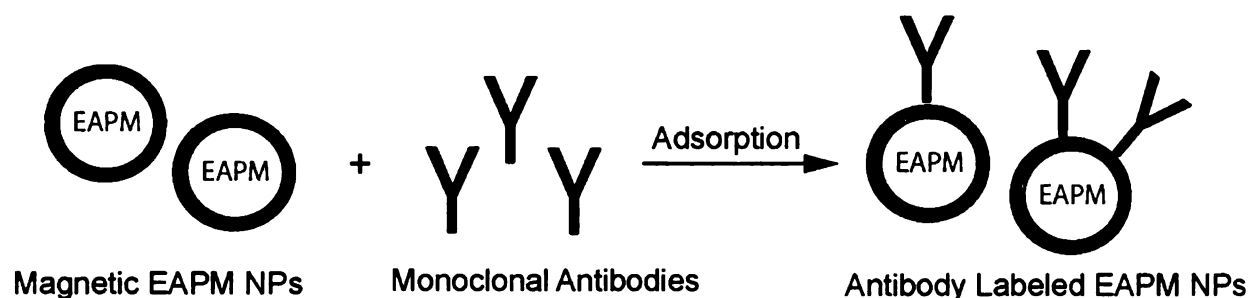
Figure 4-3. Modification of EAPM NPs with monoclonal antibodies.

4.2.2.3 Biosensor Capture Pad Functionalization

Figure 4-4 illustrates the functionalization of the biosensor capture pad for polyclonal antibody attachment. The nitrocellulose biosensor capture membrane pads were first cleaned with de-ionized water followed by 10% methanol (v/v) for 45 min and dried at room temperature. The cleaned membranes were treated with 0.5 % glutaraldehyde solution (v/v) for 1 h and dried at room temperature. After drying, the glutaraldehyde activated capture membranes were coated with polyclonal goat anti-*B. anthracis* IgG (500μg/ml) using a reagent dispensing module (Matrix 1600, Kinematic Automation Inc., CA) and incubated for 1 h at 37°C. Finally, the membrane surface was washed with blocking buffer consisting of 100 mM Tris-HCl (pH-7.6) and 0.1% (v/v) Tween 20 and incubated for 45 min at 37°C to inactivate the residual aldehyde groups.

The antibody modified membranes were dried at room temperature and stored at 4°C before use.

O=CH(CH₂)₃CH=O

Capture Pad + O=CH(CH₂)₃CH=O ⟶ Functionalized Capture Pad

Glutaraldehyde
Crosslinker

Blocking ⟵ —NH=CH(CH₂)₃CH=HN— ⟵ —NH₂ —NH₂

Antibody Attachment   Polyclonal Antibodies
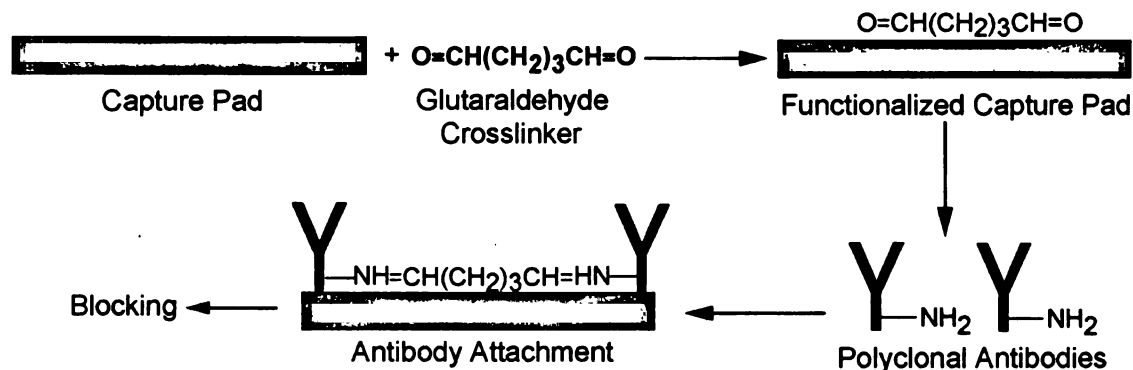
Figure 4-4. Functionalization of biosensor capture pad for attachment of polyclonal antibodies.

4.2.2.4 Application and Absorption Pad Preparation

The application and the absorption cellulose membrane pads of the biosensor were washed with de-ionized water to remove dirt and surface residues. The membranes were then air-dried and stored in a clean container before being assembled into the biosensor.

4.2.2.5 Sensor Assembly

The application, capture and the absorption pads after preparation were assembled according to the arrangement as shown in Figure 4-2 (A) with the membrane pads overlapping one another. After assembly, the biosensors were cut into 5 mm strips using a programmable shear module (Matrix 2360, Kinematics Automation Inc. CA, USA). Silver electrodes were fabricated on the capture membrane surface at 0.5 mm distances apart using silver conductive ink (Chemtronics, GA) and the biosensor strips were connected to the data acquisition systems as described as shown in Figure 4-2 (B).

4.2.2.6 Antibody Attachment Confirmation Studies

The antibody modification of the EAPM NPs was confirmed and investigated by measuring the absorption of IgG molecules using a UV-VIS-NIR Scanning Spectrophotometer (UV-3101PC, Shimadzu, Kyoto, Japan). The UV spectrum of pure anti- *B. anthracis* IgG (150μg/ml) molecules and that of the unreacted IgG molecules present in the supernatant after magnetic separation of the immuno-EAPMs was studied by scanning the samples for a wavelength range of 200 nm to 400 nm using a resolution of 1.0 nm. The attachment of polyclonal anti- *B. anthracis* IgG molecules on the biosensor capture pad was confirmed by a Laser Scanning Confocal Microscope (Olympus Fluoview 1000). The antibody modified biosensor capture pad was labeled with secondary anti-goat IgG-FITC molecules using a working dilution of 1:320. Fluorescence was observed by excitation with 488-nm line of argon-ion laser and detection of emission using a 505 nm long pass filter.

4.3 OBJECTIVE 3

Evaluation of sensitivity and specificity of the EAPM NP based immunosensor and determination of EAPM immunomagnetic capture efficiency.

This objective was aimed at determining the sensitivity of the fabricated EAPM based immunosensor in pure suspensions of *B. anthracis* spores and artificially contaminated food matrices, determining the immunosensor specificity in non-target bacterial cultures, and in determining the capture efficiency of EAPM NPs in immunomagnetic concentration procedures.

4.3.1 Bacterial Culture and Plating

Characterized strains of *Bacillus anthracis* (Sterne) and *Bacillus cereus* were obtained from the Michigan Department of Community Health (Lansing, MI) for performing sensitivity studies with the immunosensor. Generic *E. coli* and *Salmonella enterica* Serovar Enteritidis (S-64) strains from the collection of the Biosensors Laboratory were used for specificity experiments. The *Bacillus* strains and generic *E. coli* were grown in trypticase soy broth (TSB, Difco) while lactose broth (Difco) was used for growing *Salmonella* Enteritidis. The cultures were grown in an incubator (Fisher Scientific, IA) at 37°C for 24 h and were enumerated by spiral plating in the appropriate plating media followed by colony counting after 24 and 48h. Both the plating and colony counting were performed using automated equipments (Microbiology International, MD, USA).

4.3.1.1 B. anthracis Sporulation Protocol

Sporulation of *B. anthracis* (Sterne) cells was promoted following a previously published protocol (Pezard *et al.*, 1991). *B. anthracis* vegetative cells from a 24 h enrichment culture were streaked on Nutrient Yeast Broth (NYB) agar slopes and incubated at 30°C for seven days. Sporulation was monitored by Schaeffer-Fulton staining and light microscopy. Once the sporulation was greater than 90%, the spores were harvested by suspending them in 5 ml sterile de-ionized water and incubating at 65°C in waterbath for 30 min to kill the remaining vegetative cells. The spores were collected by centrifugation at 12000 rpm for 3 min, and re-suspended in 5ml of sterile de-ionized water. Finally, the total spore count was estimated using a disposable hemocytometer (C-Chip DHC-NO1, Fisher Scientific, Pittsburg, PA) and the viable

spores were enumerated by microbial plating in trypticase soy agar (TSA II) with 5% sheep blood plates (BD Biosciences, MD) and counting the colonies after 16 and 36h. The spore suspension was stored at 4°C for future use.

4.3.2 Immunomagnetic Concentration using EAPM NPs

Following the antibody modification procedure, the antibody coated EAPM NPs (immuno-EAPMs) were added to different concentrations of *B. anthracis* spore suspensions (10^1 to 10^7 spores/ml) in order to have a final immuno-EAPM concentration of 20 mg/ml. The amount of EAPM NPs to be used in the immunomagnetic concentration procedure was determined from prior studies with *B. cereus* as target pathogen. The mixture was incubated with gentle shaking in a hybridization oven (Boekel Scientific, PA) for 10 min at room temperature. The immuno-EAPM-spore complexes formed were magnetically separated from the unbound spores, to remove the supernatant and washed twice with sterile de-ionized water before re-suspending in 10 ml sterile de-ionized water.

4.3.3 Biosensor Testing

One hundred microliters of the immuno-EAPM-spore complexes obtained after immunomagnetic concentration was applied carefully to the application pad of the biosensor. The flow time of the sample from the application pad to the capture pad was approximately 1 min. Recording of the resistance signal across the biosensor electrodes was started from 2 min and carried for a total time of 6 min as determined from prior studies (Pal *et al.*, 2007). Resistance measurements were also made before applying the sample to the biosensor to ensure that the biosensor strips were not conductive before sample application. Three trials were performed for each set of experiments. All

biosensor testing were performed inside a Class II Biosafety Cabinet (Model 1284, ThermoElectron Corporation, OH).

4.3.4 Biosensor Sensitivity Study

Pure spore suspension of *B. anthracis* was used to assess the sensitivity of the EAPM biosensor. The *B. anthracis* spores stock solution was serially diluted to spore concentrations ranging from 10^0 to 10^7 spores/ml. The performance of the four different EAPM samples (1:0.1, 1:0.4, 1:0.6 and 1:0.8) was evaluated in the detection of *B. anthracis* spores prior to choosing the best nanoparticle type for the sensitivity analysis. Three different spore concentrations (10^1, 10^4 and 10^7 per ml) were used in this comparison study. The biosensor sensitivity was then determined using the EAPM NPs that showed the best biosensor performance in the above study in spore concentrations ranging from 10^0 to 10^7 per ml. All biosensors were baselined against a negative control solution containing EAPM nanoparticles in sterile water (concentration-20 mg/ml).

4.3.5 Biosensor Specificity Analysis

Pure cultures of generic *E. coli* and *S.* Enteritidis were used for determining the specificity of the EAPM biosensor. Twenty four hour enrichment cultures of generic *E. coli* and *S.* Enteritidis were serially diluted to cell concentrations ranging from 10^1 to 10^5 CFU/ml using sterile 0.1 % (w/v) peptone water. The immuno-EAPMs were added to appropriate cell concentrations of the desired bacteria to obtain a final immuno-EAPM concentration of 20mg/ml. The immunomagnetic concentration and biosensor detection procedure was similar to that as described in Sections 4.3.2 and 4.3.3. The resistance signal generated was compared statistically with positive and negative control samples of *B. anthracis* spores to evaluate the biosensor specificity.

4.3.6 Biosensor Testing in Food Matrices

The efficiency of the EAPM biosensor was tested in three different food matrices. Romaine lettuce, lean ground beef, and ultra-pasteurized whole milk, was purchased from a local grocery store. For the lettuce and beef samples, 25-g samples were weighed, mixed with 225 ml of 0.1% (w/v) peptone water in a Whirl-Pak plastic bag, and stomached in a stomacher (Microbiology International, MD) for 1 minute. The whole milk sample was used as purchased. Nine milliliters of the three kinds of liquid samples were thoroughly mixed with 1 ml of appropriate concentrations of *B. anthracis* spore stock solution. Finally, a series of 10 ml samples inoculated with *B. anthracis* spores at concentrations ranging from 10^1 to 10^7 spores/ml were obtained.

Following the food sample preparation, immuno-EAPMs (20 mg/ml) were mixed with different concentrations of the *B. anthracis* spore inoculated food matrices. Immunomagnetic concentration of *B. anthracis* spores from the food matrices and biosensor testing was performed according to the procedure described in Section 4.3.2 and 4.3.3. EAPM NPs suspended in the liquid samples (20 mg/ml) obtained from the three different food matrices without inoculated *B. anthracis* spores was used as a negative control.

4.3.7 Statistical Analysis

Statistical analysis of the biosensor data was performed using the SAS software (SAS, Cary, NC). The means and standard deviations of the biosensor resistance signals for all samples were calculated on the basis of data from three replicates and the differences between the means were compared using analysis of variance (ANOVA) to a significance of 95% (α =0.05). Factorial ANOVA analysis (Two-way ANOVA with

slicing of interactions) was performed to determine the interactive effects of EAPM NP type and spore concentration as well as the double interaction of both factors on the biosensor resistance responses in the EAPM comparison study. For sensitivity study, the two-way interaction of spore concentration and time was analyzed. For specificity analysis, interactive effects of different pathogen types, cell concentrations as well as combined effect of both factors were studied using two-way ANOVA. Single factor analysis of variance was performed on the food sample data.

4.3.8 Confirmation and EAPM Capture Efficiency Calculations

The immunomagnetic capture of *B. anthracis* spores using EAPM nanoparticles from pure spore suspension and different food matrices was confirmed by microbial plating in TSA II blood agar plates. One hundred microliters of the immuno-EAPM-spore complexes obtained after immunomagnetic concentration was used for plating. Triplets of each sample were plated. The viable spore count was enumerated after 16 to 36h. The capture efficiency (CE) of the EAPM nanoparticles was calculated using the equation:

$$CE\,(\%) = \frac{C_b}{C_t} \times 100$$

where, C_t is total concentration of viable spores in the sample (CFU/ml), and C_b is the concentration of viable spores bound to the EAPM nanoparticles (CFU/ml).

4.4   OBJECTIVE 4

Fabrication of an EAPM based electrochemical DNA biosensor for detection of *B. anthracis*.

This objective was aimed at developing an electrochemical DNA biosensor system using EAPM NPs for target DNA concentration as well as biosensor transduction for the detection of *Bacillus anthracis* protective antigen (*pagA*) gene.

4.4.1   Biosensor Design and Data Collection

A screen printed three electrode sensor (Gwent Group, UK) was used in the electrochemical detection of DNA targets. The sensor chip had an overall dimension of 22 × 12 mm with a circular working electrode of 4 mm diameter and a partially circular (270°) common reference and counter electrode of 1.5 mm width. Screen printed carbon acted as the working electrode while screen printed silver/silver chloride (Ag/AgCl) acted as the common reference and counter electrode on a polyester backing. The screen printed carbon and silver ink had a resistance of 50 Ohms at 12 microns, and 320 mOhms at 25 microns, respectively, according to the manufacturer's specifications. Figure 4-5 shows the architecture of the screen printed carbon electrode (SPCE) biosensor. For data collection, the SPCE biosensor units were connected to a Potentiostat/ Galvanostat (Model 263A, Princeton Applied Research, OakRidge, TN).
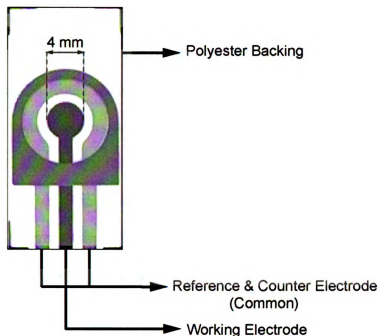
Figure 4-5. Screen printed carbon electrode biosensor.

4.4.2 Chemicals and Reagents

Sodium chloride (NaCl), sodium phosphate (monobasic and dibasic), sodium acetate, phosphate buffered saline tablets (0.01M), formamide, ethylene diamine tetra acetic acid (EDTA), isopropanol, ethanol, sodium dodecyl sulfate (SDS), proteinase K, hydrochloric acid (HCl), Trizma base, ethidium bromide, gel loading solution and Streptavidin from *Streptomyces avidinii* were purchased from Sigma Aldrich (St Loius, MS). AccuPrime[TM] *Taq* DNA Polymerase system, Ultrapure[TM] DNAse RNAse free water and Ultrapure[TM] agarose were purchased from Invitrogen Corporation (Carlsbad, CA). QIAquick PCR purification kit was procured from Qiagen Inc. Valencia, CA. EDC (1-ethyl-3-[3-dimethylaminopropyl] carbodiimide hydrochloride) was obtained from Pierce (Rockford, IL).

4.4.3   Selection and Analysis of DNA Primers and Probes

The primers pairs for PCR, and the capture and detector probes for the biosensor, were designed and selected from the protective antigen (*pag A*) gene, while the non-complementary sequence was selected from the capsular (*cap A*) gene of *Bacillus anthracis* (Song *et al.*, 2005). Detailed information on the sequences of the probes and the primer pairs has been shown in Table 4-2. The specificity of the primer and the probe sequences were analyzed using the Basic Local Alignment Search Tool (BLAST).

4.4.4   Extraction, Amplification and Characterization of *B. anthracis* DNA

4.4.4.1 DNA Extraction

Genomic DNA was extracted from a 24 h enrichment culture of *B. anthracis* using a modified protocol for mammalian DNA extraction (Laird *et al.*, 1991). One ml of the overnight culture was transferred into a 1.5 ml microcentrifuge tube and centrifuged for 10 min at 13000 rpm to precipitate the DNA. The supernatant was discarded and the remaining pellet was re-suspended in 500 μl of lysis buffer (100mM Tris HCl, 5mM EDTA, 0.2% SDS, 200 mM NaCl) and 5μl of proteinase K solution. The tube was placed in a waterbath for 75 min at 55°C and then introduced in ice. Five hundred microliters of isopropanol was added to the tube and mixed, followed by freezing the tube for 30 min at - 80°C. The precipitated DNA was recovered by centrifugation for 15 min at 13000 rpm followed by addition of 500 μl of pre-cooled ethanol solution and centrifugation at 13000 rpm for 15 min. Finally, the supernatant was discarded and the pellet was dried to and resuspended in 100 μl of DNAse and RNAse free water.

Table 4-2. Sequence information of *B. anthracis* primer pairs and probes.

Name	Target Gene	Sequence (5'-3')	No. of Bases	GenBank Accession No.	Position
Forward Primer (FP)	*pag A*	5'-AAAATGGAAGAGTGAGGGTG-3'	20	M22589	3284-3303
Reverse Primer (RP)	*pag A*	5'-CCGCCTTCTACCAGATTTA-3'	20	M22589	3383-3402
Detector Probe *(Ph-PRO)	*pag A*	5'-GGAAGAGTGAGGGTGGATACAGGCTCGAACTGGAGTGAAGTGTTACCGCA-3'	50	M22589	3289-3338
Capture Probe †(PRO-Bio)	*pag A*	5'-GGAAAAGATTTAAATCTGGTAGAAAGGCGG-3'	30	M22589	3373-3402
Non-complementary Sequence (NC)	*cap A*	5'-CCGAGTCCTAGACAGGAAGCCTTAGCAAAAGCAATGGTTGATGCAGGGGC-3'	50	M24150	2719-2768

All sequences were purchased from Integrated DNA Technologies, Inc. (Coralville, IA). The RP, Ph-PRO, PRO-Bio and NC sequences were modified with 6-FAM™ labels at 5', 3', 5' and 5' positions, respectively, for fluorescence studies.

* 5'-Phosphorylation

† 3'-Biotinylation

The concentration of the extracted double stranded target DNA was determined by measuring the absorbance of the sample at 260 nm using a spectrophotometer (Bio-Rad SmartSpec 3000).

4.4.4.2 Polymerase Chain Reaction (PCR) Amplification and Optimization

Polymerase chain reaction of the extracted target DNA was performed using a DNA thermocycler (Eppendorf, Westbury, NY). The 50μl PCR reaction mixture consisted of template DNA, forward and reverse primers, PCR buffer [1X], 2'-deoxynucleoside 5'-triphospate (dNTP) mix [0.2 mM], magnesium chloride ($MgCl_2$) [1.5 mM], and 1μl of AccuPrime^{TM} *Taq* DNA Polymerase. The PCR amplification reaction was optimized with respect to the amount of DNA template, the concentration of forward and reverse primers, the melting temperature (T_m) and the reaction time in order to obtain the best amplification of targets. All PCR reactions were performed inside a PCR Workstation (Fisher Scientific, IA).

4.4.4.3 PCR Product Purification

The amplified PCR product was purified using the QIAquick PCR purification kit. Five volumes of the buffer PB was mixed with 1 volume of the PCR product. The sample was then applied to a QIAquick column that was placed in a 2 ml collection tube for binding DNA. The column was centrifuged for 60 s and the flow-through was discarded. For washing, 750 μl of the buffer PE was added to the QIAquick column, centrifuged for 60 sec, and the flow-through was discarded. The QIAquick column was then placed back in the collection tube and centrifuged for 60 sec. Finally, to elute the DNA, the QIAquick column was placed in a clean 1.5 ml microcentrifuge tube, 50 μl of DNAse RNase free water was added to the column and it was centrifuged for 60 sec.

4.4.4.4 PCR Product Characterization

The results from PCR amplification and purification were confirmed by performing gel electrophoresis in ethidium bromide stained 2.5 % agarose gels using a mini gel electrophoresis system (EmbiTec, San Diego, CA) at 50 Volts for 30 min. The amplified PCR bands were then observed in a Gel Documentation system (Fotodyne Incorporated, Hartland, WI). The concentration of the purified PCR DNA was determined using the NanoDrop^{TM}1000 spectrophotometer (ThermoScientific, Wilmington, DE). Two microliters of the DNA sample was placed in the sample holder of the spectrophotometer and the UV-VIS absorbance was measured at 260 nm.

4.4.5 EAPM-DNA Probe Labeling Study

4.4.5.1 EAPM-DNA Modification

The EAPM NPs (1:0.6) were labeled with the single stranded phosphorylated detector DNA probes (Ph-PRO) through the formation of phosphoramidate bonds between the amino groups present in the polyaniline of EAPM NPs and the phosphate group of the oligonucleotide based on a procedure previously described by (Zhu *et al.*, 2006a). The EAPM NPs were first suspended in 100 µl of the Ph-PRO probe solution [22.5 µM] containing 10 mM sodium acetate buffer (pH 5.2) and 0.1 M 1-ethyl-3-[3-dimethylaminopropyl] carbodiimide hydrochloride (EDC). The mixture was incubated with shaking in a rotational hybridization oven at room temperature for 4 h (Amerex Instruments Inc., CA). Finally, the Ph-PRO DNA probe attached EAPM NPs (PRO-EAPMs) were separated by a magnetic separator and washed repeatedly with acetate buffer and DNAse RNAse free water to remove the unbound probes. Figure 4-6 shows the cross-linking chemistry between the NPs and the detector probe.
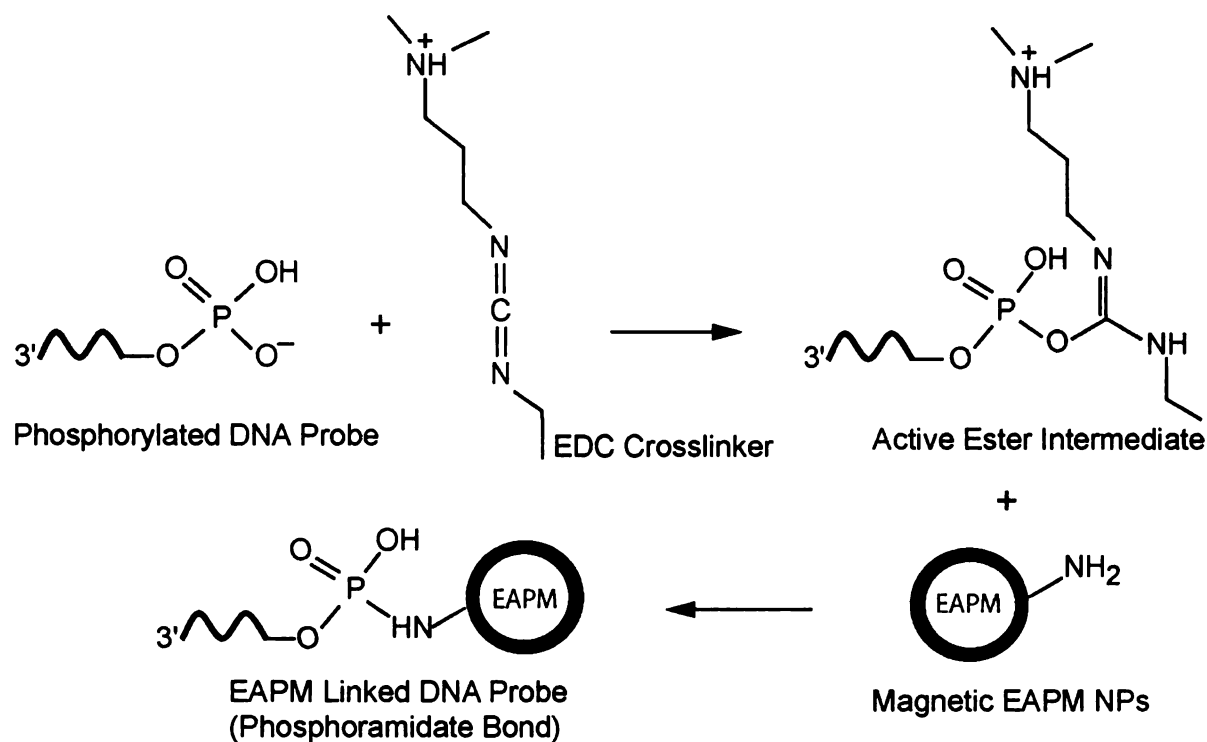
Figure 4-6. Crosslinking chemistry between the detector DNA probe and magnetic EAPM NPs.

4.4.5.2 Confirmation and Optimization

The attachment of the Ph-PRO detector probes to the EAPM NPs were confirmed by fluorescence measurements performed in a Microplate Fluorometer Reader (Victor^3, Perkin Elmer, MA) and UV-VIS absorbance measurements performed in a NanoDrop 1000 Spectrophotometer. For the fluorescence confirmatory experiment, the Ph-PRO probes were labeled with 6-carboxy flouorescein (6-FAM™) at 3' end. Fluorescence of the pure 6-FAM™ labeled Ph-PRO probe solution and that of the unreacted probes remaining in the supernatant after magnetic separation of the PRO-EAPMs was observed by excitation at 495 nm and detection of emission at 520 nm. The UV-VIS absorbance at 260 nm of the pure probe and the supernatant solution was also measured. The optimum concentration of the EAPM NPs for labeling with the Ph-PRO probes was determined

from the fluorescence and absorbance measurements by keeping the Ph-PRO probe concentration fixed at 22.5 µM and varying the NP concentrations as 0.1, 1, 10 and 20 mg/ml.

4.4.6 SPCE Surface Modification

The SPCE surface was modified with streptavidin for biosensor measurements. Forty microliters of streptavidin solution (1mg/ml) prepared in 0.1M phosphate buffer (pH-7.0) was added onto the working electrode surface and incubated for 2 h at room temperature. The electrodes were then dried for an additional 30 min and were ready for use in biosensor experiments. As a result, the working electrode surface was coated with approximately 0.8 $\mu g/mm^2$ of streptavidin.

4.5 OBJECTIVE 5

DNA hybridization on EAPM NPs and sensitivity and specificity evaluation of the EAPM based electrochemical DNA biosensor.

This objective was focused on hybridizing the amplified *B. anthracis* target gene fragment to the PRO-EAPMs for integration onto screen printed carbon electrodes for determining the sensitivity and specificity of the EAPM based electrochemical DNA biosensor.

4.5.1 Sandwiched Hybridization of DNA Targets on EAPM NPs

4.5.1.1 Sandwiched Hybridization Protocol

The PCR amplified DNA targets were hybridized dually with the detector probe labeled EAPM NPs (PRO-EAPMs) and the biotinylated capture probes (PRO-Bio) based on a hybridization protocol adapted and modified from Song *et al.* (Song *et al.*, 2006).

Before hybridization, the purified PCR product was denatured by heating at 95° for 10 min in the thermocycler and cooling in icebath for 5 min, followed by a second cycle of heating at 95° for 5 min and cooling for 5 min to separate the double stranded DNA fragments into single strands. One hundred microliters of the denatured PCR product was then diluted with 35 μl of hybridization buffer composed of 2M NaCl and 0.2M phosphate buffer (pH-7.4) and added to appropriate concentrations of the PRO-EAPMs and the PRO-Bio probes. The hybridization reaction was carried out in a hybridization oven. The EAPM-Target-Biotin DNA hybrids were then washed twice with tris ethylene diamine tetracetic acid (TE) buffer (1X, pH-7.4) for 1 min by magnetic separation of the EAPM NPs to remove the unbound target DNA. This was followed by washing the EAPM NPs with 20% formamide in 0.01M phosphate buffered saline (PBS) at 50° for 1 min by magnetic separation to remove the nonspecifically bound DNA targets. Finally, the EAPM-Target-Biotin DNA hybrids were resuspended in 40μl of DNAse RNAse free water.

4.5.1.2 Optimization of Hybridization Conditions and Confirmation

Optimization and confirmation of the hybridization conditions was performed in two steps. The first step involved hybridization of the target DNA with the PRO-EAPMs which was confirmed through fluorescence assays using the Microplate Fluorometer Reader. Fluorescence labeled PCR amplified target DNA was obtained using 5' 6-FAM labeled reverse primers in the PCR reaction. The hybridization time and temperature for the target DNA with the PRO-EAPMs was determined by observing the supernatant fluorescence after hybridization of the 6-FAM labeled PCR product with PRO-EAPMs and magnetic separation by excitation at 495 nm and measurement of emission at 520

96

nm. Three different hybridization temperatures (25°C, 45°C and 55°C) and three different hybridization times (30 min, 1h and 2h) were trialed.

The second step involved confirmation of the sandwiched hybridization of the PRO-Bio probes with the target DNA using the optimized conditions obtained from the above study through fluorescence assays. Five prime 6-FAM labeled PRO-Bio probes were used in this study. Three different concentrations of 6-FAM labeled PRO-Bio probes (1μM, 5μM and 10μM) were used to confirm the dual hybridization event by measuring the fluorescence of the pure probe solution and that of the supernatant after magnetic separation.

4.5.2 Electrochemical Detection Using SPCE Biosensor

4.5.2.1 Electrochemical Characterization of EAPM NPs

Prior to detection of the target bound EAPM NPs on the SPCE biosensor, the detection of straight EAPM NPs on the SPCE sensor surface was performed using cyclic voltammetry. One hundred microliters of EAPM NP solution (concentration -100 μg/ml) in 0.1M HCl was applied to the SPCE sensor and allowed to equilibrate for 10 min. Cyclic voltammetry was performed using a Potentiostat/Galvanostat with two vertex potentials in the ramp mode. A potential window between -0.4V and +1.0V was used. The scan rate was varied in between 20 and 200 mV/s.

4.5.2.2 Detection of EAPM-Target-Biotin DNA Hybrids

The EAPM-Target-Biotin DNA hybrids obtained after sandwiched hybridization were carefully added to the streptavidin modified working electrode surface of the SPCE biosensor. The DNA hybrids were allowed to react with the avidin coated sensor surface for 15 min at room temperature. The electrodes were then rinsed with DNAse RNAse

free water for three consecutive times to remove any unbound EAPM NPs from the surface and left to air dry for 15 min. One hundred microliters of 0.1M HCl solution was added to the SPCE surface and the electrodes were allowed to equilibrate for 5 min. Cyclic voltammetry was performed in the ramp mode with a potential window between -0.4 V and +0.1V at a scan rate of 20 mV/s. Three trials were performed for each set of experiments.

4.5.3 SPCE Biosensor Sensitivity Study

For the sensitivity study, the purified PCR products were serially diluted to concentrations ranging from 10^{-1} ng/μl to 10^{-5} ng/μl using DNAse RNAse free water. Each PCR concentration was then dually hybridized with the PRO-EAPM and the PRO-Bio probes according to the procedure described in Section 4.5.1.1. The sensitivity of the biosensor was determined by performing electrochemical detection of the hybrids obtained from the serially diluted PCR products following the procedure described in Section 4.5.2.2. A negative control consisting of EAPM NPs (concentration: 1mg/ml) suspended in DNAse RNAse free water was tested for comparison. Base line curves for bare SPCE biosensor and streptavidin modified SPCE biosensor in 0.1M HCl was obtained for each experiment.

4.5.4 Statistical Analysis

For each experiment, the cyclic voltammetry (CV) data was obtained as a current vs. potential (I vs. E) curve of 1020 pair of points, half of which corresponded to the oxidation reaction of the cycle, and the other half corresponded to the reduction reaction. The oxidation (anodic) and reduction (cathodic) peak potentials were first determined for EAPM NPs from the electrochemical characterization of the EAPM NPs. The oxidation

(anodic) and reduction (cathodic) peak currents were then determined at the corresponding peak potentials for each experimental run. For sensitivity analysis, only the anodic peak current was chosen for convenience. The means and standard deviations of the anodic peak current for all target concentrations were determined on the basis of data from three replicates and the differences between the means were compared using single factor analysis of variance (ANOVA) to a significance of 95% (α =0.05) using the SAS software.

4.5.5 Specificity Analysis

Specificity experiments for the SPCE biosensor were conducted using synthetic non-complementary (NC) DNA sequences. Dual hybridization of the NC sequences with PRO-EAPM and PRO-Bio probes were performed following the procedures described in Sections 4.5.1.1. Different concentrations of the NC sequences (1μM, 5μM, and 10μM) prepared by diluting the stock in DNAse RNAse free water. Nonspecific hybridization of the NC sequences with the PRO-EAPMs was monitored by fluorescence assays using a microplate fluorometer reader with 5' FAM labeled NC sequences. Fluorescent intensity measurements at 520 nm were compared between pure 5' FAM labeled NC sequences and the supernatant remaining after the dual hybridization event.

CHAPTER 5: RESULTS AND DISCUSSION

5.1   OBJECTIVE 1

Synthesis and characterization of electrically active polyaniline coated magnetic (EAPM) nanoparticles (NPs)

5.1.1   EAPM Nanoparticle Characterization

The change in mass magnetization (M) in the presence of a sweeping magnetic field (H) for the four different EAPM NPs (1:0.1, 1:0.4, 1:0.6, and 1:0.8) as well as the unmodified γ-Fe_2O_3 NPs is shown by the M-H hysteresis measurements performed at 300K in Figure 5-1. The key magnetic parameters are extracted from the hysteresis measurements and have been tabulated in Table 5-1. The saturation magnetization (M_S) for the unmodified γ-Fe_2O_3 NPs is found to be 64.4 emu/g, whereas for the four different EAPM NPs, the M_S values range from 61.1 to 33.5 emu/g. All five systems show a tendency to saturate at an applied field of 20 kOe. The gradual decrease in the M_S value with increase in the polymer (polyaniline) content is expected due to the surface interactions between polyaniline, which is diamagnetic in nature, and the iron oxide NPs (Alam *et al.*, 2007). As observed in Table 5-1, the coercivity (H_C) for all four EAPM NPs are the same as the unmodified Fe_2O_3 NPs i.e. 200 Oe, thus indicating that the anisotropy energy of the magnetic NPs is not affected by the presence of polyaniline (Poddar *et al.*, 2004a). The remanent magnetization (M_R) values for the NPs vary between 15.3 and 9.18 emu/g. The high H_C and finite M_R values in the EAPM NPs indicate that hysteresis is not completely absent in the NPs, thus suggesting that the NPs are still in the ferromagnetic phase (Sorensen, 2001).
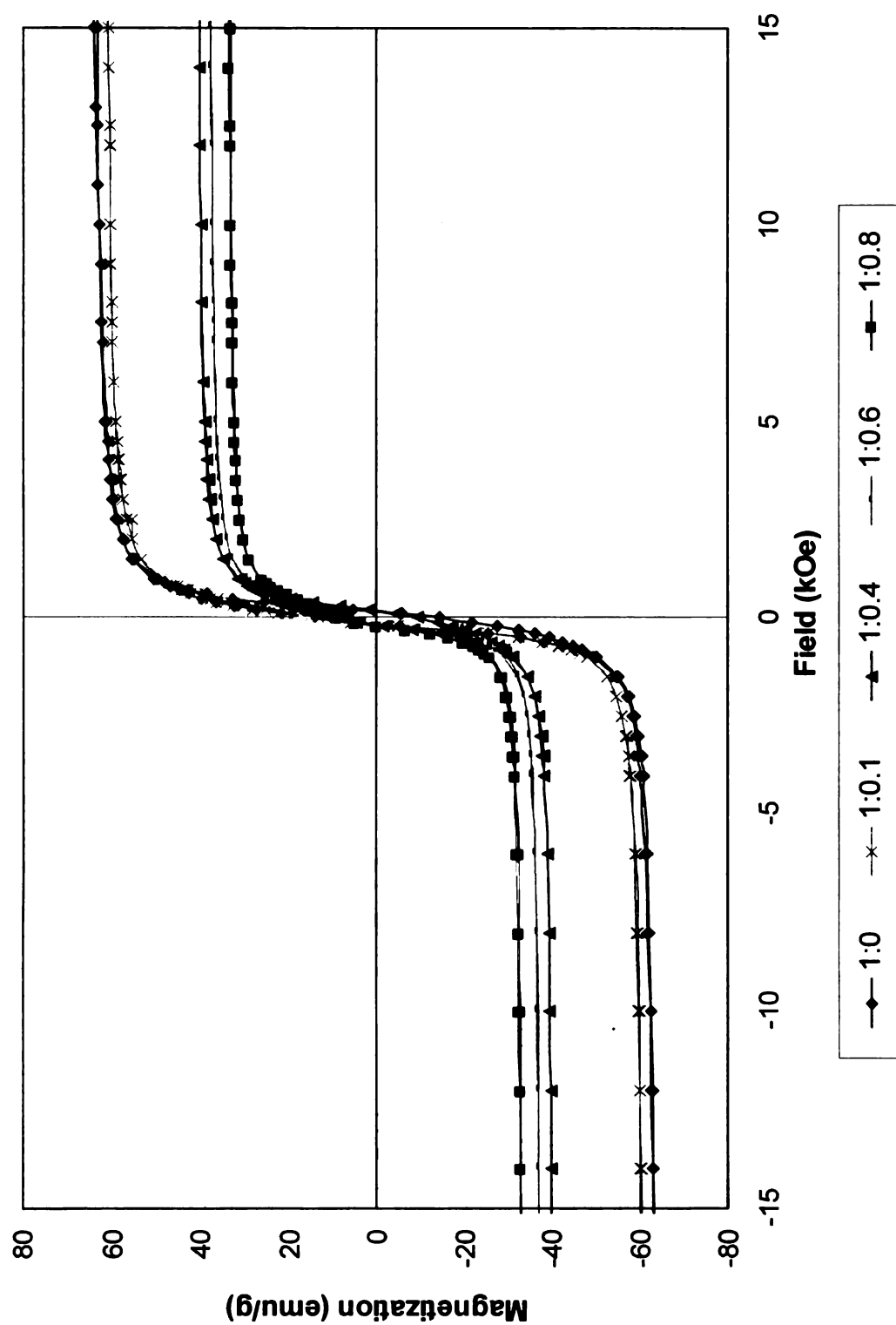
Figure 5-1. Experimental _M-H_ curves of the four different EAPM NPs and the unmodified Fe$_2$O$_3$ NPs at 300K.

101

Table 5-1. Magnetic parameters measured for the EAPM NPs.

EAPM Composition (γ-Fe$_2$O$_3$:Aniline)	Coercivity (300K) H_C (Oe)	Remanent Magnetization (300K) M_R (emu/g)	Saturation Magnetization (300K) M_S (emu/g)
1:0	200	14.4	64.4
1:0.1	200	15.3	61.1
1:0.4	200	9.57	40.3
1:0.6	200	9.48	37.7
1:0.8	200	9.18	33.5
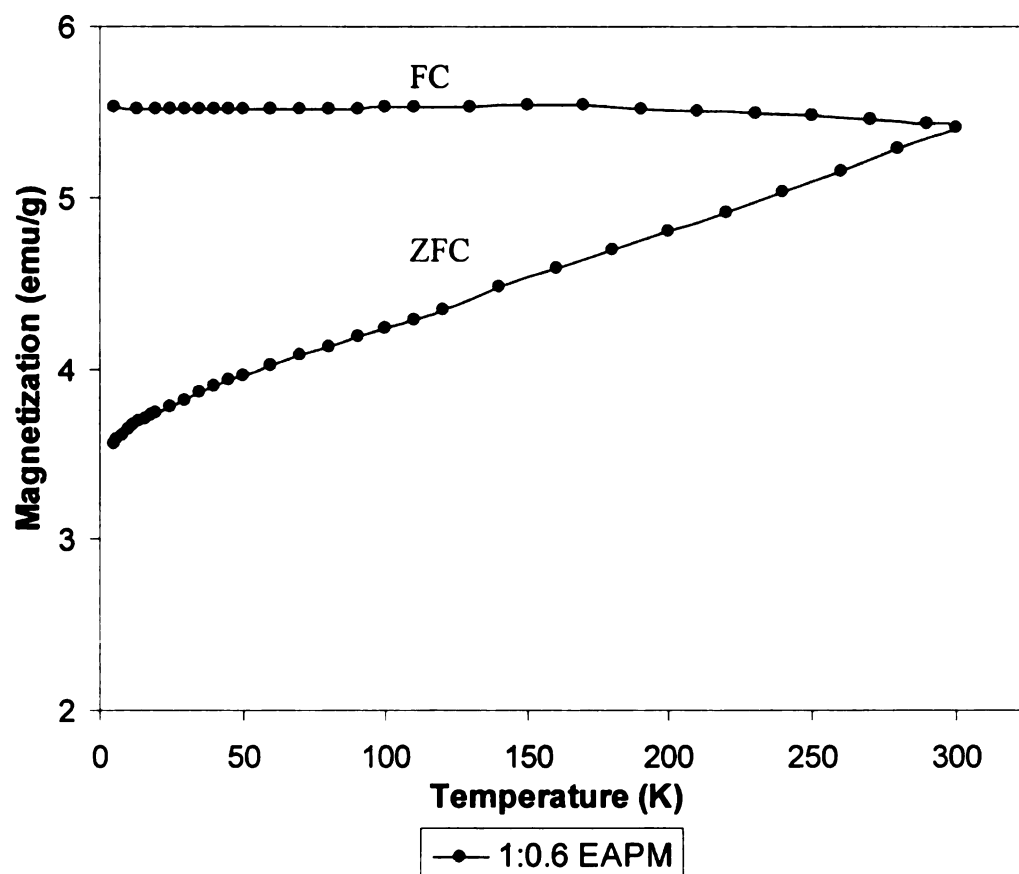
Figure 5-2. Experimental FC-ZFC magnetization curves for 1:0.6 EAPM NPs at 100 Oe.

curv

of 1

estal

abs

nan

roo

sh

lo

ha

co

co

1

is

si

sh

co

ins

ma

Figure 5-2 shows the comparison of field cooled (FC) and zero field cooled (ZFC) curves for the 1: 0.6 EAPM NPs in the temperature range of 5 to 100K at an applied field of 100 Oe. The characteristic sharp change in magnetization associated with the well established ferromagnetic to superparamagnetic transition in single domain particles is absent in the FC-ZFC curves (Sorensen, 2001). The FC-ZFC results thus indicate that the nanoparticles within the polymer matrix are predominantly in the ferromagnetic regime at room temperature and are consistent with the experimental M-H data.

Conductivity results for the unmodified γ-Fe_2O_3 and the synthesized EAPM NPs are shown in Figure 5-3 and Table 5-2. Pure iron oxide NPs have electrical conductivity as low as 10^{-5} S/cm thus exhibiting an insulating behavior. The synthesized EAPM NPs have conductivities in the range of 10^{-2} to 10^{0} S/cm. As observed in Figure 5-3, the conductivity of the EAPM NP pellets show an exponential increase in the electrical conductivity with decreasing Fe_2O_3 content from 90 wt. % to 55 wt. % in the 1:0.1 to 1:0.8 EAPM samples. The conductivity of the 1: 0.4 (71 wt. %) EAPM (7.68×10^{-1} S/cm) is an order of magnitude higher than that of the 1:0.1(90 wt. %) NP (9.2×10^{-2} S/cm) and similarly, the 1:0.6 (55 wt. %) and 1:0.8 (62 wt. %) NPs (1.1×10^{0}, 2.43×10^{0} S/cm) show conductivities an order of magnitude higher than the 1:0.4 (71 wt. %) NP. The conductivity of the EAPM NPs decrease with increasing iron oxide content due to the insulating property of the oxides which partially block the conductive path in the polymer matrix (Zhang and Wan, 2003;Zhang et al., 2005b).
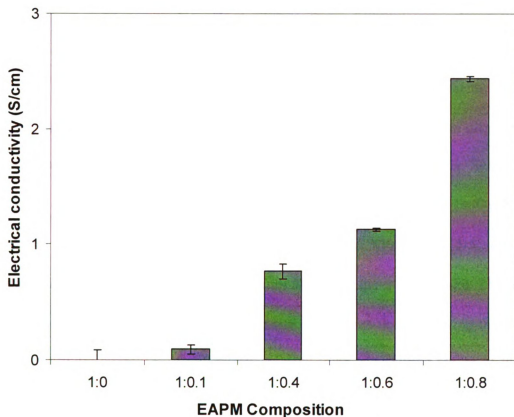
Figure 5-3. Room temperature electrical conductivity of the EAPM NPs.

Table 5-2. Conductivity values measured for the EAPM NPs.

EAPM Composition (γ-Fe_2O_3:Aniline)	Fe_2O_3 Content (Wt. %)	Pellet Thickness (μm)	Conductivity at 300K (S /cm)
1:0	100	1488	0.00005
1:0.1	90	1683	0.092
1:0.4	71	1476	0.768
1:0.6	62	1983	1.129
1:0.8	55	1938	2.436

morp

NPs

sph

10

ele

cry

tha

siz

ha

E.

Fi

Transmission electron microscope (TEM) images were used to study the structural morphology and size distribution of the unmodified $\gamma\text{-}Fe_2O_3$ and the synthesized EAPM NPs. The TEM image of the bare $\gamma\text{-}Fe_2O_3$ NPs in Figure 5-4 shows that the NPs have spherical shape and are less than 50 nm in size with an approximate size distribution of 10 to 40 nm which is consistent with the manufacturer's specifications. Selected area electron diffraction images (Figure 5-4, inset) indicate that the $\gamma\text{-}Fe_2O_3$ NPs are crystalline in nature. The TEM image of the 1:0.1 EAPM NPs (Figure 5-5, left) shows that the particles are spherical in shape similar to that of the $\gamma\text{-}Fe_2O_3$ NPs. The average size distribution of the 1:0.1 EAPMs are smaller than 50 nm thus indicating that the NPs have very minute quantities of polymer coating on them. Crystalline nature of the 1:0.1 EAPMs are confirmed through the electron diffraction rings (Figure 5-5, inset).
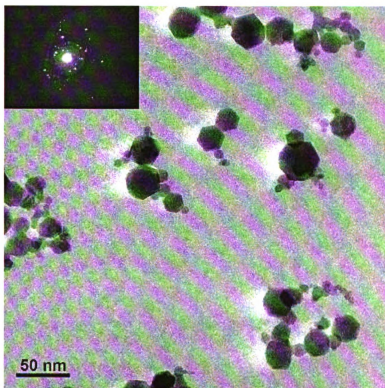
Figure 5-4. TEM and electron diffraction image of $\gamma\text{-}Fe_2O_3$ NPs.
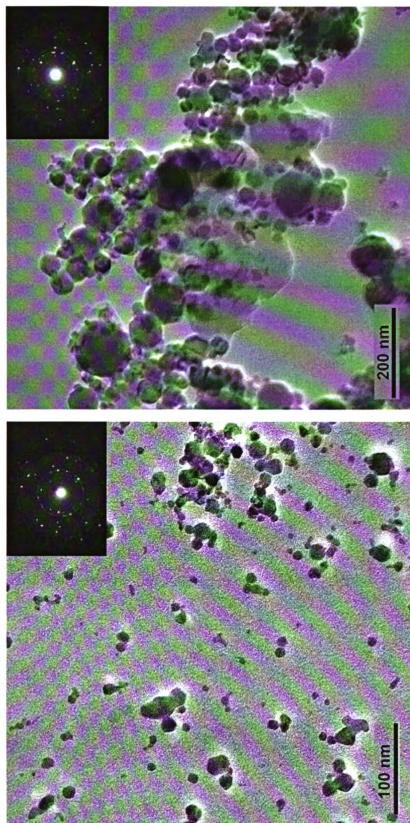
Figure 5-5. TEM and electron diffraction images of EAPM NPs: (left) 1:0.1 EAPM; (right) 1:0.4 EAPM.
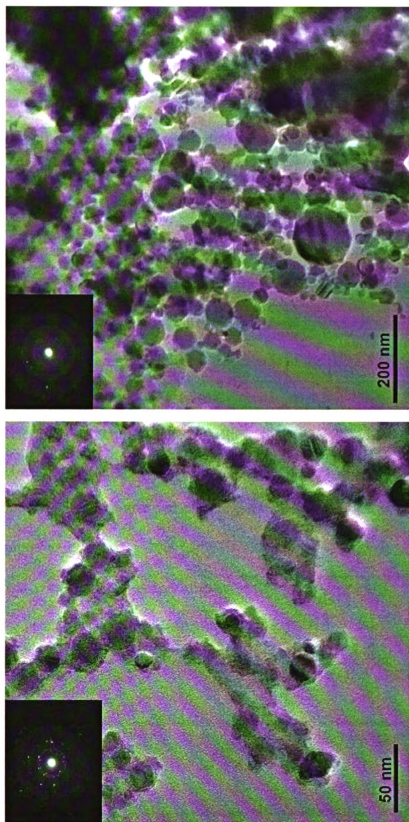
Figure 5-6. TEM and electron diffraction images of EAPM NPs: (left) 1:0.6 EAPM; (right) 1:0.8 EAPM.

The 1:0.4 EAPM (Figure 5-5, right) aggregates show spherical morphology with an average size distribution of 100 to 200 nm and are crystalline (Figure 5-5, right inset). The 1:0.6 EAPMs (Figure 5-6, left) have an approximate size distribution of 50 to 100 nm and exhibit a chain like morphology similar to observations made by Sharma *et al.* (Sharma *et al.*, 2005). The electron diffraction image (Figure 5-6, left inset) of the 1:0.6 EAPMs also reveal the crystalline nature of the samples. The 1:0.8 EAPMs (Figure 5-6, right) show the presence of excess polymer as compared to the 1:0.4 and 1:0.6 EAPMs and the aggregates are greater than 200 nm in size. The electron diffraction patterns of the 1:0.8 EAPMs (Figure 5-6, right inset) also indicate that they are mostly amorphous in nature. The TEM observations of the synthesized EAPM NPs are quite consistent with the measured magnetic and electrical parameters of the NPs.

The 1:0.6 EAPM was consequently chosen over the 1:0.1, 1:0.4 and 1:0.8 EAPMs for performing structural characterization studies as the NPs show good saturation magnetization as well as high electrical conductivity values thus suggesting a uniform distribution of the polymer and the magnetic core in the sample. The presence of both polyaniline and γ-Fe_2O_3 in the 1:0.6 EAPM NPs as well as its conductive nature was therefore confirmed by energy-dispersive X-ray microanalysis (EDS) of the EAPM samples using a scanning electron microscope and through UV-VIS spectral analysis.

Element	Weight (%)	Atomic (%)
C K	28.72	44.33
N K	6.96	9.22
O K	29.44	34.12
Cl K	3.98	2.08
Fe K	30.98	10.25
Total	100	
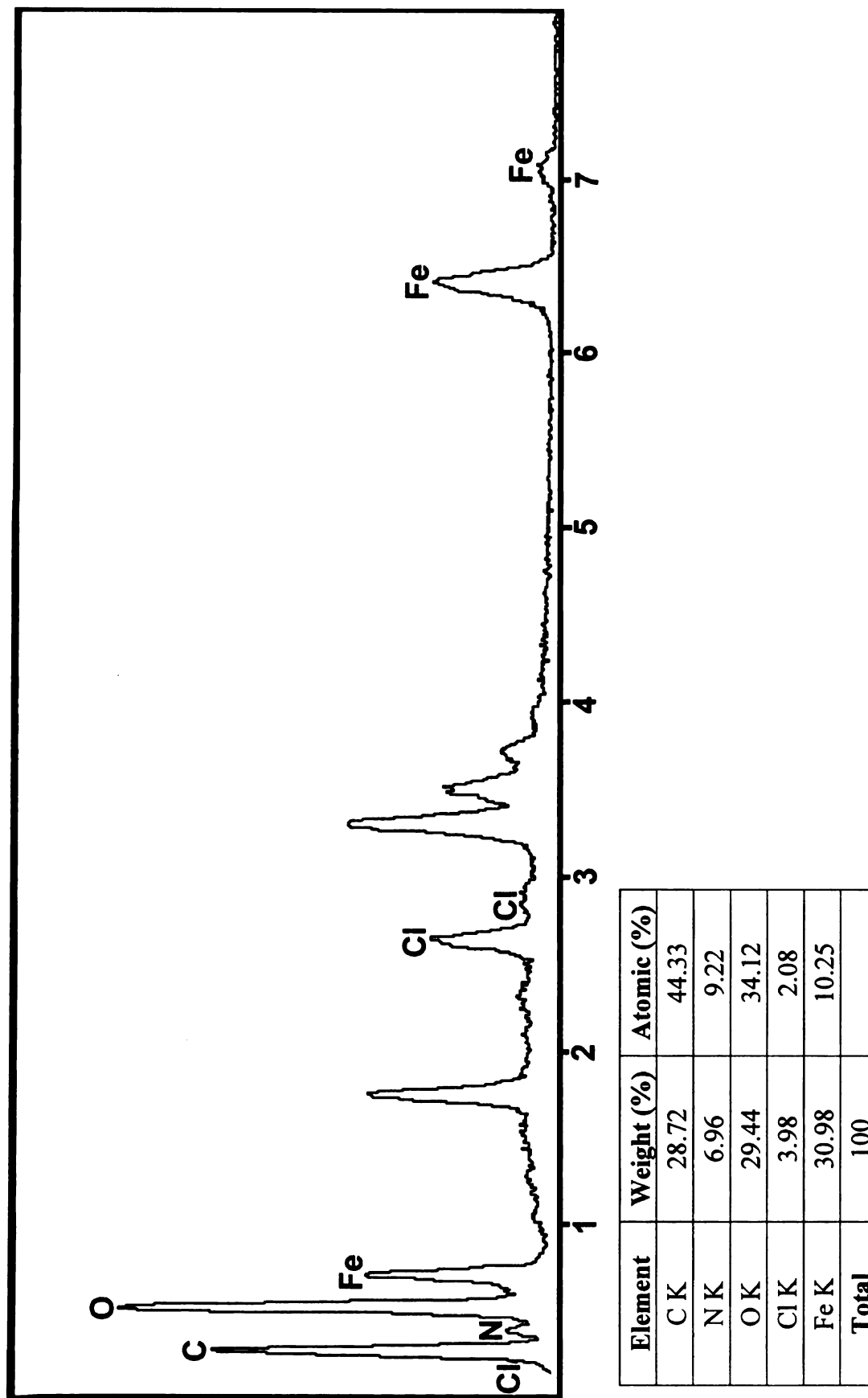
Figure 5-7. Elemental analysis of the 1:0.6 EAPM NPs using energy-dispersive spectroscopy (EDS) in SEM.

Figure 5-7 shows the EDS elemental analysis data of the 1:0.6 EAPMs. All the elements barring hydrogen present in polyaniline i.e. carbon (C), nitrogen (N), and chlorine (Cl) could be detected in the 1:0.6 EAPM sample. The absence of hydrogen in the EDS data was due to instrumental limitations of the EDS detector in the SEM microscope which could only detect elements having atomic numbers higher than 5. The dopant Cl atoms in the EDS data also suggest that polyaniline is present in its conductive form in the EAPM NPs. High percentages of Iron (Fe) and oxygen (O) atoms are also detected in the 1:0.6 EAPM NPs thus confirming presence of γ-Fe_2O_3.

Figure 5-8 shows the result of UV-vis spectral analysis of pure polyaniline and the 1:0.6 EAPM NPs dispersed in water. As observed in the figure, the characteristics peaks of pure polyaniline appear at 356 nm, 433 nm and 862 nm. The peak at 356 nm can be attributed to π-π^* transition of the benzenoid ring, while the peaks at 433 nm and 862 nm are associated with polaron- π^* and π-polaron band transitions of polyaniline, respectively (Stafstrom *et al.*, 1987;Lv *et al.*, 2005;Dallas *et al.*, 2006). For the EAPM NPs, characteristic absorption peaks are observed at 441 nm and 864 nm that can be related to the polaron- π^* and π-polaron band transitions of polyaniline. For the EAPM NPs, the polaron- π^* peak shows an 8 nm shift and the π-polaron peak shows a 2 nm shift from that of pure polyaniline. These red shifts observed in the spectrum can be explained by interactions between the Fe_2O_3 nanoparticles and the polymer backbone. However, the π-π^* transition peak of the polymer is not properly distinguished in the absorbance spectrum of the EAPM NPs. The absorbance data further confirms that the polymer is present in the doped (conductive) state in the EAPM NPs (Ohira *et al.*, 1987).
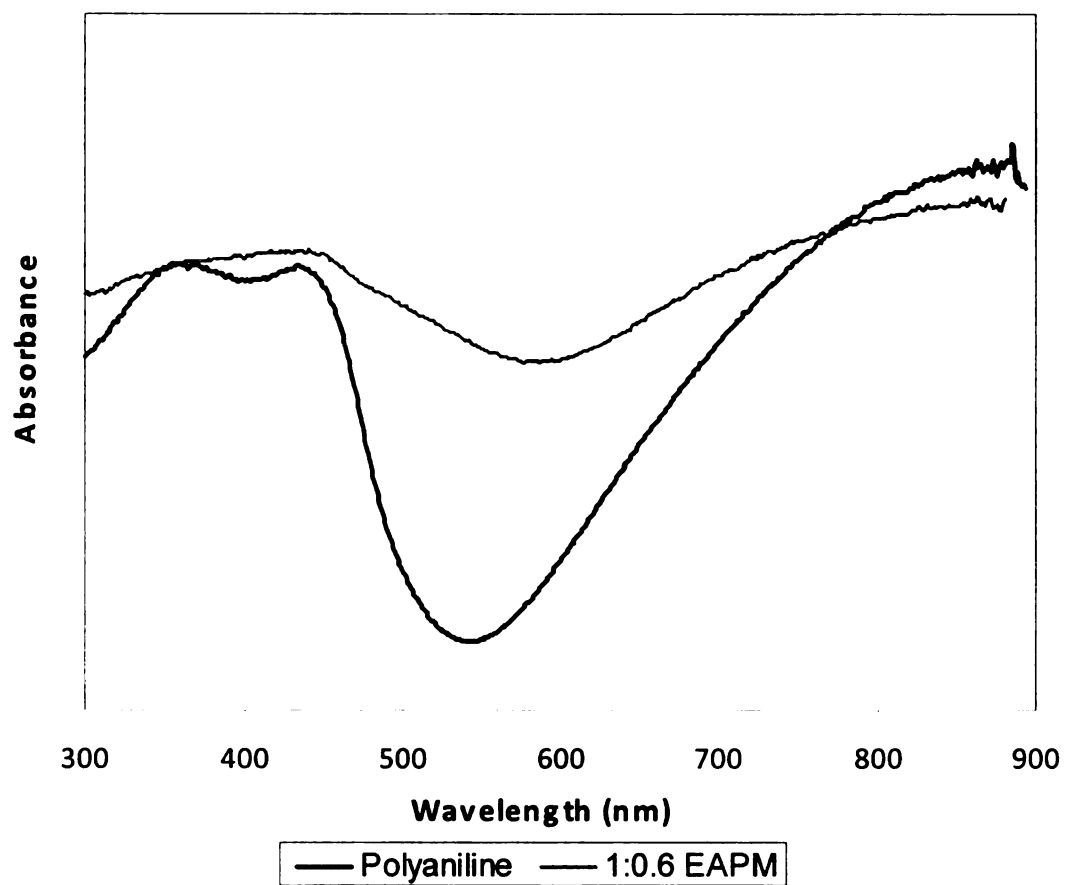
Figure 5-8. UV-VIS absorption spectra of pure polyaniline and EAPM NPs.

5.2   OBJECTIVE 2

Design and fabrication of an EAPM NP based immunosensor for detection of *B. anthracis* spores.

5.2.1   EAPM Based Immunosensor Fabrication

5.2.1.1 Confirming EAPM Antibody Modification

The labeling of the EAPM NPs with antibodies was confirmed by spectrophotometric studies. Figure 5-9 shows the UV spectrum of pure anti-*B. anthracis* IgG (150μg/ml) molecules and that of the unreacted IgG molecules in the supernatant after magnetic separation of the immuno-EAPMs measured by a UV-VIS-NIR scanning spectrophotometer. As evident in the figure, pure IgG solution shows a characteristic peak of protein molecules at 280 nm. However, the supernatant from the immuno-EAPMs shows no characteristic peak at 280 nm, thus implying that the anti-*B. anthracis* IgG molecules are adsorbed onto the EAPM NPs and no unreacted IgG molecules remain in the supernatant. Physical adsorption was used for bio-modification of the EAPM NPs with IgG molecules because the conjugation procedure is simple and allows IgG molecules to retain their activity and conformation. Physical adsorption is affected by several factors, such as van der Waals interaction, electrostatic interaction, hydrophobic effect and hydrogen bonding (Zhou *et al.*, 2004). Literature suggests that IgG adsorption occurs preferentially through Fc fragment of the molecule (Buijs *et al.*, 1996). Hence, it can be suggested that electrostatic interactions between negatively charged Fc fragments of IgG molecules and positively charged polymer surfaces of EAPM NPs play a significant role in the physical adsorption process.

112
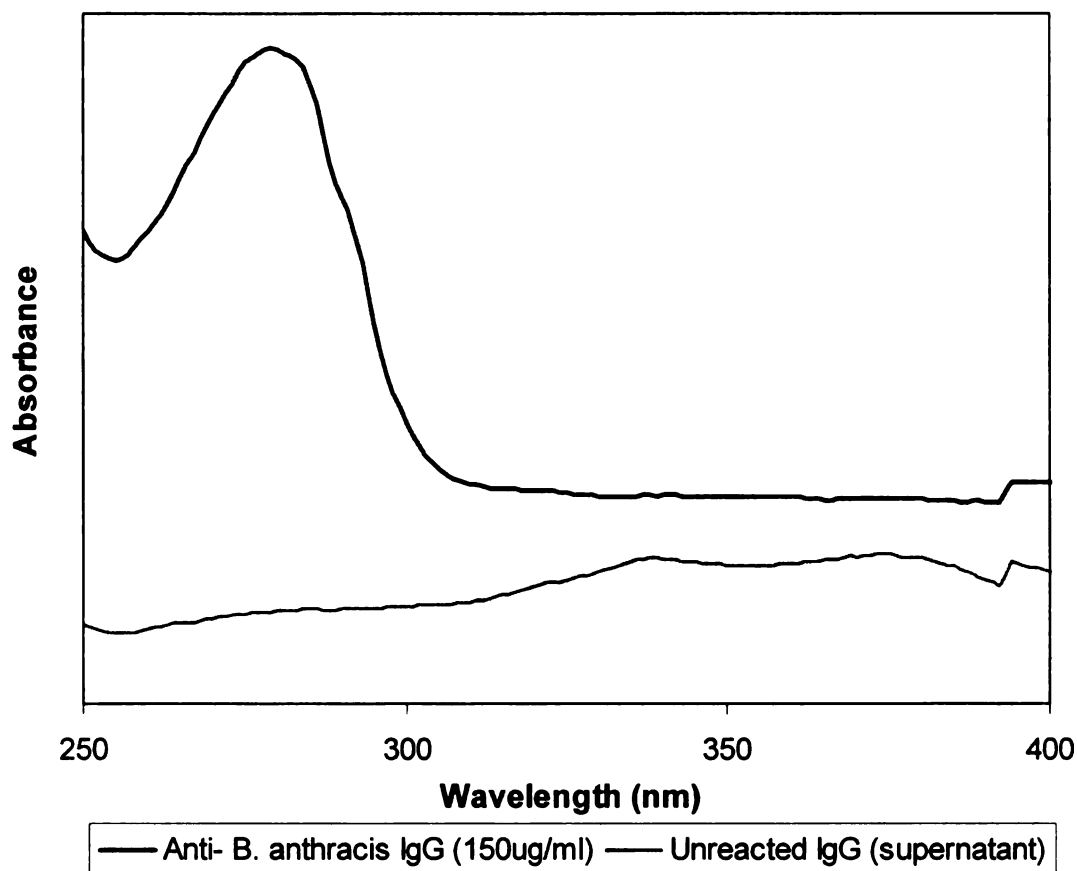
Figure 5-9. UV spectrum of pure anti-*B. anthracis* IgG molecules and unreacted IgG molecules after magnetic separation from EAPM NPs.

5.2.1.2 Confirming Biosensor Capture Pad Functionalization

The successful immobilization of polyclonal goat anti-*B. anthracis* IgG (500μg/ml) on the biosensor capture pad was confirmed by fluorescent images obtained from the Laser Scanning Confocal Microscope. The anti-*B. anthracis* IgG immobilized biosensor capture pads were modified with secondary antibodies (FITC-anti-goat IgG) using a working dilution of 1:320. Figure 5-10 (left) shows the fluorescent image of the capture pad labeled with the secondary FITC anti-goat IgG and Figure 5-10 (right) shows the image of the capture pad without the FITC label (control), observed by excitation with

488-nm line of argon ion laser, and the detection of emission using a 505 nm long pass filter. The bright green fluorescence emission in Figure 5-10 (left) confirms the immobilization of anti-*B. anthracis* IgG on the capture pad which is detected by the FITC label of the secondary anti-goat IgG molecules. In contrast, the control image (Figure 5-10, right) shows no significant fluorescence emission because of the absence of the secondary FITC labeled antibody in the control. The appearance of a few fluorescent dots in the control image can be explained by the tendency of the nitrocellulose membrane to fluoresce when exposed to the argon ion laser.
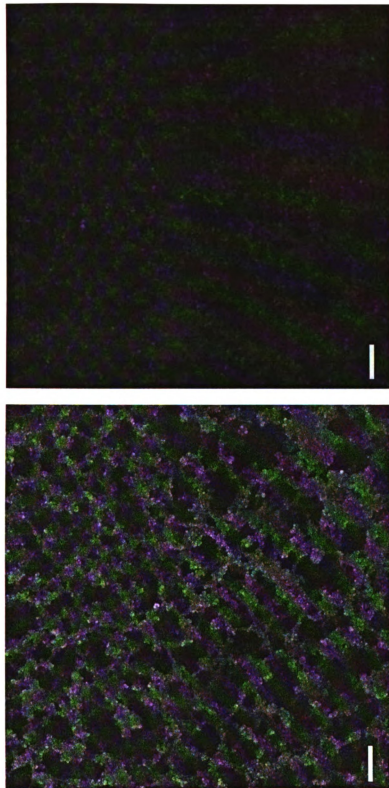
Figure 5-10. Laser scanning confocal microscope images of antibody modified biosensor capture pad with FITC anti-goat IgG label (left) and capture pad without FITC anti-goat IgG label (right) (scale bar = 20 μm).

5.2.2 EAPM Based Immunosensor Detection Concept

Figure 5-11 is a schematic representation of the immunomagnetic separation technique and the detection procedure of the EAPM based immunosensor. The detection principle involves a sandwich immunoassay, with a capture antibody (polyclonal anti- *B. anthracis* IgG) immobilized on the biosensor capture pad and a detector antibody (monoclonal anti- *B. anthracis* IgG) conjugated with the synthesized EAPM NPs. The detector antibody conjugated EAPM NPs are first added to the target antigen contaminated samples (Figure5-11, step 1) to capture the antigen by applying a magnetic field (step 2). The immunomagnetically captured target antigens are then washed to remove unbound antigens and other materials (step 3) and applied to the sample application pad of the biosensor (step 4). The antigen-antibody-EAPM complex flows to the capture pad, where the antigen is anchored by the capture antibodies present on the sensor capture pad and a sandwich structure is formed (step 5). The electrically active EAPM NPs bound to the antigens in the sandwich aid in direct electron transfer across the silver electrodes thus acting as a voltage controlled "ON" switch and generating an electrical signal which is recorded (step 6) (Muhammad-Tahir and Alocilja, 2003b;Pal *et al.*, 2007). In the absence of antigens, the sandwich complex is not generated and as a result of which the electron transfer by the EAPM NPs between the electrodes is not facilitated.
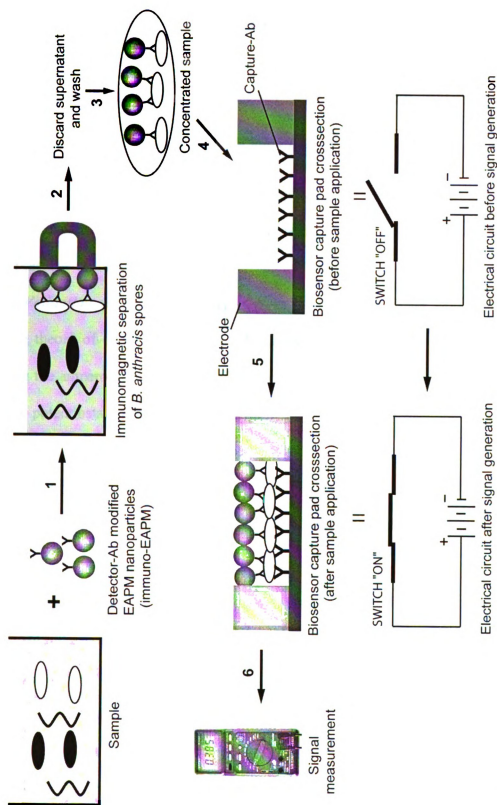
Figure 5-11. Schematic representation of the EAPM based immunosensor for detection of *B. anthracis* spores.

The biosensor detection concept is based on the difference between the electric signal in the absence of the target and the signal in the presence of the target. The electrical signal generated across the electrodes on the biosensor surface can be measured in terms of current (I) or in terms of resistance (R) when a fixed potential (V) is applied across the electrodes. Thus, from Ohm's law ($I = \dfrac{V}{R}$), it can be theoretically suggested that at a fixed applied potential, the current response of the biosensor should increase in the presence of an antigen, while the resistance response of the biosensor should decrease in the presence of the antigen.

5.2.2.1 Validation of Detection Concept

The theory of detection of the EAPM based immunosensor was first validated by studying the amperometric response of the sensors in presence and absence of the target using a potentiostat. A potentistat was initially used for the validation of detection concept because of its higher precision over the hand-held multimeter that was subsequently used in later biosensor experiments. The biosensors were tested for an antigen concentration of 10^6 spores per ml and a control solution which had no antigens, using 100 µl of the antigen-antibody-EAPM complex obtained after immunomagnetic concentration. The current responses of the sensors were recorded over a total time of 20 minutes (1200 seconds) at a constant potential of 0.05 V chosen arbitrarily as the input signal. As observed in figure 5-12, the biosensor current response at high antigen concentration increases rapidly to a maximum value of 0.46µA before saturating. On the contrary, the control amperometric signal only attains a value of 0.128 µA before saturation. This increase in the amperometric response of the biosensor at high antigen concentration in comparison to the control suggests the formation of a sandwich structure

(Figure 5-11, step 5) on the capture pad where electrically active EAPM NPs act as an 'ON' switch and increase the electron flow across the electrodes. The finding is in agreement with the proposed theory of detection of the biosensor discussed earlier. For the control solution, the formation of a sandwich 'bridge' is hindered due to the absence of antigens as a result of which the electron transfer process across the electrodes is not facilitated and a decrease in the amperometric response is observed. The experimental results demonstrate the novel concept of employing EAPM NPs as a transducer for electric signal generation in biosensors in contrast to straight polyaniline that has been used for signal amplification in biosensors by Kim *et al* and Sergeyeva *et al.* (Kim *et al.*, 2000;Sergeeva *et al.*, 1996).

As evident in Figure 5-12, initial fluctuations are observed in the biosensor amperometric responses for approximately 100 sec as a result of which the control signal is not significantly differentiable from the sample. Resultantly, a data acquisition time starting from 2 min after sample application was considered to be applicable for subsequent studies. A total data acquisition time limited to 6 min was acceptable for distinction between the blank or control signal and a sample containing the antigens from prior studies (Pal *et al.*, 2007).
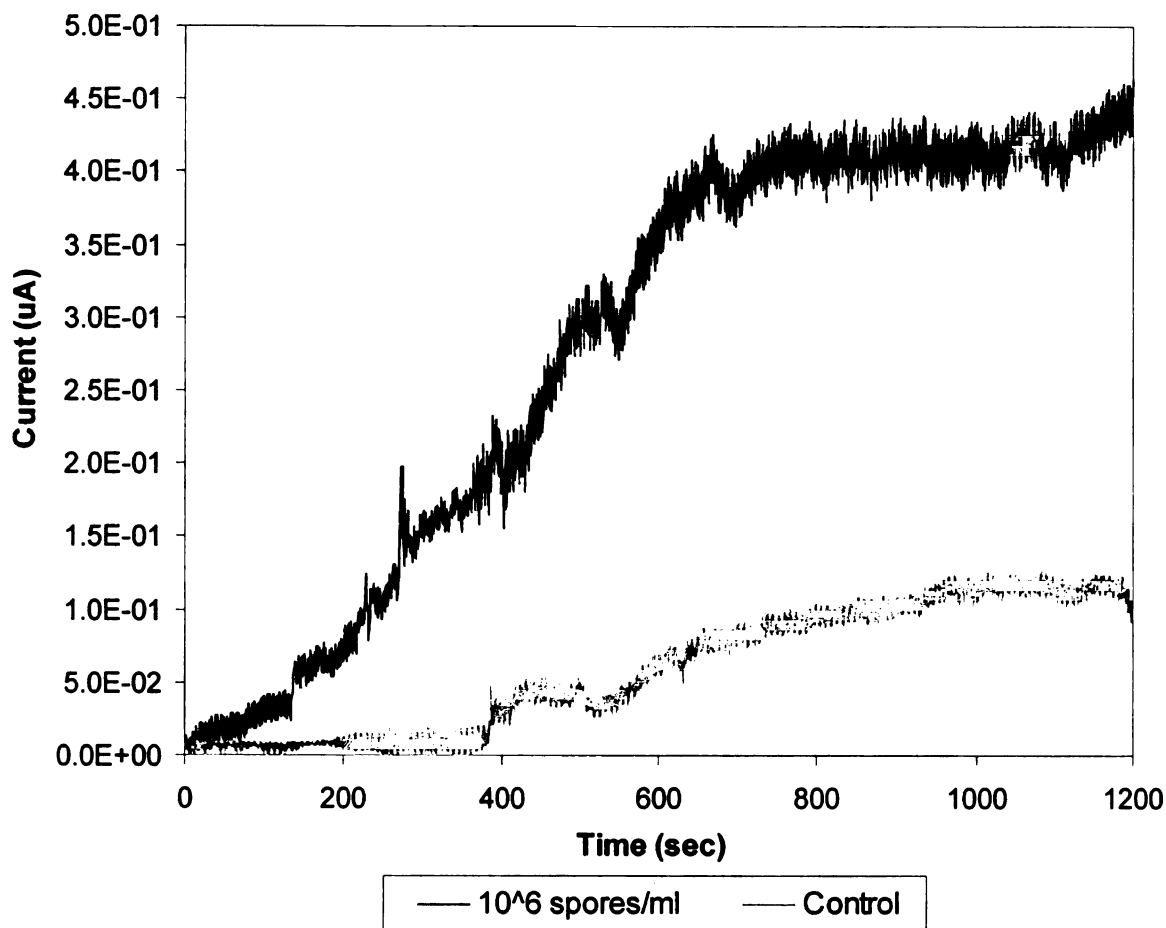
Figure 5-12. Amperometric response of the EAPM based immunosensor in the presence and absence of the target antigen.

Figure 5-13 shows the plot of resistance versus time for the EAPM immunosensors calculated from the measured amperometric response. The resistance values were calculated for 6 min at 2 min intervals as discussed earlier. As seen in Figure 5-13, the resistance values for the control solution varies between 2.5 MOhm and 18.5 MOhms, whereas, in the presence of antigens, the resistance values varies between 300 and 1000 kOhms. This decrease in resistance in the presence of antigens once again corroborates the fact that the EAPM NPs result in enhanced electron transfer across the immunosensor electrodes.
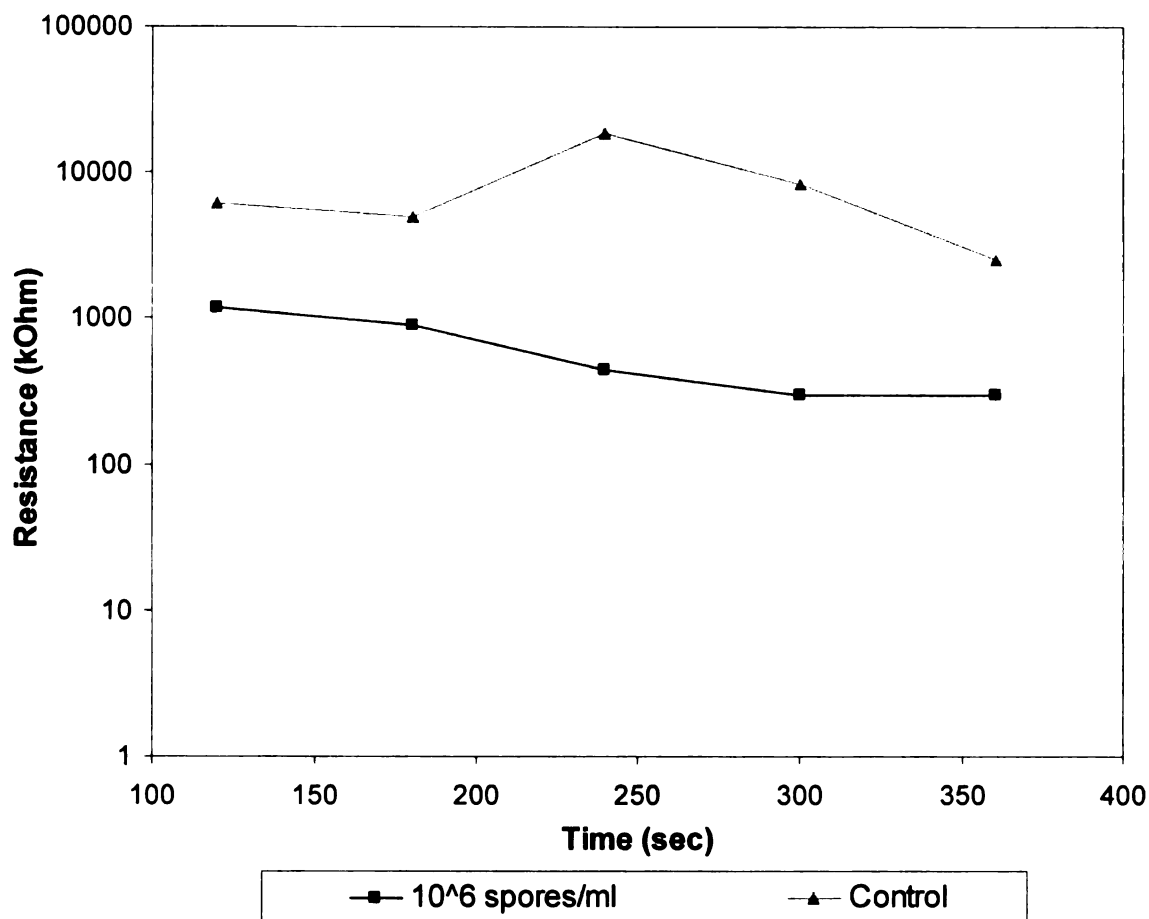
Figure 5-13. Resistance changes of the EAPM immunosensor in the presence and absence of the target antigen calculated from the measured amperometric response.

The NP concentration to be used in the EAPM based immunosensor was determined based on optimization experiments previously performed in a *B. cereus* biosensor (data in Appendix B). *B. cereus* was chosen as the model pathogen for its genetic similarities with *B. anthracis*. The antibody concentration for EAPM modifications was fixed at 150 μg/ml from prior studies and preliminary experiments with *B. cereus* (Pal *et al.*, 2007). The optimum NP concentration for the best biosensor response as determined from preliminary experiments was 20 mg/ml and was used in subsequent immunosensor studies for *B. anthracis* detection. For immunomagnetic concentration, the antibody

coated EAPM NPs were allowed to react with the antigens and a 10 min incubation time was found to be adequate for attachment of the antigens to the antibodies. The antibody modified EAPM NPs were only used for single measurements in both the magnetic concentration and biosensor detection steps and the reusability of these NPs for both procedures need to be determined.

5.3   OBJECTIVE 3

Evaluation of sensitivity and specificity of the EAPM NP based immunosensor and determination of EAPM immunomagnetic capture efficiency.

All biosensor experiments were performed in pure spore suspensions of *B. anthracis*. A spore stock solution was created using a previously published protocol that has been elaborated in Chapter 3 of this dissertation. Sporulation was monitored by light microscopy and the spore image results have been presented in Appendix B (Figure B-3). The spore count of the stock solution as estimated by counting using a hemacytometer (cell counting chamber) was 420 spores per ml. For all sensitivity, specificity and food matrix studies, the spore dilutions were created from the above stock solution.

5.3.1   Immunosensor Performances Using Different EAPM Types

The biosensor performances of the four different EAPM NPs (1:0.1, 1:0.4, 1:0.6, and 1:0.8) were assessed in pure spore suspensions of *B. anthracis*. Biosensor tests were carried out for three different spore concentrations (10^1, 10^4 and 10^7 per ml) for each NP type. Multi-factor analysis of variance (Two-way ANOVA) to a significance of 95% was used to compare the interactive effects of the different spore concentrations as well as the different EAPM types on the biosensor resistance signals (results in Appendix A). Figure

5-14 shows a comparison of the mean resistance signals generated with the four different types of magnetic NPs. The effect of the different EAPM NPs and the different spore concentrations on the biosensor resistance responses is found to be statistically significant ($P < 0.0001$) from the Type 3 Tests of Fixed Effects table (Table A-1).

As evident in Figure 5-14, at high spore concentration (10^7 per ml), all four EAPM NP types show significant statistical differences ($P < 0.05$) in resistance values from the control thus implying detection. However, the effect of the different EAPM types on the resistance signal is not statistically significant at this concentration ($P = 0.7351$). This could be explained by the very high antigen concentration that was capable of generating a strong biosensor signal. At 10^4 spores per ml, only the 1:0.4 and 1:0.6 EAPM NPs show resistance values statistically different from the control ($P < 0.0001$) whereas at the lowest spore concentration (10^1 per ml), none of the EAPM NPs show significant differences from the control thus implying no detection at this concentration ($P > 0.05$). These results suggest that the effect of different EAPM types is more pronounced at 10^4 spores per ml.

Figure 5-14 also shows that the 1:0.1 EAPM NPs can only detect the spores at the highest concentration level (10^7 per ml) and hence was not considered further for subsequent experiments. Similarly, the 1:0.8 EAPM NPs have no statistically significant effect on the biosensor resistance signals ($P = 0.8227$). This can be due to the greater agglomeration and larger size observed in the 1:0.8 NPs (in Figure5-6) which have an impeding effect on the flow of the EAPM NPs as well as the EAPM-antibody-spore complexes through the capture pad thus resulting in a high background signal which makes the control signal indistinguishable from that of the different spore concentrations.

The 1:0.6 EAPM NPs were consequently chosen for biosensor sensitivity and specificity studies. The high electrical conductivity and competent magnetic properties of the NPs confirmed by DC SQUID and four point probe measurements as well as the low variability in the resistance responses of the biosensor (Figure 5-14) at high antigen concentrations with these NPs suggests that the 1:0.6 EAPMs offers the best trade off between desired NP characteristics and biosensor signal generation.
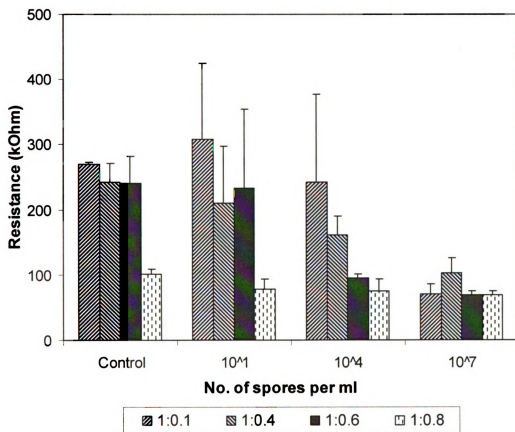
Figure 5-14. Comparison of biosensor resistance response of the four EAPM NPs at three different spore concentrations (Mean resistance ± SD, n = 3).

5.3.2 Immunosensor Sensitivity Study

The sensitivity study for the EAPM based *B. anthracis* immunosensor was performed for spore concentrations ranging from 10^0 to 10^7 spores per ml. Figure 5-15 shows the average biosensor resistance measured from three trials using the 1:0.6 EAPM NPs. Multi factor analysis of variance (Two-way ANOVA with time as repeated measures) to a significance of 95% ($P < 0.05$) was used to study the effect of cell concentrations and time on the biosensor resistance responses and to compare the differences in the resistance readings between the control and the different spore concentrations (results in Appendix A). The type 3 Tests of Fixed Effects table (Table A-6) indicates that only spore concentration and not time has a significant effect on the biosensor resistance signal (P- value for concentration: < 0.0001, P- value for time: 0.9983). The average resistance recorded for the different spore concentrations show significant statistical differences from the control solutions ($P < 0.0001$). The clarity in signal can be attributed to the magnetic concentration procedures in this assay which provide advantages such as low interference from other biological materials, concentration of target pathogens into smaller volumes, and reduced background signal (Kriz *et al.*, 1998).

In figure 5-15, a gradual increase in the mean resistance signal is observed as the spore concentration decreases from 10^7 to 10^0 spores/ml with an exception to the signal at 10^3 spores/ml. This can be explained by the fact that a higher concentration of pathogen will have a higher concentration of EAPM NPs bound to them resulting in an increased electron transfer between the electrodes and a concomitant decrease in the resistance signal. However, the resistance values recorded for the different spore

concentrations are not statistically different from one another. This disparities observed in the biosensor signal can be explained by a number of factors such as imperfections in biosensor fabrication, non-uniformity in EAPM samples, probabilistic interactions between the antigens and antibodies, antibody orientations on the capture pad surface and stability of the sandwich complex formed on the capture pad.

The lowest *B. anthracis* spore concentration which produces a resistance signal statistically ($P < 0.05$) lower than the control is considered to be the analytical sensitivity or the detection limit of the biosensor. Since the biosensor signal at the threshold concentration of 4.2×10^2 spores per ml (estimated from spore count) is statistically significant from the control, the sensitivity of the biosensor was determined to be 4.2×10^2 spores/ml. This is an excellent sensitivity in terms of rapid identification since the ID 50 (median infectious dose) for *B. anthracis* has been reported to be in between 8000 and 10,000 spores and most biosensors developed for the detection of *B. anthracis* spores have sensitivities greater than 10^3 spores/ml (Cieslak and Eitzen, 1999;Krebs *et al.*, 2006;Liu *et al.*, 2007).

At this stage of research, the biosensor can only be considered as qualitative device as the resistance signal at different spore concentrations are not statistically differentiable. Futhermore, the higher data variability observed in the control as well as at very low spore concentrations (viz. 10^1 and 10^2 spores/ml) could not be explained at this stage and would require further investigations. However, the biosensor signal demonstrates the success of the immunomagnetic capture process by the EAPM NPs, which is further confirmed by microbial plating results and capture efficiency calculations discussed in Section 5.3.5 of this chapter.
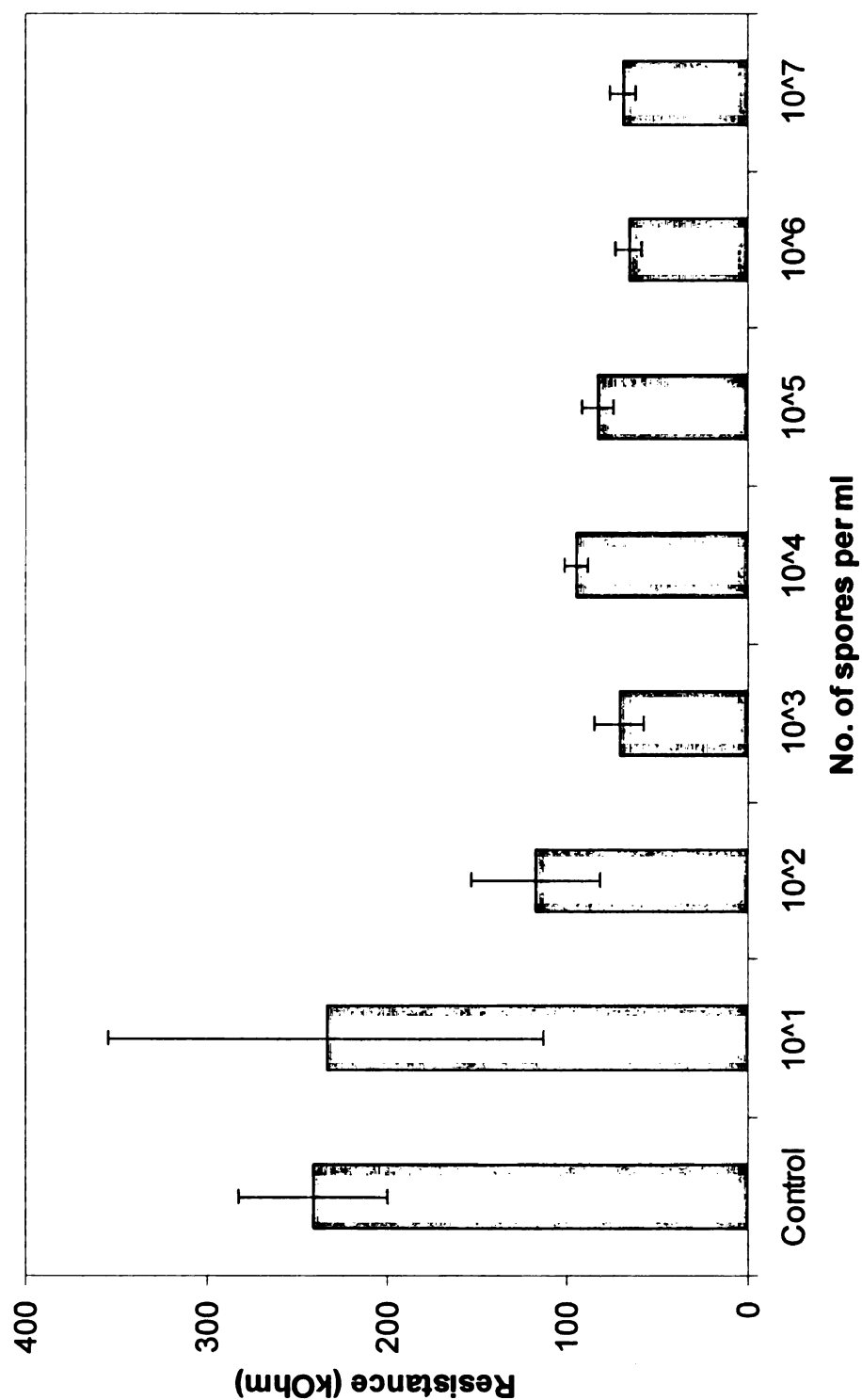
Figure 5-15. EAPM based immunosensor resistance response in pure spore suspensions of *B. anthracis* (mean resistance ± SD, n = 3). Different superscripts over the bars indicate significantly different resistance response ($P < 0.05$).

5.3.3 Immunosensor Specificity Analysis

Figure 5-16 shows the specificity analysis of the EAPM nanoparticle based immunosensor. A comparison of the biosensor resistance responses in pure cultures of $E.$ $coli$ with cell concentrations ranging from 1.7×10^1 to 1.7×10^5 CFU/ml, in pure cultures of S. Enteritidis with cell concentrations ranging from 1.6×10^1 to 1.6×10^5 CFU/ml, and pure spore suspensions of $B.$ $anthracis$ with spore concentrations ranging from 4.2×10^1 to 4.2×10^5 spores/ml, is presented in this figure. Multi factor analysis of variance (Two-way ANOVA) to a significance of 95% ($P < 0.05$) was used to study the effect of different cell concentrations and the effect of the two pathogen types on the biosensor resistance responses and to compare the differences in the resistance readings between the control and the different cell concentrations (results in Appendix A). The type 3 Tests of Fixed Effects table (Table A-10) indicates that neither the pathogen type nor the cell concentration had a significant effect on the biosensor resistance signal (P- value for concentration: 0.6084, P- value for pathogen type: 0.1537).

As observed in Figure 5-16, the biosensor average resistance values for different concentrations of the non-target bacteria (i.e. $E.$ $coli$ and $S.$ Enteritidis) are similar to the values observed for the control with no statistically significant differences. The P-values range from 0.1171 to 0.8398 for $E.$ $coli$, and from 0.5210 to 0.9905 for $S.$ Enteritidis. The results indicate that the effects of non-specific interactions are insignificant for the range of cell concentrations tested on the biosensor. In comparison, for pure $B.$ $anthracis$ spore suspensions, the biosensor average resistance responses show significant differences between the control and spore concentrations ranging from 10^2 to 10^5 spore/ml (P-value < 0.0001) which is expected since the antibodies used in the biosensor are specific for $B.$

anthracis. However, at a low *B. anthracis* spore concentration of 10^1 spores/ml, the

biosensor resistance response is similar to that of the control which implies no detection

at this concentration (*P*-value: 0.5440).
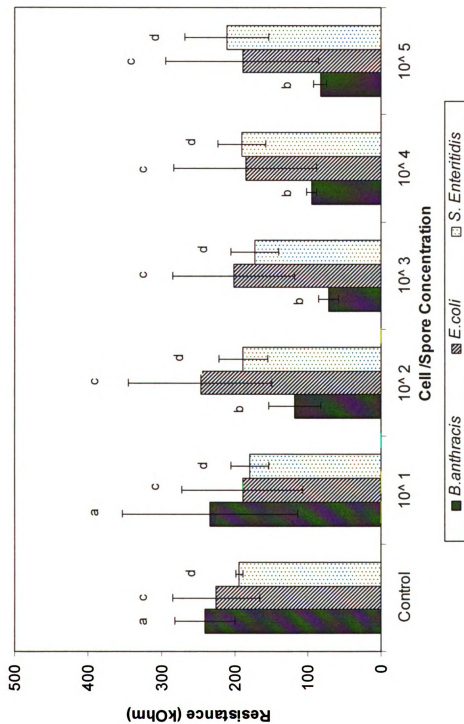
Figure 5-16. Comparison of immunosensor resistance response in pure spore suspensions of *B. anthracis* and pure cultures of generic *E. coli* and *S. Enteritidis*. For each pathogen, different superscripts over bars indicate significantly different resistance response ($P < 0.05$).

5.3.4 Immunosensor Testing in Food Matrices

Figure 5-17 shows the average resistance readings measured with the EAPM NP based immunosensor in lettuce, whole milk, and ground beef samples inoculated with *B. anthracis* spores. The average resistance signals obtained from three replicates are plotted for the control that consisted of uninoculated food samples containing EAPM NPs at a concentration of 20 mg/ml and the food samples contaminated with spore concentrations ranging from 4.2×10^1 to 4.2×10^7 spores/ml. As observed, the resistance values recorded for the different spore concentrations are much lower than the values for the control solution that has no spores in it. The average resistances for the control are in the range of 288.2 ± 68 kΩ and 353.8 ± 51 kΩ, whereas the average resistances for the different spore concentrations in the three food samples vary from 75.1 ± 14 to 132.6 ± 19 kΩ for the detectable spore concentrations. The reduced resistance values further support the formation of a sandwich structure on the capture pad that was hypothesized earlier where the conductive EAPM NPs help in electron transfer causing a drop in the resistance signal across the silver electrodes (Kim *et al.*, 2000;Pal *et al.*, 2007).

Single factor analysis of variance tests (One-way ANOVA) to a significance of 95% ($P < 0.05$) were conducted to compare the differences in the resistance values between the control and the different spore concentrations to determine the biosensor sensitivity in food matrices. For the lettuce and ground beef samples, the biosensor sensitivity is 4.2×10^2 spores/ml as estimated from spore stock concentration with statistically significant differences from the control (P-value for lettuce at 10^2 spores/ml < 0.0001; P-value for ground beef at 10^2 spores/ml < 0.0001). For whole milk samples, the biosensor can reach a sensitivity of 4.2×10^3 spores/ml where statistically significant differences can be

observed from the control (P-value at 10^3 spores/ml was < 0.0001). The reduced biosensor sensitivity in whole milk samples can be explained by interferences due to proteins molecules viz. antibodies and fat molecules that influence binding kinetics of the spores with the EAPM NPs during the immunomagnetic capture process.

As observed in the figure, at a particular spore concentration, the resistance signals for the different food matrices are not statistically differentiable from one another in most cases although the values are lower than the control. Similarly, the differences in the resistance signal in between different spore concentration of each food sample is also not statistically significant. These results are consistent with the sensitivity data of the biosensor in pure spore suspensions thus emphasizing the fact that at this stage the biosensor can only be considered as a qualitative device for a yes/no diagnosis of *B. anthracis* spores. However, the biosensor shows high sensitivity and fast detection time in comparison to the very few rapid detection systems for *B. anthracis* in food matrices that have been reported in the literature (Cheun *et al.*, 2001;Tims and Lim, 2004). The biosensor results also indicate that the EAPM NPs are successful in concentrating the *B. anthracis* spores from the different food matrices. This is further confirmed by microbial plating of the spore-antibody-EAPM complexes, the results of which are discussed in Section 5.3.5 of this chapter.
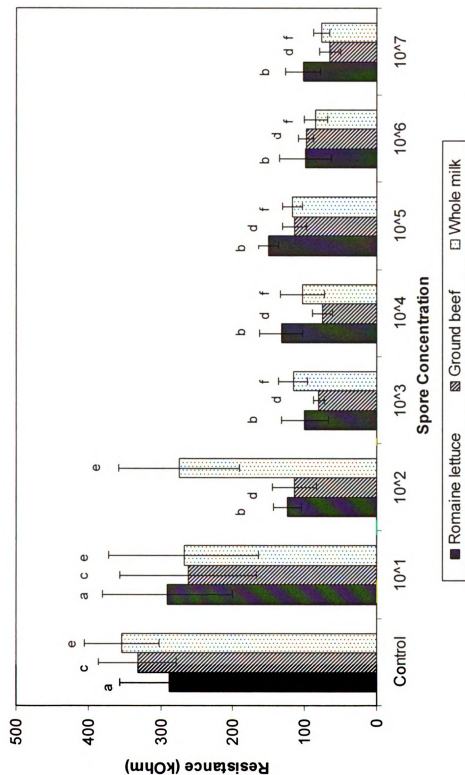
Figure 5-17. Resistance response of the EAPM based immunosensor in food matrices contaminated with *B. anthracis* spores. For each food sample, different superscripts over bars indicate significantly different resistance response ($P < 0.05$).

133

5.3.5 Confirmation and EAPM Capture Efficiency Determination

The immunomagnetic target capture process (step 1 in Figure 5-11) using the EAPM NPs performed before the biosensor detection was confirmed by microbial plating of the immuno-EAPM-spore complexes. The capture efficiency (CE) of the EAPM NPs was calculated using the equation described in Section 4.3.8 of Chapter 4.

Table 5-3 shows the plate count data and the CE calculations of the immuno-EAPMs in pure spore suspensions of *B. anthracis*. As observed in Table 5-3, the EAPM NPs has very high CE values ranging in between 95.8% and 76.0% for viable *B. anthracis* spore concentrations of 4.73 $\times 10^7$ CFU/ml to 4.73 $\times 10^1$ CFU/ml. The highest CE value of 95.8% is observed at a viable spore concentration of 4.73 $\times 10^2$ CFU/ml. The immuno-EAPMs also demonstrate efficient capture from *B. anthracis* spores concentrations as low as 10^1/ml with a CE value of 91.6%. The CE values are determined only after an immuno-reaction time of 10 min between the EAPM NPs and the different spore concentrations before applying the complexes to the biosensor. From the CE results, it can be concluded that the immuno-EAPMs are very efficient in rapid capturing of *B. anthracis* spores from pure spore suspensions. The high capture efficiency of the EAPM NPs can be attributed to their small sizes that make them ideal for achieving efficient diffusion and rapid binding kinetics in solutions (Soukka *et al.*, 2001;Varshney *et al.*, 2005).

Table 5-4 shows the plate count data and the CE calculations of the immuno-EAPMs in the three different food matrices (romaine lettuce, whole milk, and ground beef) contaminated with *B. anthracis* spores. As evident in Table 5-4, the capture effect of the immuno-EAPMs in the lettuce and ground beef samples are quite similar to the capture

effect observed in the pure spore suspensions. In both food samples, the CE values are highest at a viable spore concentration of 1.52×10^2 CFU/ml with a CE value of 97% for lettuce and that of 72% for ground beef. Similarly, the EAPM NPs can achieve an immunomagnetic capture at viable spore concentration as low as 1.52×10^1 CFU/ml from both lettuce and ground beef samples. However, the CE values for both food samples are lower than the CE values of the pure spore suspensions. For lettuce, the CE values of the immuno-EAPMs range in between 14.6 and 96.7 %, while, for beef samples, the CE values range between 9 and 72.3 %. This decrease can be explained by the interference from food matrices in the antigen-antibody binding kinetics. For whole milk samples, the immunomagnetic capture of the viable *B. anthracis* spores can only go as low as 1.52×10^2 CFU/ml and the capture effects are the same for all viable spore concentrations with CE values in the range of 6% and 11%. The presence of gangliosides (a class of glycolipids) in milk fat globule membranes of whole milk samples can lead to competitive binding of *B. anthracis* spores with the gangliosides and the immuno-EAPMs and is thought to be a possible reason for the low CE values observed in the whole milk samples. The use of gangliosides as nonspecific receptors of pathogens and toxins is well reported in literature (Desai *et al.*, 2008; Mason *et al.*, 2006).

The CE results demonstrated that the immuno-EAPMs were successful in rapidly concentrating *B. anthracis* spores from pure spore suspensions and food matrices with very high capture efficiencies at low spore concentrations. Since the CE values of the EAPM NPs were calculated based on an EAPM concentration of 20 mg/ml and antibody concentration of 150 μg/ml, it is expected that higher capture efficiencies can be attained

with the EAPM NPs by increasing both EAPM and antibody concentrations in the capture process.

Table 5-3. Capture Efficiency (CE) of immuno-EAPMs in pure spore suspensions of _B. anthracis_ estimated from plate count data.

Dilution Factor	Total Viable Spore Count ± SD (n=3) C_t (CFU/ml)	Viable Spores Bound to EAPM NPs ± SD (n=3) C_b (CFU/ml)	Capture Efficiency CE (%)
10^1	$4.73 \times 10^7 \pm 9.07$	$4.07 \times 10^7 \pm 9.07$	86.0
10^2	$4.73 \times 10^{6*}$	$3.59 \times 10^6 \pm 4.93$	76.0
10^3	$4.73 \times 10^{5*}$	$3.97 \times 10^5 \pm 3.05$	83.9
10^4	$4.73 \times 10^{4*}$	$4.07 \times 10^4 \pm 9.29$	86.0
10^5	$4.73 \times 10^{3*}$	$4.33 \times 10^3 \pm 2.51$	91.6
10^6	$4.73 \times 10^{2*}$	$4.53 \times 10^2 \pm 7.09$	95.8
10^7	$4.73 \times 10^{1*}$	$4.33 \times 10^1 \pm 1.52$	91.6
10^8	$4.73 \times 10^{0*}$	0	0
Control	0	0	0

* Estimated spore concentrations
SD = Standard Deviation, n = no. of replicates

Table 5-4. Capture efficiency (CE) of immuno-EAPMs in romaine lettuce, whole milk, and ground beef contaminated with *B. anthracis* spores estimated from plate count data.

Dilution Factor	Total Viable Spore Count ± SD (n=3) C_t (CFU/ml)	Romaine Lettuce		Whole Milk		Ground Beef	
		Viable Spores Bound to EAPM ± SD (n=3) C_b (CFU/ml)	Capture Efficiency (CE) (%)	Viable Spores Bound to EAPM ± SD (n=3) C_b (CFU/ml)	Capture Efficiency (CE) (%)	Viable Spores Bound to EAPM ± SD (n=3) C_b (CFU/ml)	Capture Efficiency CE (%)
10^1	$1.52 \times 10^7 \pm 23$	$6.07 \times 10^6 \pm 55.3$	39.9	$1.41 \times 10^6 \pm 10.5$	9.3	$3.02 \times 10^6 \pm 32.5$	20.0
10^2	$1.52 \times 10^{6*}$	$2.30 \times 10^5 \pm 15.8$	15.1	$1.63 \times 10^5 \pm 10.3$	11.0	$3.17 \times 10^5 \pm 34.4$	20.8
10^3	$1.52 \times 10^{5*}$	$3.40 \times 10^4 \pm 17.6$	22.3	$1.22 \times 10^4 \pm 8.2$	8.0	$2.85 \times 10^4 \pm 6.5$	18.7
10^4	$1.52 \times 10^{4*}$	$2.23 \times 10^3 \pm 11.5$	14.6	$9.10 \times 10^2 \pm 19.5$	6.0	$1.38 \times 10^3 \pm 14.8$	9.0
10^5	$1.52 \times 10^{3*}$	$5.53 \times 10^2 \pm 7.1$	36.4	$1.40 \times 10^2 \pm 2.6$	9.2	$5.10 \times 10^2 \pm 9.5$	34.0
10^6	$1.52 \times 10^{2*}$	$1.47 \times 10^2 \pm 1.1$	96.7	$1.00 \times 10^1 \pm 0.5$	7.0	$1.10 \times 10^2 \pm 0.6$	72.3
10^7	$1.52 \times 10^{1*}$	$1.00 \times 10^1 \pm 1.1$	65.7	0	0	$1.00 \times 10^1 \pm 1.2$	65.7
10^8	$1.52 \times 10^{0*}$	0	0	0	0	0	0
Control	0	0	0	0	0	0	0

* Estimated spore concentrations
SD = Standard Deviation, n = no. of replicates

137

5.4   OBJECTIVE 4

Fabrication of an EAPM based electrochemical DNA biosensor for detection of *B. anthracis*.

5.4.1   Selection and Analysis of DNA Primers and Probes

B. anthracis Sterne strain, a strain with attenuated virulence, was used as the model organism in this study. Virulent strains of *B. anthracis* have two virulent plasmids: pXO1 (184 kb), which encodes toxins and pXO2 (95 kb), which encodes the capsule (Reif *et al.*, 1994). The *B. anthracis* Sterne strain lacks the pXO2 plasmid encoding the poly-γ-D glutamic capsule which is a major determinant of virulence in anthrax. For this reason, the PCR primers and the DNA probes were selected from a fragment of the *pag A* gene, which is present in the plasmid pXO1. The specificity of the selected probes and primers were checked using the BLAST analysis tool. BLAST results indicated that both the probe and primer pairs had a high degree of specificity (ΔE value: 8e-19, Max ident: 100% for the detector probe; ΔE value: 3e-7, Max ident: 100% for the capture probe; ΔE value: 0.43, Max ident: 100% for the primer pairs) for the *B. anthracis* Sterne strain plasmid pXO1 *pag A* gene. The only *Bacillus* species with which the sequences showed high similarity was *B. cereus* (*B. cereus* strain G9241 plasmid pBCXO1, Max ident: 100%).

5.4.2   Extraction, Amplification and Characterization of *B. anthracis* DNA

Genomic DNA was extracted from overnight cultures of *B. anthracis* grown in TSB broth using a procedure for mammalian DNA extraction. The concentration of the double stranded DNA (dsDNA) after the extraction process was determined to be 326.6 µg/ml by measuring the absorbance at 260 nm in a spectrophotometer following which the

DNA was diluted according to the requirements of PCR reaction. The PCR amplification reaction was optimized with respect to the concentration of the reactants, the melting temperature (T_m) and the amplification time in order to obtain the best amplification of targets in the shortest possible time. Table 5-5 shows the optimized concentrations of the reactants used in the PCR reaction.

Table 5-5. Optimum concentration of PCR components.

PCR Component	Final Concentration in PCR Reaction Mixture
Buffer	1X
dNTP mix	0.2mM
MgCl2	1.5mM
Accuprime Taq DNA Polymerase	1 μl
Forward Primer	100 nM
Reverse Primer	100 nM
DNA Template	100 ng

The PCR amplification reaction was optimized and run under the following conditions: 95°C for 2 min; 35 cycles of 95°C for 30 s, 55°C for 30s, 72°C for 60s; and 72°C for 5 min in the DNA thermal cycler. The PCR products obtained were first purified using the QIAquick kit and then characterized by gel electrophoresis and spectrophotometric measurements.
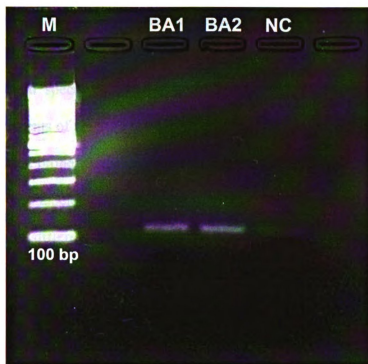
Figure 5-18. Gel Electrophoresis of PCR amplified *Bacillus anthracis*. (M- Marker, BA1 and BA2 – *B. anthracis*, NC- Negative Control)

Figure 5-18 shows the result of the PCR reaction after purification on 2.5 % agarose gel. The appearance of distinct bands in lanes BA1 and BA2 just above the 100 bp band of the marker confirms the length of the PCR product (120 bp). The appearance of bands in lanes BA1 and BA2 and no bands in lane NC also confirms the successful optimization of the PCR reaction conditions along with the PCR purification process. The dsDNA concentration in the purified PCR products (BA1 and BA2 pooled together), when tested in the NanoDrop Spectrophotometer, ranged in between of 7.0 and 12.0 ng/µl with $A_{260/280}$ ratios in between 1.63 and 2.38, thus indicating the high quality of the PCR product.

5.4.3 Confirming EAPM -DNA Probe Modification

The biomodification of the EAPM NPs with DNA probes (Ph-PRO) was confirmed

by fluorescence and spectrophotometric studies. Figure 5-19 shows the fluorescence

intensity measurements of the pure 6-FAM labeled Ph-PRO probe solution [22.5μM] and

that of the unreacted probes remaining in the supernatant after magnetic separation of the

PRO-EAPMs (probe labeled EAPMs) by excitation at 495 nm and detection of emission

at 520 nm for four different EAPM NP concentrations (0.1, 1, 10 and 20 mg/ml). As

evident in the figure, the 6-FAM labelled Ph-PRO probes (pure probe) show the highest

fluorescence signal since there are no EAPM NPs present in the solution. In comparison,

the supernatant obtained from magnetic separation of the PRO-EAPMs after the labeling

study using different EAPM NP concentrations show significantly lower fluorescence

signal than that of the pure probe thus indicating the attachment of the probes to the NPs.

A linear decrease in the fluorescence signal is also observed as the NP concentration

increases from 0.1 to 20 mg/ml which is expected since an increased EAPM NP

concentration would result in a greater number of attachment sites (terminal amine

groups of polyaniline) for the phosphorylated probes. The single-stranded DNA (ss-

DNA) concentration measurements of the pure probes and the supernatants using the

NanoDrop spectrophotometer further confirmed the attachment of the probes to the

EAPM NPs. As observed in figure 5-19, the ss-DNA concentration for the pure probe is

385.2 ng/ul, whereas for the supernatants from PRO-EAPMs, the ss-DNA concentration

decreases and is in the range of 310.2 and 0 ng/ul. From the fluorescence and the

absorbance results, an EAPM concentration of 1 mg/ml was chosen for subsequent

hybridization studies, since at this concentration, the EAPM NPs were saturated with

adequate concentrations of the DNA probes required for hybridization with the target DNA.
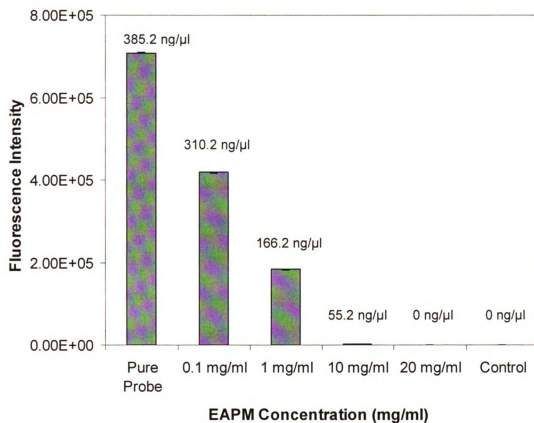
Figure 5-19. Fluorescence signal of pure Ph-PRO probes and unreacted Ph-PRO probes after magnetic separation from the EAPM NPs.

5.4.4 EAPM Based Electrochemical DNA Biosensor Detection Concept

Figure 5-20 is a schematic representation of the detection mechanism of the EAPM based electrochemical DNA biosensor. The detection principle involves an electrochemical sandwich assay engaging a detector DNA probe and a capture DNA probe. The detector probe is labeled with EAPM NPs whereas the capture probe is labeled with biotin. Both the EAPM labeled detector probe and biotinylated capture probe are first added to the target sequence, where the target undergoes sandwiched hybridization with both probes. The EAPM-target-biotin DNA hybrids thus formed are separated from other noncomplementary sequences and unreacted DNA by magnetic separation of the EAPM NPs. The EAPM-target-biotin DNA hybrids are then added directly to the surface of streptavidin modified screen printed electrodes for anchoring the hybrids on the electrode surface by streptavidin-biotin interactions. After a short incubation period, the electrode surface is washed to remove the excess EAPM NPs and the unbound DNA hybrids. The target DNA is finally detected on the SPCE biosensor surface by the redox activity of the EAPM NPs using cyclic voltammetry.
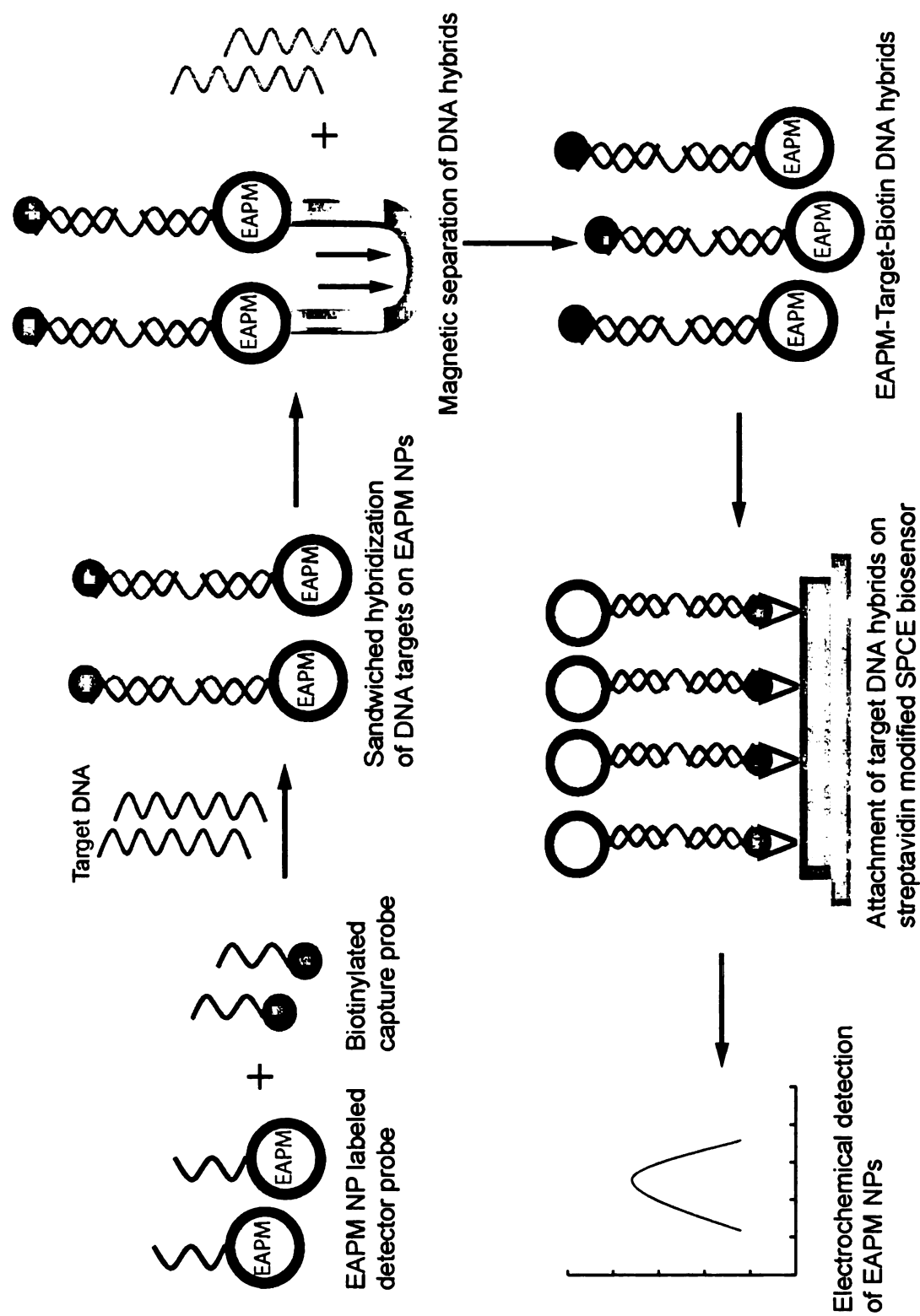
Figure 5-20. Schematic representation of the EAPM based electrochemical DNA biosensor for detecting *B. anthracis pag* gene.

5.5   OBJECTIVE 5

DNA hybridization on EAPM NPs and sensitivity and specificity evaluation of the

EAPM based electrochemical DNA biosensor.

5.5.1   Sandwiched Hybridization of DNA Targets on EAPM NPs

5.5.1.1 Determination of Hybridization Conditions

The EAPM labeled detector probes (PRO-EAPMs) were hybridized with the target

DNA obtained from the PCR product. The optimum temperature required for the

hybridization reaction was determined by fluorescence assays using 6-FAM labeled PCR

products ($\lambda_{excitation}$: 495 nm, $\lambda_{emission}$: 520 nm). To determine the optimum temperature,

the hybridization reaction was performed for 1 hour at three different temperatures: at 25

°C (room temperature), at 45 °C (25 °C below the melting temperature, T_m, of the Ph-

PRO probe) and at 55°C (15 °C below the T_m of the probe). Figure 5-21 shows the

normalized fluorescence intensity of the DNA targets obtained from PCR reaction before

and after hybridization with the PRO-EAPMs at the three different temperatures. At each

temperature, the fluorescence signal of the PCR target is normalized against the PCR

negative control to eliminate the effect of any background fluorescence.

It is evident from figure 5-21 that the highest decrease in fluorescence signal for the

PCR target DNA is observed at 45 °C with the reduction in normalized fluorescence

being 11448 ± 106.4 counts/0.1 s. This is expected since a hybridization temperature 25

°C below the T_m (T_m of Ph-PRO probe is 70.4°C) allows the maximum rate of

hybridization (Mehlen *et al.*, 2004). For the hybridization studies at 25 °C and 55 °C, the

reduction in normalized fluorescence are only 5030 ± 117.5 and 448 ± 110.9 counts/0.1 s,

respectively. Therefore, the hybridization temperature was kept at 45 ℃ for subsequent studies.
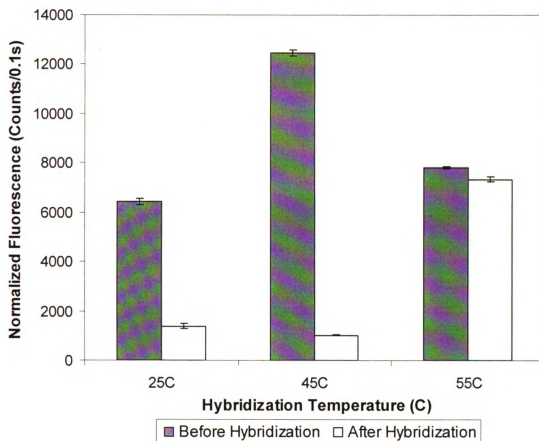
Figure 5-21. Normalized fluorescence signal of PCR DNA targets before and after hybridization at different hybridization temperatures.

In order to ensure a fast hybridization reaction between the target DNA and the Ph-PRO probe labeled EAPM NPs (PRO-EAPMs), the hybridization time was optimized by fluorescence assays using 6-FAM labeled PCR products. The DNA hybridization reaction was performed for 30 min, 1 h and 2 h at 45 ℃. Figure 5-22 shows the normalized fluorescence intensity (background subtracted) of the PCR targets before and after hybridization with the PRO-EAPMs at three different times. As observed in the

figure, the decrease in the fluorescence signals of the PCR targets after the hybridization event are almost the same for the three hybridization times trialed. The reduction in the normalized fluorescence values for hybridization times of 30 min, 1 h, and 2 h are 10862 ± 107.6, 10380 ± 64.5, and 10226 ± 300.8 counts/0.1s, respectively. Thus, the hybridization time was limited to 30 min in the succeeding studies.
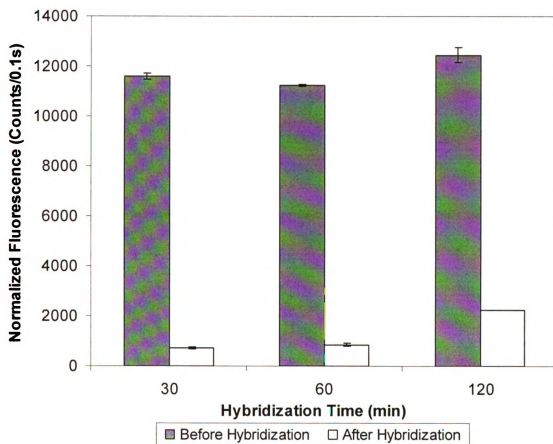
Figure 5-22. Normalized fluorescence signal of PCR DNA targets before and after hybridization at different hybridization times.

5.5.1.2 Confirming Sandwiched Hybridization on EAPM NPs

The sandwiched hybridization of the PCR targets with the EAPM labeled detector probe (PRO-EAPMs) and the biotinylated capture probe (PRO-Bio) was confirmed by

fluorescent assays using 6-FAM labeled PRO-Bio probes ($\lambda_{excitation}$: 495 nm, $\lambda_{emission}$: 520 nm). The hybridization temperature and time was fixed at 45°C and 30 min, respectively, to ensure maximum hybridization of the targets with the detector probes. Three different concentrations of the PRO-Bio probes (1μM, 5μM, and 10μM) were trialed in the sandwich hybridization event. Figure 5-23 shows a comparison of the change in fluorescence signal of the PRO-Bio probes in the presence and absence of the PCR targets during the sandwiched hybridization.
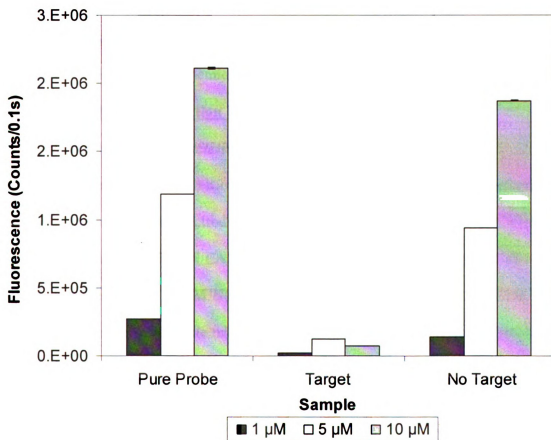
Figure 5-23. Change in fluorescence of PRO-Bio probes in the presence and absence of PCR targets during sandwiched hybridization.

As evident in Figure 5-23, the fluorescence signal of the PRO- Bio probes reduces by an order of magnitude in the presence of the PCR targets during the dual hybridization process for all three probe concentrations. This signal reduction confirms the successful sandwiched hybridization of the biotinylated capture probes with the PCR targets. In the absence of the PCR targets, a small decrease in fluorescence is observed at all capture probe concentrations. This can be attributed to mild bleaching of the fluorescent labels during the stringent hybridization and washing procedures. From the above results a PRO-Bio probe concentration of 5μM was fixed for the successive detection experiments and the resulting EAPM-target-biotin DNA hybrids from the sandwiched hybridization were used directly for electrochemical detection.

5.5.2 Electrochemical Detection Using SPCE Biosensor

5.5.2.1 Electrochemical Characterization of EAPM NPs

Electrochemical characterization of the synthesized EAPM NPs was performed on the screen printed carbon electrodes (SPCEs) using cyclic voltammetry (CV) before proceeding to the detection of EAPM captured DNA hybrids. Figure 5-24 shows the cyclic voltammogram of EAPM NPs in 0.1 M HCl scanned from -0.4 V to 1.0 V at a scan rate of 20 mV/s. Two stable redox peaks are observed in the voltammogram that can be related to the presence of the polymer, polyaniline, in the EAPM samples. The anodic peaks at 0.12 V and 0.59 V correspond to the switching of the leucoemeraldine base to emeraldine salt and emeraldine to pernigraniline salt respectively (Arora *et al.*, 2007;Gospodinova *et al.*, 1996). The corresponding cathodic peaks for the reduction process are observed at 0.53 V and -0.07 V, respectively.

Figure 5-25 shows the effect of scan rate on the rate of electron transfer to the SPCE electrodes by the EAPM NPs. The two characteristic redox peaks of the EAPM NPs are visible at all scan rates. With an increase in the scan rate, the anodic peak potential of the EAPM NPs is shifted to a more positive value and the cathodic peak potential is shifted to a negative direction. Figure 5-25 (inset) shows a plot of the dependence of the anodic peak current and the cathodic peak current versus the scan rate. As observed in the figure, the peak currents exhibits a linear relationship with increasing scan rate thus suggesting surface controlled behavior and diffusion controlled system (Bard and Faulkner, 2001). However, the ratio of the peak currents at different scan rates $I_{pa}/I_{pc} \neq 1$ which indicates a quasi-reversible chemistry of the EAPM NPs and the SPCE electrode process (Bard and Faulkner, 2001;Ram et al., 1999).
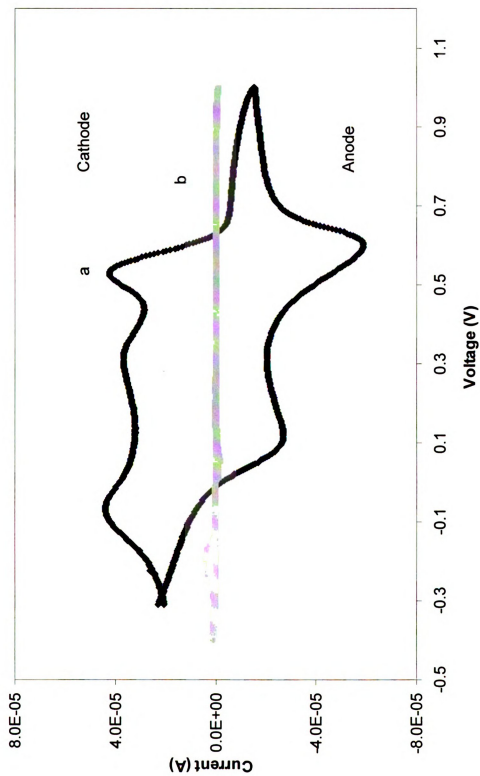
Figure 5-24. Cyclic voltammograms of (a) EAPM NPs on SPCE and (b) bare SPCE in 0.1M HCl at 20 mV/s.
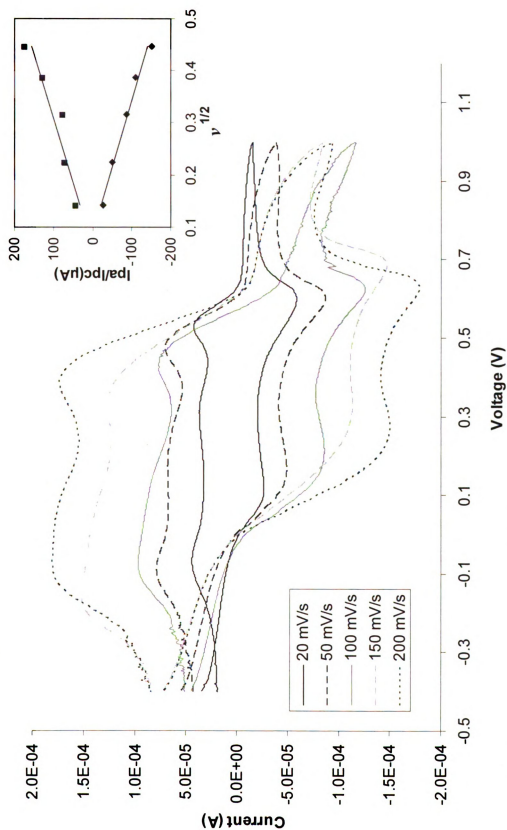
Figure 5-25. Cyclic voltammograms of EAPM NPs in 0.1M HCl at scan rates of 20, 50, 100, 150 and 200 mV/s. Inset- Plots of anodic and cathodic peak current vs. scan rate.

5.5.2.2 Detection of EAPM-Target-Biotin DNA Hybrids

Following the sandwiched hybridization of the PCR DNA targets with the EAPM-PRO probes and the PRO-Bio probes, the EAPM-target-biotin DNA hybrids were directly detected electrochemically on the SPCE electrodes. Figure 5-26 shows the electrochemical response of the EAPM captured target DNA hybrids from undiluted PCR products (concentration-7.3ng/µl) on the SPCE electrode. The electrochemical responses of the bare SPCEs and streptavidin modified SPCEs were compared as control. As observed in the figure, the cyclic voltammogram of the EAPM captured targets shows the two characteristic redox peaks of the EAPM NPs that were absent in the control. The anodic peak potentials are located at 0.12 V and 0.59 V, whereas the cathodic peak potentials are located at 0.53 V and -0.09 V, similar to the CV response obtained with just EAPM NPs in 0.1M HCl. The CV response demonstrates the fact that the EAPM NPs maintained their native electrochemical behavior after the probe labeling and sandwiched target hybridization procedures. The appearance of the EAPM redox peaks in the CV response of the PCR targets also confirms the successful capture of the EAPM-target DNA-biotin hybrids and detection of the EAPM NPs on the streptavidin modified SPCE electrodes.
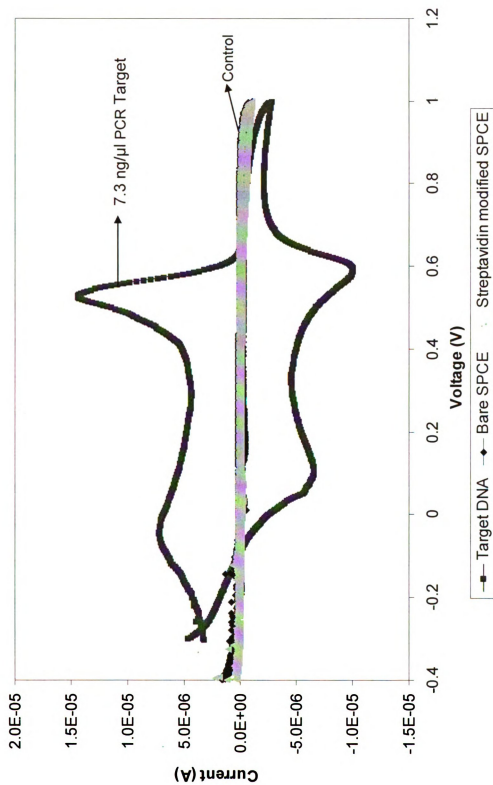
Figure 5-26. Electrochemical responses of EAPM captured target DNA hybrids on SPCE, of bare SPCE, and of streptavidin modified SPCE in 0.1M HCl at 20 mV/s.

5.5.3   SPCE Biosensor Sensitivity Study

The sensitivity of the EAPM based SPCE biosensor was estimated in different concentrations of the PCR target DNA obtained by serially diluting the PCR product. Figure 5-27 shows the electrochemical response (cyclic voltammograms) of the biosensor in PCR target concentrations ranging from 10 ng/μl to 1 pg/μl and the control. The control consists of just EAPM NPs with no PCR target (shown as 0 ng/μl in the figure). As observed in the CV response, the two characteristic redox peaks of the EAPM NPs are present in different concentrations of the PCR target. A gradual decrease in the intensity of the redox peaks is also noted with a decrease in the target concentration. This is expected since a lower concentration of the target would result in lower concentration of the EAPM-target DNA-biotin hybrids bound on the streptavidin coated electrode. The presence of the EAPM redox peaks at lower target concentrations also shows that the EAPM NPs are capable of generating redox signals at very low concentrations.

Although both redox peaks of EAPM NPs are evident at lower target concentrations, the anodic peak current (oxidation peak) at an anodic peak potential of 0.59V was chosen for further analysis due to the minimal shift observed in the peak current in repeated observations at this peak potential. Figure 5-28 shows a plot of the anodic (oxidation) current in the potential range of 0.3 V to 0.7V obtained from the cyclic voltammograms of the different PCR target concentrations and the control.
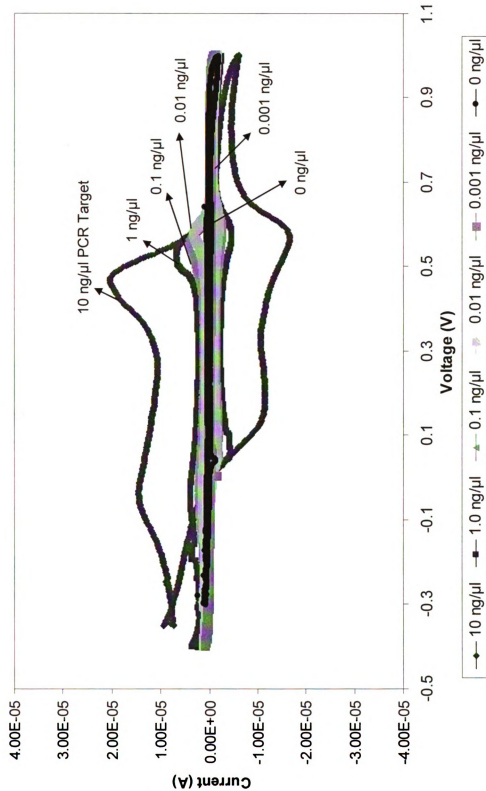
Figure 5-27. Cyclic voltammograms of the EAPM based SPCE biosensor for different concentrations of PCR target DNA in 0.1M HCl at a scan rate of 20 mV/s.
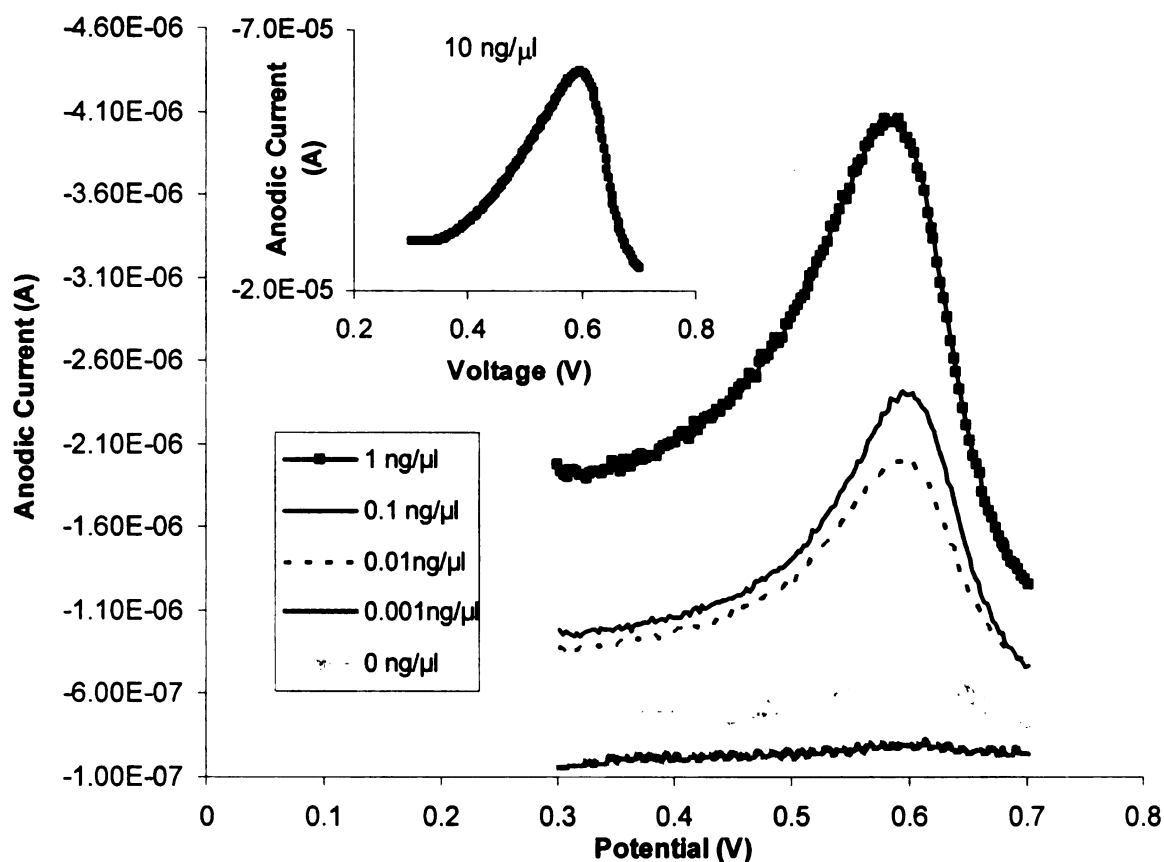
Figure 5-28. Anodic (oxidation) peaks of PCR target concentrations ranging from 1 ng/µl to 0 ng/µl. Inset- anodic peak of 10 ng/µl PCR target (obtained from cyclic voltammograms).

As evident in Figure 5-28 (Inset), the anodic peak current at 0.59 V is maximum (62µA) for the highest PCR target concentration (10ng/µl) and decreases from 62µA to 2 µA as the PCR target concentration decreases from 10 to 0.01 ng/µl. The anodic peak currents for the control and for a target concentration of 0.001 ng/µl are 0.84 and 0.29 µA, respectively. The higher current values of the control than 0.001 ng/µl of the target indicate that there is no detection at this concentration and the peak current signal is generated by the nonspecifically adsorbed EAPM NPs on the electrode surface for both cases.
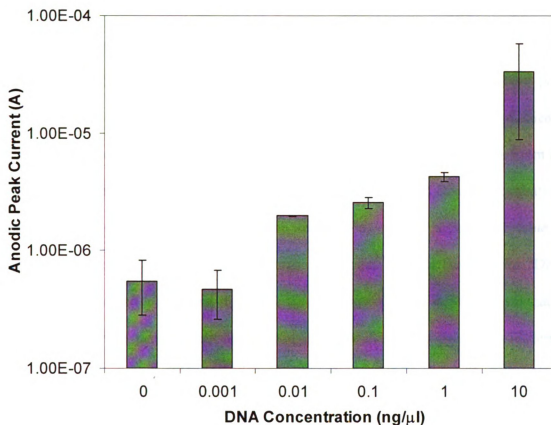
Figure 5-29. CV mediated anodic peak current at different PCR target concentrations from three experimental trials (mean current ± SD, n = 3).

Figure 5-29 shows the mean anodic peak current of different concentrations of PCR targets obtained from three experimental trials of the EAPM based SPCE biosensor. It is evident from the above figure that the mean anodic peak current for the SPCE biosensor increases with increasing target concentration. A linear increase in the anodic current is observed for target concentrations between 0.01 and 1 ng/µl which is followed by an exponential increase in the anodic current at the highest target concentration of 10 ng//µl. It is also noted that the lowest PCR target concentration for which the mean anodic peak current can be differentiated from that of the control is 0.01 ng/µl. Based on these results

from the cyclic voltammetry experiments, the lowest detection limit of the EAPM based SPCE biosensor is determined to be 0.01 ng/µl of PCR DNA.

To confirm the sensitivity results obtained from CV response, the anodic peak current signal of the biosensor for the different PCR concentrations were statistically analyzed by one-way ANOVA using the SAS software (results in Appendix A). From the tests of fixed effects table (Table A-21), it is evident that the PCR DNA concentrations have significant effect ($P < 0.0001$) on the anodic peak current signal. The table of estimates (Table A-22) further shows that the peak current values for DNA concentrations ranging from 10 ng/µl to 0.01 ng/µl are significantly different from that of control, whereas, the peak current at 0.001 ng/µl of DNA is not significantly different from the control ($P = 0.6943$). Thus, the statistical analysis results affirm the SPCE biosensor sensitivity to be 0.01 ng/µl of PCR DNA. Furthermore, the differences of least squares means table (Table A-24) shows that the anodic peak current signal is significantly different for different DNA concentrations ($P \leq 0.05$) thus indicating that the SPCE biosensor is quantitative for the range of DNA concentrations tested.

Results of the SPCE DNA biosensor conclude that EAPM nanoparticles can be successfully used as a redox indicator in biosensor detection systems. This is a unique approach for DNA detection that has not been investigated in current literature and its potential needs to be explored in future studies. Other studies have reported DNA detection on polyaniline modified electrodes using redox indicators such as methylene blue and duanorubicin (Arora et al., 2007;Chang et al., 2007a).

5.5.4 Specificity Analysis

The specificity of the detector probe labeled EAPM NPs (Pro-EAPMs) was evaluated by fluorescence assays using 6-FAM labeled noncomplementary sequence (NC). The NC sequence was designed from the *cap A* gene of *Bacillus anthracis*. Theoretical alignment of the NC sequence with the detector probe sequence using the BLAST analysis tool indicated no significant similarity between the sequences.

Figure 5-30 shows fluorescence results before and after hybridization of the Pro-EAPMs with the 6-FAM labeled NC sequences at three different concentrations ($1\mu M$, $5\mu M$ and $10\ \mu M$). As evident in the figure, a small decrease in the fluorescence signal is observed for the 6-FAM labeled NC sequences at the three concentrations tested after hybridization with the Pro-EAPMs. This can be attributed to the occurrence of small amounts of cross reactions between the detector probe and the NC sequence as both sequences were designed from the same microorganism. Although theoretical results (BLAST analysis) indicated highly dissimilar sequences but such ideal conditions are hard to achieve in real samples. However, the reduction in fluorescence signal for the NC sequences were not significant as none of the concentrations showed a decrease in fluorescence intensity by an order of magnitude. Therefore, specificity studies with different noncomplementary sequences designed from different microorganisms are required in future for further specificity analysis.
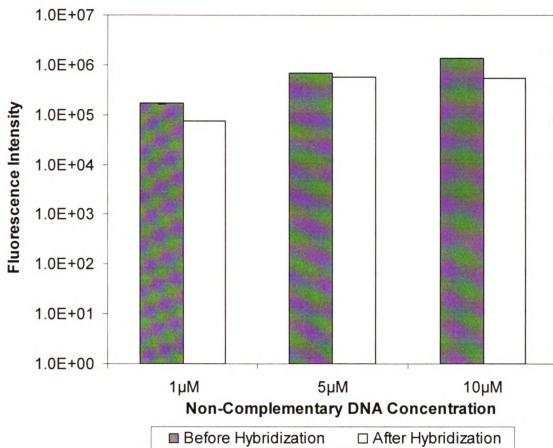
Figure 5-30. Change in fluorescence intensity of non-complementary sequences before and after sandwiched hybridization on EAPM NPs.

CHAPTER 6: CONCLUSION AND FUTURE RESEARCH

In this dissertation the potential of electrically active polyaniline coated magnetic nanoparticles (EAPM) as a novel nanostructured transducer and as a magnetic concentrator was explored for biosensor applications. The five major objectives of this research describe synthesis and characterization studies of the EAPM nanoparticles, fabrication and implementation of an EAPM nanoparticle based immunosensor, and fabrication and implementation of an EAPM based DNA biosensor.

The EAPM nanoparticles were synthesized by a chemical polymerization method using γ-Fe_2O_3 nanoparticles and the monomer aniline. DC Squid magnetism and Four point probe conductivity studies showed that the synthesized nanoparticles were in the ferromagnetic regime and had room temperature electrical conductivity as high as 2.4 S/cm. TEM analysis indicated that the nanoparticle size was related to polymer concentration and SEM EDS analysis as well as UV-VIS spectral analysis further confirmed the presence of the polymer in the EAPM nanoparticles in the doped or conductive state.

An integrated antibody based biosensor (immunosensor) using EAPM nanoparticles as an immunomagnetic concentrator and transducer was designed and fabricated. The fabricated biosensor was implemented in the detection of *B. anthracis* Sterne spores. The detection process was fast and included a magnetic concentration time of 10 min and signal detection time of 6 min. A comparison study showed that the 1:0.6 EAPM nanoparticles performed better in the detection system and hence was chosen for successive experiments. The EAPM based immunosensor had a lower detection limit of 4.2×10^2 *B. anthracis* spores/ml in pure spore suspensions that was well below the

reported ID 50 for *B. anthracis*. The immunosensor sensitivity was also evaluated in food matrices and was found to be $4.2 \times 10^2/4.2 \times 10^3$ spores/ml. Specificity analysis indicated no cross reactivity in the sensor signal with non-target pathogens such as *E. coli* and *S. Enteritidis*. Capture efficiency (CE) experiments using EAPM nanoparticles confirmed successful immunomagnetic concentration of the target pathogens with the highest CE value of 97% in concentrations as low as 10^1 spores/ml.

A DNA biosensor was developed based on sandwiched hybridization of DNA targets on probe labeled EAPM nanoparticles and electrochemical detection of the hybridization process through the redox signal of EAPM nanoparticles. The EAPM based DNA biosensor was fabricated and implemented in the detection of *B. anthracis pag A* gene. Fluorescence assays confirmed the sandwiched hybridization of PCR amplified DNA targets with EAPM labeled detector probes and biotinylated capture probes. The EAPM DNA biosensor was able to detect *B. anthracis* DNA with a lower detection limit of 0.01 ng/µl of PCR amplified targets. The electrochemical detection process was completed in 60 min.

In summary, this research shows the feasibility of using EAPM nanoparticles for magnetic concentration and biosensor transduction in more than one detection system. Table 6-1 compiles the specifications of the two different EAPM nanoparticle based biosensors that were developed.

163

Table 6-1. Specifications of EAPM based biosensors.

Parameters	Immunosensor	DNA sensor
Detection mechanism	Charge transfer resistance	Redox activity
Target	*B. anthracis* spores	*B. anthracis pag A* gene
Lower detection limit	4.2×10^2 spores/ml	0.01 ng/μl PCR DNA
Range of Detection	10^2 to 10^7 spores/ml	10 - 0.01 ng/μl
Detection time	16 min	60 min
Specificity	Specific	Specific

Future research should be directed toward a number of different activities: (1) synthesizing uniform EAPM nanostructures with excellent electrical and magnetic properties and minimum nanoparticle aggregation; (2) advancing the EAPM based immunosensor toward quantitative evaluation of samples; (3) implementing the DNA based biosensor in detection of genomic DNA for field based applications; (4) exploring different techniques for electrochemical detection of EAPM nanostructures; (5) advancing EAPM nanostructures as an efficient magnetic concentrator; (6) developing EAPM nanostructure based biosensors for different targets , and (6) developing low-cost EAPM based magnetic detection devices.

APPENDIX A: STATISTICAL ANALYSIS RESULTS

A.1   ANOVA ANALYSIS OF DIFFERENT EAPM BASED IMMUNOSENSORS

The Mixed Procedure

Table A-1. Type 3 Tests of Fixed Effects

Effect	Num DF	Den DF	F Value	Pr > F
Concentration	3	128	31.73	<.0001
Sample	3	128	22.89	<.0001
Sample*Concentration	9	128	5.47	<.0001

Table A-2. Tests of Effect Slices

Effect	Conc.	Sample	Num DF	Den DF	F Value	Pr > F
Sample*Concentration	10^1		3	128	14.29	<.0001
Sample*Concentration	10^4		3	128	8.88	<.0001
Sample*Concentration	10^7		3	128	0.43	0.7351
Sample*Concentration	Control		3	128	15.71	<.0001
Sample*Concentration		1 : 0.1	3	128	17.14	<.0001
Sample*Concentration		1 : 0.4	3	128	5.81	0.0009
Sample*Concentration		1 : 0.6	3	128	24.89	<.0001
Sample*Concentration		1 : 0.8	3	128	0.3	0.8227

Table A-3. Estimates

Label	Estimate	Standard Error	DF	t Value	Pr > |t|
10^1 vs. Control for sample 0.1	38.8	35.7967	128	1.08	0.2804
10^4 vs. Control for sample 0.1	-27.9444	35.7967	128	-0.78	0.4365
10^7 vs. Control for sample 0.1	-198.67	35.7967	128	-5.55	<.0001
10^1 vs. Control for sample 0.4	-31.4889	35.7967	128	-0.88	0.3807
10^4 vs. Control for sample 0.4	-81.5222	35.7967	128	-2.28	0.0244
10^7 vs. Control for sample 0.4	-139.53	35.7967	128	-3.9	0.0002
10^1 vs. Control for sample 0.6	-105.82	35.7967	128	-2.96	0.0037
10^4 vs. Control for sample 0.6	-244.7	35.7967	128	-6.84	<.0001
10^7 vs. Control for sample 0.6	-270.57	35.7967	128	-7.56	<.0001
10^1 vs. Control for sample 0.8	-21.8556	35.7967	128	-0.61	0.5426
10^4 vs. Control for sample 0.8	-26.0778	35.7967	128	-0.73	0.4676
10^7 vs. Control for sample 0.8	-31.9667	35.7967	128	-0.89	0.3735

Table A-4. Least Squares Means

Effect	Conc.	Sample	Estimate	Standard Error	DF	t Value	Pr >|t|
Sample*Conc.	10^1	0.1	308.4	25.3121	128	12.18	<.0001
Sample*Conc.	10^4	0.1	241.66	25.3121	128	9.55	<.0001
Sample*Conc.	10^7	0.1	70.9333	25.3121	128	2.8	0.0059
Sample*Conc.	Control	0.1	269.6	25.3121	128	10.65	<.0001
Sample*Conc.	10^1	0.4	210.46	25.3121	128	8.31	<.0001
Sample*Conc.	10^4	0.4	160.42	25.3121	128	6.34	<.0001
Sample*Conc.	10^7	0.4	102.41	25.3121	128	4.05	<.0001
Sample*Conc.	Control	0.4	241.94	25.3121	128	9.56	<.0001
Sample*Conc.	10^1	0.6	233.6	25.3121	128	9.23	<.0001
Sample*Conc.	10^4	0.6	94.7222	25.3121	128	3.74	0.0003
Sample*Conc.	10^7	0.6	68.8556	25.3121	128	2.72	0.0074
Sample*Conc.	Control	0.6	339.42	25.3121	128	13.41	<.0001
Sample*Conc.	10^1	0.8	78.7	25.3121	128	3.11	0.0023
Sample*Conc.	10^4	0.8	74.4778	25.3121	128	2.94	0.0039
Sample*Conc.	10^7	0.8	68.5889	25.3121	128	2.71	0.0077
Sample*Conc.	Control	0.8	100.56	25.3121	128	3.97	0.0001

Table A-5. Differences of Least Squares Means

Effect	Sample	Conc.	_Conc.	Estimate	Standard Error	DF	t Value	Pr > |t|
Sample*Conc.	0.1	10^1	10^4	66.7444	35.7967	128	1.86	0.0645
Sample*Conc.	0.1	10^1	10^7	237.47	35.7967	128	6.63	<.0001
Sample*Conc.	0.1	10^1	Control	38.8	35.7967	128	1.08	0.2804
Sample*Conc.	0.1	10^4	10^7	170.72	35.7967	128	4.77	<.0001
Sample*Conc.	0.1	10^4	Control	-27.9444	35.7967	128	-0.78	0.4365
Sample*Conc.	0.1	10^7	Control	-198.67	35.7967	128	-5.55	<.0001
Sample*Conc.	0.4	10^1	10^4	50.0333	35.7967	128	1.4	0.1646
Sample*Conc.	0.4	10^1	10^7	108.04	35.7967	128	3.02	0.0031
Sample*Conc.	0.4	10^1	Control	-31.4889	35.7967	128	-0.88	0.3807
Sample*Conc.	0.4	10^4	10^7	58.0111	35.7967	128	1.62	0.1076
Sample*Conc.	0.4	10^4	Control	-81.5222	35.7967	128	-2.28	0.0244
Sample*Conc.	0.4	10^7	Control	-139.53	35.7967	128	-3.9	0.0002
Sample*Conc.	0.6	10^1	10^4	138.88	35.7967	128	3.88	0.0002
Sample*Conc.	0.6	10^1	10^7	164.74	35.7967	128	4.6	<.0001
Sample*Conc.	0.6	10^1	Control	-105.82	35.7967	128	-2.96	0.0037
Sample*Conc.	0.6	10^4	10^7	25.8667	35.7967	128	0.72	0.4712
Sample*Conc.	0.6	10^4	Control	-244.7	35.7967	128	-6.84	<.0001
Sample*Conc.	0.6	10^7	Control	-270.57	35.7967	128	-7.56	<.0001
Sample*Conc.	0.8	10^1	10^4	4.2222	35.7967	128	0.12	0.9063
Sample*Conc.	0.8	10^1	10^7	10.1111	35.7967	128	0.28	0.778
Sample*Conc.	0.8	10^1	Control	-21.8556	35.7967	128	-0.61	0.5426
Sample*Conc.	0.8	10^4	10^7	5.8889	35.7967	128	0.16	0.8696
Sample*Conc.	0.8	10^4	Control	-26.0778	35.7967	128	-0.73	0.4676
Sample*Conc.	0.8	10^7	Control	-31.9667	35.7967	128	-0.89	0.3735

A.2   ANOVA ANALYSIS FOR IMMUNOSENSOR SENSITIVITY

The Mixed Procedure

Table A-6. Type 3 Tests of Fixed Effects

Effect	Num DF	Den DF	F Value	Pr > F
Concentration	8	54	10.32	<.0001
Time	2	54	0.34	0.7122
Concentration*Time	16	54	0.25	0.9983

Table A-7. Estimates

Label	Estimate	Error	DF	t Value	Pr > |t|
10^1 vs. Control	-23.8222	39.0112	54	-0.61	0.544
10^2 vs. Control	-139.83	39.0112	54	-3.58	0.0007
10^3 vs. Control	-186.43	39.0112	54	-4.78	<.0001
10^4 vs. Control	-162.7	39.0112	54	-4.17	0.0001
10^5 vs. Control	-174.7	39.0112	54	-4.48	<.0001
10^6 vs. Control	-191.94	39.0112	54	-4.92	<.0001
10^7 vs. Control	-188.57	39.0112	54	-4.83	<.0001

Table A-8. Least Squares Means

Effect	Conc.	Estimate	Standard Error	DF	t Value	Pr > |t|
Conc.	10^1	233.6	27.5851	54	8.47	<.0001
Conc.	10^2	117.59	27.5851	54	4.26	<.0001
Conc.	10^3	70.9889	27.5851	54	2.57	0.0128
Conc.	10^4	94.7222	27.5851	54	3.43	0.0012
Conc.	10^5	82.7222	27.5851	54	3	0.0041
Conc.	10^6	65.4778	27.5851	54	2.37	0.0212
Conc.	10^7	68.8556	27.5851	54	2.5	0.0156
Conc.	Control	257.42	27.5851	54	9.33	<.0001

Table A-9. Differences of Least Squares Means

Effect	Conc.	_Conc.	Estimate	Standard Error	DF	t Value	Pr > |t|
Conc.	10^1	10^2	116.01	39.0112	54	2.97	0.0044
Conc.	10^1	10^3	162.61	39.0112	54	4.17	0.0001
Conc.	10^1	10^4	138.88	39.0112	54	3.56	0.0008
Conc.	10^1	10^5	150.88	39.0112	54	3.87	0.0003
Conc.	10^1	10^6	168.12	39.0112	54	4.31	<.0001
Conc.	10^1	10^7	164.74	39.0112	54	4.22	<.0001
Conc.	10^1	Control	-23.8222	39.0112	54	-0.61	0.544
Conc.	10^2	10^3	46.6	39.0112	54	1.19	0.2375
Conc.	10^2	10^4	22.8667	39.0112	54	0.59	0.5602
Conc.	10^2	10^5	34.8667	39.0112	54	0.89	0.3754
Conc.	10^2	10^6	52.1111	39.0112	54	1.34	0.1872
Conc.	10^2	10^7	48.7333	39.0112	54	1.25	0.217
Conc.	10^2	Control	-139.83	39.0112	54	-3.58	0.0007
Conc.	10^3	10^4	-23.7333	39.0112	54	-0.61	0.5455
Conc.	10^3	10^5	-11.7333	39.0112	54	-0.3	0.7647
Conc.	10^3	10^6	5.5111	39.0112	54	0.14	0.8882
Conc.	10^3	10^7	2.1333	39.0112	54	0.05	0.9566
Conc.	10^3	Control	-186.43	39.0112	54	-4.78	<.0001
Conc.	10^4	10^5	12	39.0112	54	0.31	0.7596
Conc.	10^4	10^6	29.2444	39.0112	54	0.75	0.4567
Conc.	10^4	10^7	25.8667	39.0112	54	0.66	0.5101
Conc.	10^4	Control	-162.7	39.0112	54	-4.17	0.0001
Conc.	10^5	10^6	17.2444	39.0112	54	0.44	0.6602
Conc.	10^5	10^7	13.8667	39.0112	54	0.36	0.7236
Conc.	10^5	Control	-174.7	39.0112	54	-4.48	<.0001
Conc.	10^6	10^7	-3.3778	39.0112	54	-0.09	0.9313
Conc.	10^6	Control	-191.94	39.0112	54	-4.92	<.0001
Conc.	10^7	Control	-188.57	39.0112	54	-4.83	<.0001

A.3   ANOVA ANALYSIS FOR IMMUNOSENSOR SPECIFICITY

The Mixed Procedure

Table A-10. Type 3 Tests of Fixed Effects

Effect	Num DF	Den DF	F Value	Pr > F
Pathogen	1	96	2.07	0.1537
Concentration	5	96	0.72	0.6084
Pathogen*Concentration	5	96	0.83	0.5284

Table A-11. Estimates

Label	Estimate	Standard Error	DF	t Value	Pr > |t|
10^1 vs. Control for *E. coli*	-50.8222	34.6163	96	-1.47	0.1453
10^2 vs. Control for *E. coli*	7.0167	34.6163	96	0.2	0.8398
10^3 vs. Control for *E. coli*	-38.4889	34.6163	96	-1.11	0.269
10^4 vs. Control for *E. coli*	-54.7333	34.6163	96	-1.58	0.1171
10^5 vs. Control for *E. coli*	-50.7111	34.6163	96	-1.46	0.1462
10^1 vs. Control for *S.* Enteritidis	-9.4778	34.6163	96	-0.27	0.7848
10^2 vs. Control for *S.* Enteritidis	-0.4111	34.6163	96	-0.01	0.9905
10^3 vs. Control for *S.* Enteritidis	-16.4333	34.6163	96	-0.47	0.6361
10^4 vs. Control for *S.* Enteritidis	0.9667	34.6163	96	0.03	0.9778
10^5 vs. Control for *S.* Enteritidis	22.3	34.6163	96	0.64	0.521

A.4 ANOVA ANALYSIS FOR LETTUCE TESTING

The Mixed Procedure

Table A-12. Type 3 Tests of Fixed Effects

Effect	Num DF	Den DF	F Value	Pr > F
Concentration	7	64	25.37	<.0001

Table A-13. Least Squares Means

Effect		Estimate	Standard Error	DF	t Value	Pr > |t|
Concentration	10^1	290.86	16.1587	64	18	<.0001
Concentration	10^2	123.69	16.1587	64	7.65	<.0001
Concentration	10^3	99.7889	16.1587	64	6.18	<.0001
Concentration	10^4	132.66	16.1587	64	8.21	<.0001
Concentration	10^5	150.48	16.1587	64	9.31	<.0001
Concentration	10^6	99.1	16.1587	64	6.13	<.0001
Concentration	10^7	102.37	16.1587	64	6.34	<.0001
Concentration	Control	288.23	16.1587	64	17.84	<.0001

Table A-14. Differences of Least Squares Means

Effect	Conc.	_Conc.	Estimate	Standard Error	DF	t Value	Pr > |t|
Conc.	10^1	10^2	167.17	22.8518	64	7.32	<.0001
Conc.	10^1	10^3	191.07	22.8518	64	8.36	<.0001
Conc.	10^1	10^4	158.2	22.8518	64	6.92	<.0001
Conc.	10^1	10^5	140.38	22.8518	64	6.14	<.0001
Conc.	10^1	10^6	191.76	22.8518	64	8.39	<.0001
Conc.	10^1	10^7	188.49	22.8518	64	8.25	<.0001
Conc.	10^1	Control	2.6222	22.8518	64	0.11	0.909
Conc.	10^2	10^3	23.9	22.8518	64	1.05	0.2996
Conc.	10^2	10^4	-8.9667	22.8518	64	-0.39	0.6961
Conc.	10^2	10^5	-26.7889	22.8518	64	-1.17	0.2454
Conc.	10^2	10^6	24.5889	22.8518	64	1.08	0.286
Conc.	10^2	10^7	21.3222	22.8518	64	0.93	0.3543
Conc.	10^2	Control	-164.54	22.8518	64	-7.2	<.0001
Conc.	10^3	10^4	-32.8667	22.8518	64	-1.44	0.1552
Conc.	10^3	10^5	-50.6889	22.8518	64	-2.22	0.0301
Conc.	10^3	10^6	0.6889	22.8518	64	0.03	0.976
Conc.	10^3	10^7	-2.5778	22.8518	64	-0.11	0.9105
Conc.	10^3	Control	-188.44	22.8518	64	-8.25	<.0001
Conc.	10^4	10^5	-17.8222	22.8518	64	-0.78	0.4383
Conc.	10^4	10^6	33.5556	22.8518	64	1.47	0.1469
Conc.	10^4	10^7	30.2889	22.8518	64	1.33	0.1897
Conc.	10^4	Control	-155.58	22.8518	64	-6.81	<.0001
Conc.	10^5	10^6	51.3778	22.8518	64	2.25	0.028
Conc.	10^5	10^7	48.1111	22.8518	64	2.11	0.0392
Conc.	10^5	Control	-137.76	22.8518	64	-6.03	<.0001
Conc.	10^6	10^7	-3.2667	22.8518	64	-0.14	0.8868
Conc.	10^6	Control	-189.13	22.8518	64	-8.28	<.0001
Conc.	10^7	Control	-185.87	22.8518	64	-8.13	<.0001

A.5   ANOVA ANALYSIS FOR GROUND BEEF TESTING

The Mixed Procedure

Table A-15. Type 3 Tests of Fixed Effects

Effect	Num DF	Den DF	F Value	Pr > F
Concentration	7	64	37.93	<.0001

Table A-16. Least Squares Means

Effect	Conc.	Estimate	Standard Error	DF	t Value	Pr > |t|
Concentration	10^1	262.02	16.0192	64	16.36	<.0001
Concentration	10^2	113.8	16.0192	64	7.1	<.0001
Concentration	10^3	80.2556	16.0192	64	5.01	<.0001
Concentration	10^4	75.1889	16.0192	64	4.69	<.0001
Concentration	10^5	114.28	16.0192	64	7.13	<.0001
Concentration	10^6	98.0889	16.0192	64	6.12	<.0001
Concentration	10^7	64.9889	16.0192	64	4.06	0.0001
Concentration	Control	331.83	16.0192	64	20.71	<.0001

Table A-17. Differences of Least Squares Means

Effect	Conc.	_Conc.	Estimate	Standard Error	DF	t Value	Pr > |t|
Conc.	10^1	10^2	148.22	22.6545	64	6.54	<.0001
Conc.	10^1	10^3	181.77	22.6545	64	8.02	<.0001
Conc.	10^1	10^4	186.83	22.6545	64	8.25	<.0001
Conc.	10^1	10^5	147.74	22.6545	64	6.52	<.0001
Conc.	10^1	10^6	163.93	22.6545	64	7.24	<.0001
Conc.	10^1	10^7	197.03	22.6545	64	8.7	<.0001
Conc.	10^1	Control	-69.8111	22.6545	64	-3.08	0.3030
Conc.	10^2	10^3	33.5444	22.6545	64	1.48	0.1436
Conc.	10^2	10^4	38.6111	22.6545	64	1.7	0.0932
Conc.	10^2	10^5	-0.4778	22.6545	64	-0.02	0.9832
Conc.	10^2	10^6	15.7111	22.6545	64	0.69	0.4905
Conc.	10^2	10^7	48.8111	22.6545	64	2.15	0.035
Conc.	10^2	Control	-218.03	22.6545	64	-9.62	<.0001
Conc.	10^3	10^4	5.0667	22.6545	64	0.22	0.8237
Conc.	10^3	10^5	-34.0222	22.6545	64	-1.5	0.1381
Conc.	10^3	10^6	-17.8333	22.6545	64	-0.79	0.4341
Conc.	10^3	10^7	15.2667	22.6545	64	0.67	0.5028
Conc.	10^3	Control	-251.58	22.6545	64	-11.1	<.0001
Conc.	10^4	10^5	-39.0889	22.6545	64	-1.73	0.0893
Conc.	10^4	10^6	-22.9	22.6545	64	-1.01	0.3159
Conc.	10^4	10^7	10.2	22.6545	64	0.45	0.6541
Conc.	10^4	Control	-256.64	22.6545	64	-11.33	<.0001
Conc.	10^5	10^6	16.1889	22.6545	64	0.71	0.4775
Conc.	10^5	10^7	49.2889	22.6545	64	2.18	0.0333
Conc.	10^5	Control	-217.56	22.6545	64	-9.6	<.0001
Conc.	10^6	10^7	33.1	22.6545	64	1.46	0.1489
Conc.	10^6	Control	-233.74	22.6545	64	-10.32	<.0001
Conc.	10^7	Control	-266.84	22.6545	64	-11.78	<.0001

A.6   ANOVA ANALYSIS FOR WHOLE MILK TESTING

The Mixed Procedure

Table A-18. Type 3 Tests of Fixed Effects

Effect	Num DF	Den DF	F Value	Pr > F
Concentration	7	64	32.15	<.0001

Table A-19. Least Squares Means

Effect	Conc.	Estimate	Standard Error	DF	t Value	Pr > |t|
Concentration	10^1	267.94	18.9017	64	14.18	<.0001
Concentration	10^2	274.57	18.9017	64	14.53	<.0001
Concentration	10^3	116.21	18.9017	64	6.15	<.0001
Concentration	10^4	103.44	18.9017	64	5.47	<.0001
Concentration	10^5	116.61	18.9017	64	6.17	<.0001
Concentration	10^6	84.6889	18.9017	64	4.48	<.0001
Concentration	10^7	76.4	18.9017	64	4.04	0.0001
Concentration	Control	353.88	18.9017	64	18.72	<.0001

Table A-20. Differences of Least Squares Means

Effect	Conc.	_Conc.	Estimate	Standard Error	DF	t Value	Pr > t
Conc.	10^1	10^2	-6.6222	26.731	64	-0.25	0.8051
Conc.	10^1	10^3	151.73	26.731	64	5.68	<.0001
Conc.	10^1	10^4	164.5	26.731	64	6.15	<.0001
Conc.	10^1	10^5	151.33	26.731	64	5.66	<.0001
Conc.	10^1	10^6	183.26	26.731	64	6.86	<.0001
Conc.	10^1	10^7	191.54	26.731	64	7.17	<.0001
Conc.	10^1	Control	-85.9333	26.731	64	-3.21	0.2020
Conc.	10^2	10^3	158.36	26.731	64	5.92	<.0001
Conc.	10^2	10^4	171.12	26.731	64	6.4	<.0001
Conc.	10^2	10^5	157.96	26.731	64	5.91	<.0001
Conc.	10^2	10^6	189.88	26.731	64	7.1	<.0001
Conc.	10^2	10^7	198.17	26.731	64	7.41	<.0001
Conc.	10^2	Control	-79.3111	26.731	64	-2.97	0.4002
Conc.	10^3	10^4	12.7667	26.731	64	0.48	0.6346
Conc.	10^3	10^5	-0.4	26.731	64	-0.01	0.9881
Conc.	10^3	10^6	31.5222	26.731	64	1.18	0.2427
Conc.	10^3	10^7	39.8111	26.731	64	1.49	0.1413
Conc.	10^3	Control	-237.67	26.731	64	-8.89	<.0001
Conc.	10^4	10^5	-13.1667	26.731	64	-0.49	0.624
Conc.	10^4	10^6	18.7556	26.731	64	0.7	0.4854
Conc.	10^4	10^7	27.0444	26.731	64	1.01	0.3155
Conc.	10^4	Control	-250.43	26.731	64	-9.37	<.0001
Conc.	10^5	10^6	31.9222	26.731	64	1.19	0.2368
Conc.	10^5	10^7	40.2111	26.731	64	1.5	0.1374
Conc.	10^5	Control	-237.27	26.731	64	-8.88	<.0001
Conc.	10^6	10^7	8.2889	26.731	64	0.31	0.7575
Conc.	10^6	Control	-269.19	26.731	64	-10.07	<.0001
Conc.	10^7	Control	-277.48	26.731	64	-10.38	<.0001

A.7 ANOVA ANALYSIS FOR SPCE BIOSENSOR SENSITIVITY

The Mixed Procedure

Table A-21. Type 3 Tests of Fixed Effects

Effect	Num DF	Den DF	F Value	Pr > F
DNA Conc.	5	12	72.19	<.0001

Table A-22. Estimates

Label	Estimate	Standard Error	DF	t Value	Pr > |t|
0.001 vs. Control	-0.8033	1.9949	12	-0.4	0.6943
0.01 vs. Control	14.3433	1.5827	12	9.06	<.0001
0.1 vs. Control	19.9767	2.2137	12	9.02	<.0001
1 vs. Control	37.3767	2.7075	12	13.8	<.0001
10 vs. Control	330.21	143.02	12	2.31	0.0396

Table A-23. Least Squares Means

Effect	DNA Conc.	Estimate	Standard Error	DF	t Value	Pr > |t|
DNA Conc.	0.001	4.72	1.2258	12	3.85	0.0023
DNA Conc.	0.01	19.8667	0.1667	12	119.2	<.0001
DNA Conc.	0.1	25.5	1.5567	12	16.38	<.0001
DNA Conc.	1	42.9	2.203	12	19.47	<.0001
DNA Conc.	10	335.73	143.01	12	2.35	0.0369
DNA Conc.	Control	5.5233	1.5739	12	3.51	0.0043

Table A-24. Differences of Least Squares Means

Effect	DNA Conc.	_DNA Conc.	Estimate	Standard Error	DF	t Value	Pr > |t|
DNA Conc.	0.001	0.01	-15.1467	1.2371	12	-12.24	<.0001
DNA Conc.	0.001	0.1	-20.78	1.9814	12	-10.49	<.0001
DNA Conc.	0.001	1	-38.18	2.5211	12	-15.14	<.0001
DNA Conc.	0.001	10	-331.01	143.02	12	-2.31	0.0392
DNA Conc.	0.001	Control	-0.8033	1.9949	12	-0.4	0.6943
DNA Conc.	0.01	0.1	-5.6333	1.5656	12	-3.6	0.0037
DNA Conc.	0.01	1	-23.0333	2.2093	12	-10.43	<.0001
DNA Conc.	0.01	10	-315.87	143.01	12	-2.21	0.0474
DNA Conc.	0.01	Control	14.3433	1.5827	12	9.06	<.0001
DNA Conc.	0.1	1	-17.4	2.6975	12	-6.45	<.0001
DNA Conc.	0.1	10	-310.23	143.02	12	-2.17	0.0509
DNA Conc.	0.1	Control	19.9767	2.2137	12	9.02	<.0001
DNA Conc.	1	10	-292.83	143.03	12	-2.05	0.0432
DNA Conc.	1	Control	37.3767	2.7075	12	13.8	<.0001
DNA Conc.	10	Control	330.21	143.02	12	2.31	0.0396
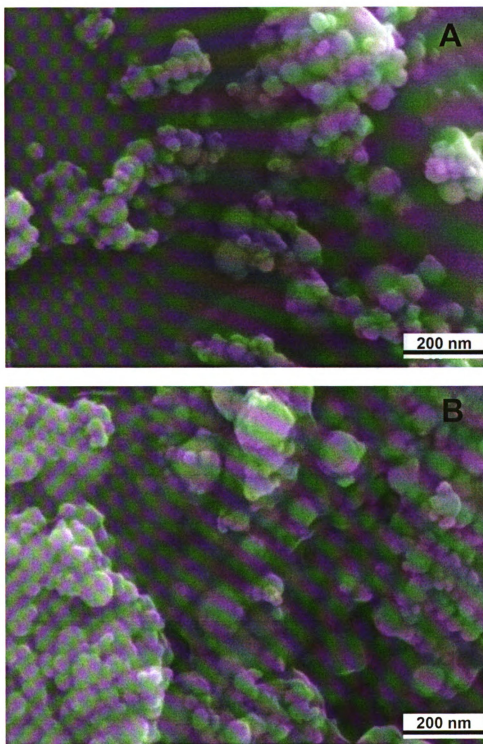
Figure B-1. SEM images of (A) Iron oxide NPs and (B) EAPM NPs
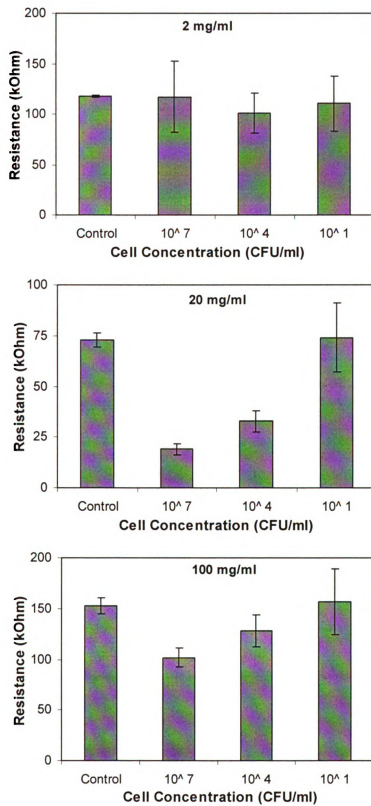
Figure B-2. Immunosensor responses of different EAPM concentrations in _B. cereus_
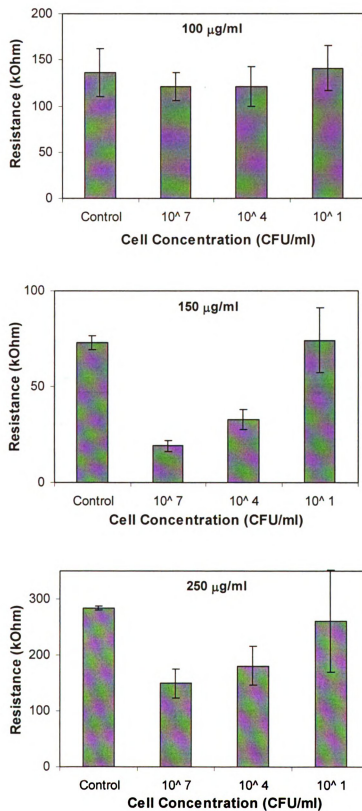
Figure B-3. Immunosensor responses of different *B. cereus* antibody concentrations.
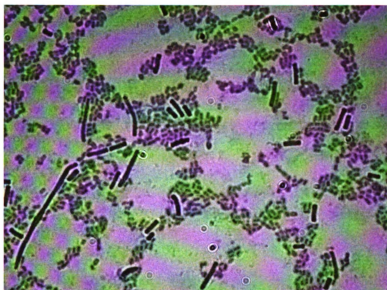
B. anthracis spores monitored after 7 day incubation period
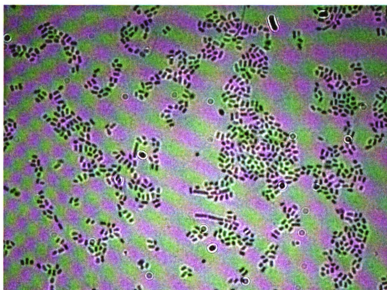
B. anthracis spores monitored after 10 day incubation period

Figure B-4. Light microscopy images of *B. anthracis* spores after two different incubation periods. (Final Spore Count – 4.2 × 10^8 spores/ml)

REFERENCES

Abrahamsson, D., Kriz, K., Lu, M., and Kriz, D. (2004) A preliminary study on DNA detection based on relative magnetic permeability measurements and histone H1 conjugated superparamagnetic nanoparticles as magnetic tracers. *Biosensors and Bioelectronics* 19(11): 1549-1557.

Aguilar, Z.P., and Sirisena, M. (2007) Development of automated amperometric detection of antibodies against *Bacillus anthracis* protective antigen. *Analytical and Bioanalytical Chemistry* 389(2): 507-515.

Ahuja, T., Mir, I.A., Kumar, D., and Rajesh (2007) Biomolecular immobilization on conducting polymers for biosensing applications. *Biomaterials* 28(5): 791-805.

Alam, J., Riaz, U., and Ahmad, S. (2007) Effect of ferrofluid concentration on electrical and magnetic properties of the Fe_3O_4/PANI nanocomposites. *Journal of Magnetism and Magnetic Materials* 314(2): 93-99.

Arora, K., Prabhakar, N., Chand, S., and Malhotra, B.D. (2007) *Escherichia coli* genosensor based on polyaniline. *Analytical Chemistry* 79(16): 6152-6158.

Asmatulu, R., Zalich, M.A., Claus, R., and Riffle, J.S. (2005) Synthesis, characterization and targeting of biodegradable magnetic nanocomposite particles by external magnetic fields. *Journal of Magnetism and Magnetic Materials* 292: 108-119.

Bard, A.J., and Faulkner, L.R. (2001) Electrochemical Methods: Fundamentals and Applications John Wiley & Sons, Inc.

Bereket, G. and Sahin, Y. (2005) Electrochemical synthesis and anti-corrosive properties of polyaniline, poly(2-anisidine), and poly(aniline-co-2-anisidine) films on stainless steel. *Progress in Organic Coatings* 54(1): 63-72.

Berkenpas, E., Millard, P., and da Cunha, M.P. (2006) Detection of *Escherichia coli* O157 : H7 with langasite pure shear horizontal surface acoustic wave sensors. *Biosensors & Bioelectronics* 21(12): 2255-2262.

Bisoffi, M., Hjelle, B., Brown, D.C., Branch, D.W., Edwards, T.L., Brozik, S.M. *et al.* (2008) Detection of viral bioagents using a shear horizontal surface acoustic wave biosensor. *Biosensors & Bioelectronics* 23(9): 1397-1403.

Boissiere, M., Meadows, P.J., Brayner, R., Helary, C., Livage, J., and Coradin, T. (2006) Turning biopolymer particles into hybrid capsules: the example of silica/alginate nanocomposites. *Journal of Materials Chemistry* 16(12): 1178-1182.

Bothara, M., Venkatraman, V., Reddy, R.K.K., Barrett, T., Carruthers, J., and Prasad, S. (2008) Nanomonitors: electrical immunoassays for protein biomarker profiling. *Nanomedicine* 3(4): 423-436.

Branch, D.W., and Brozik, S.M. (2004) Low-level detection of a Bacillus anthracis simulant using Love-wave biosensors on 36 degrees YX LiTaO₃. *Biosensors & Bioelectronics* 19(8): 849-859.

Buijs, J., vandenBerg, P.A.W., Lichtenbelt, J.W.T., Norde, W., and Lyklema, J. (1996) Adsorption dynamics of IgG and its F(ab')(2) and Fc fragments studied by reflectometry. *Journal of Colloid and Interface Science* 178(2): 594-605.

Campbell, G.A., and Mutharasan, R. (2006) Piezoelectric-excited millimeter-sized cantilever (PEMC) sensors detect *Bacillus anthracis* at 300 spores/mL. *Biosensors & Bioelectronics* 21(9): 1684-1692.

Carrascosa, L.G., Moreno, M., Alvarez, M., and Lechuga, L.M. (2006) Nanomechanical biosensors: a new sensing tool. *Trac-Trends in Analytical Chemistry* 25(3): 196-206.

CDC (2001) Anthrax Overview [WWW document]. URL, http://www.bt.cdc.gov/agent/anthrax/SlideSetAnthrax.pdf, Accessed March 15, 2009.

CDC (2009) Bioterrorism Agents/Diseases [WWW document]. URL, http://www.bt.cdc.gov/agent/agentlist-category.asp, Accessed March 15, 2009.

Chang, H.X., Yuan, Y., Shi, N.L., and Guan, Y.F. (2007a) Electrochemical DNA biosensor based on conducting polyaniline nanotube array. *Analytical Chemistry* 79(13): 5111-5115.

Chang, H.X., Yuan, Y., Shi, N.L., and Guan, Y.F. (2007b) Electrochemical DNA biosensor based on conducting polyaniline nanotube array. *Analytical Chemistry* 79(13): 5111-5115.

Chang, M., Glynn, M.K., and Groseclose, S.L. (2003) Endemic, notifiable bioterrorism related diseases, United States, 1002-1999. *Emerging Infectious Diseases* 9(5): 556-564.

Chang, Z., Pan, H., Zhao, K., Chen, M., He, P.G., and Fang, Y.Z. (2008) Electrochemical DNA biosensors based on palladium nanoparticles combined with carbon nanotubes. *Electroanalysis* 20(2): 131-136.

Chang, Z., Zhou, J., Zhao, K., Zhu, N., He, P., and Fang, Y. (2006) Ru(bpy)32+-doped silica nanoparticle DNA probe for the electrogenerated chemiluminescence detection of DNA hybridization. *Electrochimica Acta* 52(2): 575-580.

Chen, L.L., Deng, L., Liu, L.L., and Peng, Z.H. (2007) Immunomagnetic separation and MS/SPR end-detection combined procedure for rapid detection of *Staphylococcus aureus* and protein A. *Biosensors & Bioelectronics* 22(7): 1487-1492.

Cheun, H.I., Makino, S.I., Wataral, M., Shirahata, T., Uchida, I., and Takeshi, K. (2001) A simple and sensitive detection system for *Bacillus anthracis* in meat and tissue. *Journal of Applied Microbiology* 91(3): 421-426.

Chung, J.W., Kim, S.D., Bernhardt, R., and Pyun, J.C. (2005) Application of SPR biosensor for medical diagnostics of human hepatitis B virus (hHBV). *Sensors and Actuators B-Chemical* 111: 416-422.

Cieslak, T.J., and Eitzen, E.M. (1999) Clinical and epidemiological principles of anthrax. *Emerging Infectious Diseases* 5: 552-555.

Collier, R.J., and Young, J.A.T. (2003) Anthrax toxin. *Annual Review of Cell and Developmental Biology* 19: 45-70.

Comparelli,R., Curri,M.L., Cozzoli,P.D., and Striccoli,M. (2007) Optical Biosensing Based on Metal and Semiconductor Colloidal Nanocrystals. In Nanomaterials for Biosensors. Kumar,C.S.S.R. (ed). Wiley-VCH, pp. 123-174.

185

Cooper, M.A., and Singleton, V.T. (2007) A survey of the 2001 to 2005 quartz crystal microbalance biosensor literature: applications of acoustic physics to the analysis of biomolecular interactions. *Journal of Molecular Recognition* 20(3): 154-184.

Costa-Fernandez, J.M. (2006) Optical sensors based on luminescent quantum dot. *Analytical and Bioanalytical Chemistry* 384(1): 37-40.

Cui, Y., Zhong, Z.H., Wang, D.L., Wang, W.U., and Lieber, C.M. (2003) High performance silicon nanowire field effect transistors. *Nano Letters* 3(2): 149-152.

Dai, Z., Bai, H., Hong, M., Zhu, Y., Bao, J., and Shen, J. (2008) A novel nitrite biosensor based on the direct electron transfer of hemoglobin immobilized on CdS hollow nanospheres. *Biosensors and Bioelectronics* 23(12): 1869-1873.

Dallas, P., Moutis, N., Devlin, E., Niarchos, D., and Petridis, D. (2006) Characterization, electrical and magnetic properties of polyaniline/maghemite nanocomposites. *Nanotechnology* 17(19): 5019-5026.

Dastagir, T., Forzani, E.S., Zhang, R., Amlani, I., Nagahara, L.A., Tsui, R., and Tao, N. (2007) Electrical detection of hepatitis C virus RNA on single wall carbon nanotube-field effect transistors. *Analyst* 132(8): 738-740.

Davila, A.P., Jang, J., Gupta, A.K., Walter, T., Aronson, A., and Bashir, R. (2007) Microresonator mass sensors for detection of *Bacillus anthracis* Sterne spores in air and water. *Biosensors & Bioelectronics* 22(12): 3028-3035.

Delvaux, M., Duchet, J., Stavaux, P.Y., Legras, R., and moustier-Champagne, S. (2000) Chemical and electrochemical synthesis of polyaniline micro- and nano-tubules. *Synthetic Metals* 113(3): 275-280.

Deng, J., He, C., Peng, Y., Wang, J., Long, X., Li, P., and Chan, A.S.C. (2003) Magnetic and conductive Fe3O4-polyaniline nanoparticles with core-shell structure. *Synthetic Metals* 139(2): 295-301.

Deng, Z., and Alocilja, E.C. (2008) Characterization of Nanoporous Silicon-Based DNA Biosensor for the Detection of *Salmonella* Enteritidis. *Sensors Journal, IEEE* 8(6): 775-780.

Deobagkar, D.D., Limaye, V., Sinha, S., and Yadava, R.D.S. (2005) Acoustic wave immunosensing of *Escherichia coli* in water. *Sensors and Actuators B-Chemical* 104(1): 85-89.

Desai, P.T., Walsh, M.K., and Weimer, B.C. (2008). Solid-phase capture of pathogenic bacteria by using gangliosides and detection with real-time PCR. *Applied and Environmental Microbiology*, 74(7): 2254-2258.

Diamond, D. (1998) Principles of Chemical and Biological Sensors John Wiley & Sons, Inc.

Ding, H., Liu, X.M., Wan, M., and Fu, S.Y. (2008) Electromagnetic functionalized cage-like polyaniline composite nanostructures. *Journal of Physical Chemistry B* 112(31): 9289-9294.

Dong, X.C., Fu, D.L., Xu, Y.P., Wei, J.Q., Shi, Y.M., Chen, P., and Li, L.J. (2008) Label-free electronic detection of DNA using simple double-walled carbon nanotube resistors. *Journal of Physical Chemistry C* 112(26): 9891-9895.

Drummond, T.G., Hill, M.G., and Barton, J.K. (2003) Electrochemical DNA sensors. *Nature Biotechnology* 21(10): 1192-1199.

Duic, L., Mandic, Z., and Kovacicek, F. (1994) Effect of supporting electrolyte on the electrochemical synthesis, morphology, and conductivity of polyaniline. *Journal of Polymer Science, Part A: Polymer Chemistry* 32(1): 105-111.

Duic, L., Mandic, Z., and Kovac, S. (1995) Polymer-dimer distribution in the electrochemical synthesis of polyaniline. *Electrochimica Acta* 40(11): 1681-1688.

Dungchai, W., Siangproh, W., Chaicumpa, W., Tongtawe, P., and Chailapakul, O. (2008) Salmonella typhi determination using voltammetric amplification of nanoparticles: A highly sensitive strategy for metalloimmunoassay based on a copper-enhanced gold label. *Talanta* 77(2): 727-732.

Edelstein, R.L., Tamanaha, C.R., Sheehan, P.E., Miller, M.M., Baselt, D.R., Whitman, L.J., and Colton, R.J. (2000) The BARC biosensor applied to the detection of biological warfare agents. *Biosensors and Bioelectronics* 14(10-11): 805-813.

Eggins, B.R. (2002) Chemical Sensors and Biosensors John Wiley & Sons, Ltd.

El-Tantawy, F., bdel-Kader, K.M., Kaneko, F., and Sung, Y.K. (2004) Physical properties of CdS-poly (vinyl alcohol) nanoconducting composite synthesized by organosol techniques and novel application potential. *European Polymer Journal* 40(2): 415-430.

Elsholz, B., Worl, R., Blohm, L., Albers, J., Feucht, H., Grunwald, T. *et al.* (2006) Automated Detection and Quantitation of Bacterial RNA by Using Electrical Microarrays. *Analytical Chemistry* 78(14): 4794-4802.

Epstein, A.J., Ginder, J.M., Zuo, F., Woo, H.S., Tanner, D.B., Richter, A.F. *et al.* (1987) Insulator-To-Metal Transition in Polyaniline - Effect of Protonation in Emeraldine. *Synthetic Metals* 21(1): 63-70.

Epstein, J.R., Biran, I., and Walt, D.R. (2002) Fluorescence-based nucleic acid detection and microarrays. *Analytica Chimica Acta* 469(1): 3-36.

Ercole, C., Del Gallo, M., Mosiello, L., Baccella, S., and Lepidi, A. (2003) Escherichia coli detection in vegetable food by a potentiometric biosensor. *Sensors and Actuators B-Chemical* 91(1-3): 163-168.

Erickson, D., Mandal, S., Yang, A.H.J., and Cordovez, B. (2008) Nanobiosensors: optofluidic, electrical and mechanical approaches to biomolecular detection at the nanoscale. *Microfluidics and Nanofluidics* 4(1-2): 33-52.

Erickson, M.C., and Kornacki, J.L. (2003) Bacillus anthracis: Current knowledge in relation to contamination of food. *Journal of Food Protection* 66(4): 691-699.

Fan, Y., Chen, X.T., Trigg, A.D., Tung, C.H., Kong, J.M., and Gao, Z.Q. (2007) Detection of microRNAs using target-guided formation of conducting polymer nanowires in nanogaps. *Journal of the American Chemical Society* 129(17): 5437-5443.

Farabullini, F., Lucarelli, F., Palchetti, I., Marrazza, G., and Mascini, M. (2007) Disposable electrochemical genosensor for the simultaneous analysis of different bacterial food contaminants. *Biosensors & Bioelectronics* 22(7): 1544-1549.

Feast, W.J., Tsibouklis, J., Pouwer, K.L., Groenendaal, L., and Meijer, E.W. (1996) Synthesis, processing and material properties of conjugated polymers. *Polymer* 37(22): 5017-5047.

Fu, J., Park, B., Siragusa, G., Jones, L., Tripp, R., Zhao, Y.P., and Cho, Y.J. (2008) An Au/Si hetero-nanorod-based biosensor for *Salmonella* detection. *Nanotechnology* 19(15).

Galipeau, D.W., Story, P.R., Vetelino, K.A., and Mileham, R.D. (1997) Surface acoustic wave microsensors and applications. *Smart Materials & Structures* 6(6): 658-667.

Gao, Z.Q., Agarwal, A., Trigg, A.D., Singh, N., Fang, C., Tung, C.H. *et al.* (2007) Silicon nanowire arrays for label-free detection of DNA. *Analytical Chemistry* 79(9): 3291-3297.

Geng, T., Uknalis, J., Tu, S.I., and Bhunia, A.K. (2006) Fiber-optic biosensor employing Alexa-Fluor conjugated antibody for detection of *Escherichia coli* O157: H7 from ground beef in four hours. *Sensors* 6(8): 796-807.

Gerard, M., Chaubey, A., and Malhotra, B.D. (2002) Application of conducting polymers to biosensors. *Biosensors & Bioelectronics* 17(5): 345-359.

Goldman, E.R., Clapp, A.R., Anderson, G.P., Uyeda, H.T., Mauro, J.M., Medintz, I.L., and Mattoussi, H. (2004) Multiplexed toxin analysis using four colors of quantum dot fluororeagents. *Analytical Chemistry* 76(3): 684-688.

Gong, P., He, X., Wang, K., Tan, W., Xie, W., Wu, P., and Li, H. (2008) Combination of functionalized nanoparticles and polymerase chain reaction-based method for SARS-CoV gene detection. *Journal of Nanoscience and Nanotechnology* 8(1): 293-300.

Gorman,C.B., and Grubbs, R.H. (1991) Conjugated Polymers: The Interplay Between Synthesis, Structure, and Properties. In Conjugated Polymers. Bredas, J.L., and Silbey, R. (eds). Kluwer Academic Publishers, pp. 1-48.

Gospodinova, N., Mokreva, P., and Terlemezyan, L. (1996) Concomitant processes in the redox switching of polyaniline. *Polymer International* 41(1): 79-84.

Grzeszczuk, M., and Szostak, R. (2003) Electrochemical and Raman studies on the redox switching hysteresis of polyaniline. *Solid State Ionics* 157(1-4): 257-262.

Hafeman, D.G., Parce, J.W., and Mcconell,H.M. (1988) Light-addressable potentiometric sensor for biochemical systems. *Science* 240(4856): 1182-1185.

Hahm, J., and Lieber, C.M. (2004) Direct ultrasensitive electrical detection of DNA and DNA sequence variations using nanowire nanosensors. *Nano Letters* 4(1): 51-54.

Hansen, J.A., Wang, J., Kawde, A.N., Xiang, Y., Gothelf, K.V., and Collins, G. (2006) Quantum-dot/aptamer-based ultrasensitive multi-analyte electrochemical biosensor. *Journal of the American Chemical Society* 128(7): 2228-2229.

Heeger, A., and Smith, P. (1991) Solution Processing of Conducting Polymers: Opportunities for Science and Technology. In Conjugated Polymers. Bredas, J.L., and Silbey, R. (eds). Kluwer Academic Publishers, pp. 141-210.

Hill, H.D., Vega, R.A., and Mirkin, C.A. (2007) Nonenzymatic detection of bacterial genomic DNA using the bio bar code assay. *Analytical Chemistry* 79(23): 9218-9223.

Hnaiein, M., Hassen, W.M., Abdelghani, A., Fournier-Wirth, C., Coste, J., Bessueille, F. *et al.* (2008) A conductometric immunosensor based on functionalized magnetite nanoparticles for *E. coli* detection. *Electrochemistry Communications* 10(8): 1152-1154.

Hoa, X.D., Kirk, A.G., and Tabrizian, M. (2007) Towards integrated and sensitive surface plasmon resonance biosensors: A review of recent progress. *Biosensors & Bioelectronics* 23: 151-160.

Hohnholz, D., Okuzaki, H., and Macdiarmid, A.G. (2005) Plastic electronic devices through line patterning of conducting polymers. *Advanced Functional Materials* 15(1): 51-56.

Homola, J. (2008) Surface plasmon resonance sensors for detection of chemical and biological species. *Chemical Reviews* 108(2): 462-493.

Hong, S.Y., and Park, S.M. (2005) Electrochemistry of conductive polymers 36. pH dependence of polyaniline conductivities studied by current-sensing atomic force microscopy. *Journal of Physical Chemistry B* 109(19): 9305-9310.

Ilic, B., Czaplewski, D., Zalalutdinov, M., Craighead, H.G., Neuzil, P., Campagnolo, C., and Batt, C. (2001) Single cell detection with micromechanical oscillators. *Journal of Vacuum Science & Technology B* 19(6): 2825-2828.

Inglesby, T.V. (2000) Anthrax as a biological weapon: Medical and public health management. *Jama-Journal of the American Medical Association* 283(15): 1963.

Inglesby, T.V., Dennis, D.T., Henderson, D.A., Bartlett, J.G., Ascher, M.S., Eitzen, E. *et al.* (2000) Plague as a biological weapon - Medical and public health management. *Jama-Journal of the American Medical Association* 283(17): 2281-2290.

Jernigan, J.A., Stephens, D.S., Ashford, D.A., Omenaca, C., Topiel, M.S., Galbraith, M. *et al.* (2001) Bioterrorism-related inhalational anthrax: The first 10 cases reported in the United States. *Emerging Infectious Diseases* 7(6): 933-944.

Jiang, J., Li, L.C., and Xu, F. (2006) Preparation, characterization and magnetic properties of PANI/La-substituted LiNi ferrite nanocomposites. *Chinese Journal of Chemistry* 24(12): 1804-1809.

Jin,X., Gao,Z., Pan,H., Zhu,H., Zhou,M., and Chen,H. The surface acoustic wave biosensor for detecting the gene of Staphylococal Enterotoxin B. Proceedings of the International Symposium on Test and Measurement 1, 261-264. 2003.

Johnson, L., Gupta, A.T.K., Ghafoor, A., Akin, D., and Bashir, R. (2006) Characterization of vaccinia virus particles using microscale silicon cantilever resonators and atomic force microscopy. *Sensors and Actuators B-Chemical* 115(1): 189-197.

Jyoung, J.Y., Hong, S.H., Lee, W., and Choi, J.W. (2006) Immunosensor for the detection of *Vibrio cholerae* O1 using surface plasmon resonance. *Biosensors & Bioelectronics* 21(12): 2315-2319.

Kaittanis, C., Naser, S.A., and Perez, J.M. (2007) One-step, nanoparticle-mediated bacterial detection with magnetic relaxation. *Nano Letters* 7(2): 380-383.

Kaneto, K., Fujisue, H., Kunifusa, M., and Takashima, W. (2007) Conducting polymer soft actuators based on polypyrrole films - energy conversion efficiency. *Smart Materials & Structures* 16(2): S250-S255.

Katz, E., and Willner, I. (2003) Probing biomolecular interactions at conductive and semiconductive surfaces by impedance spectroscopy: Routes to impedimetric immunosensors, DNA-Sensors, and enzyme biosensors. *Electroanalysis* 15(11): 913-947.

Kaufmann, A.F., Meltzer, M.I., and Schmid, G.P. (1997) The eonomic impact of a bioterrotism attack: Are prevention and postattack intervention programs justifiable? *Emerging Infectious Diseases* 3(2): 83-94.

191

Kim, H., Kane, M.D., Kim, S., Dominguez, W., Applegate, B.M., and Savikhin, S. (2007a) A molecular beacon DNA microarray system for rapid detection of *E. coli* O157: H7 that eliminates the risk of a false negative signal. *Biosensors & Bioelectronics* 22(6): 1041-1047.

Kim, J.H., Cho, J.H., Cha, G.S., Lee, C.W., Kim, H.B., and Paek, S.H. (2000) Conductimetric membrane strip immunosensor with polyaniline-bound gold colloids as signal generator. *Biosensors & Bioelectronics* 14(12): 907-915.

Kim, S.N., Rusling, J.F., and Papadimitrakopoulos, F. (2007b) Carbon nanotubes for electronic and electrochemical detection of biomolecules. *Advanced Materials* 19(20): 3214-3228.

Ko, S., and Jang, J. (2008) Label-free target DNA recognition using oligonucleotide-functionalized polypyrrole nanotubes. *Ultramicroscopy* 108(10): 1328-1333.

Ko, S.H., and Grant, S.A. (2006) A novel FRET-based optical fiber biosensor for rapid detection of *Salmonella* Typhimurium. *Biosensors & Bioelectronics* 21(7): 1283-1290.

Kong, J., Franklin, N.R., Zhou, C.W., Chapline, M.G., Peng, S., Cho, K.J., and Dai, H.J. (2000) Nanotube molecular wires as chemical sensors. *Science* 287(5453): 622-625.

Krebs, M.D., Mansfield, B., Yip, P., Cohen, S.J., Sonenshein, A.L., Hitt, B.A., and Davis, C.E. (2006) Novel technology for rapid species-specific detection of *Bacillus* spores. *Biomolecular Engineering* 23(2-3): 119-127.

Kriz, K., Gehrke, J., and Kriz, D. (1998) Advancements toward magneto immunoassays. *Biosensors and Bioelectronics* 13(7-8): 817-823.

Kryszewski, M., and Jeszka, J.K. (1998) Nanostructured conducting polymer composites - superparamagnetic particles in conducting polymers. *Synthetic Metals* 94(1): 99-104.

Laird, P.W., Zijderveld, A., Linders, K., Rudnicki, M.A., Jaenisch, R., and Berns, A. (1991) Simplified Mammalian DNA Isolation Procedure. *Nucleic Acids Research* 19(15): 4293.

Lan, Y.B., Wang, S.Z., Yin, Y.G., Hoffmann, W.C., and Zheng, X.Z. (2008) Using a Surface Plasmon Resonance Biosensor for Rapid Detection of *Salmonella* Typhimurium in Chicken Carcass. *Journal of Bionic Engineering* 5(3): 239-246.

Lange, K., Rapp, B.E., and Rapp, M. (2008) Surface acoustic wave biosensors: a review. *Analytical and Bioanalytical Chemistry* 391(5): 1509-1519.

Langer, J.J., Filipiak, M., Kecinska, J., Jasnowska, J., Wodarczak, J., and Buadowski, B. Polyaniline biosensor for choline determination. Proceedings of the 9th International Fischer Symposium, July 21, 2003 - July 23, 2003. 573(1), 140-145. 2004. Munich, Germany, Elsevier. Surface Science.

Lazcka, O., Del Campo, F.J., and Munoz, F.X. (2007) Pathogen detection: A perspective of traditional methods and biosensors. *Biosensors & Bioelectronics* 22(7): 1205-1217.

Lee, H., Lee, E., Kim, D.K., Jang, N.K., Jeong, Y.Y., and Jon, S. (2006) Antibiofouling polymer-coated superparamagnetic iron oxide nanoparticles as potential magnetic resonance contrast agents for in vivo cancer imaging. *Journal of the American Chemical Society* 128(22): 7383-7389.

Lee, S.H., Stubbs, D.D., Cairney, J., and Hunt, W.D. (2005) Rapid detection of bacterial spores using a quartz crystal microbalance (QCM) immunoassay. *Ieee Sensors Journal* 5(4): 737-743.

Leppla, S.H. (1982) Anthrax Toxin Edema Factor - A Bacterial Adenylate-Cyclase That Increases Cyclic-Amp Concentrations in Eukaryotic Cells. *Proceedings of the National Academy of Sciences of the United States of America-Biological Sciences* 79(10): 3162-3166.

Lermo, A., Campoy, S., Barbe, J., Hernandez, S., Alegret, S., and Pividori, M. (2007) In situ DNA amplification with magnetic primers for the electrochemical detection of food pathogens. *Biosensors & Bioelectronics* 22(9-10): 2010-2017.

Li, C., Liu, Y., Li, L., Du, Z., Xu, S., Zhang, M. *et al.* (2008) A novel amperometric biosensor based on NiO hollow nanospheres for biosensing glucose. *Talanta* 77(1): 455-459.

Li, G., Jiang, L., and Peng, H. (2007a) One-dimensional polyaniline nanostructures with controllable surfaces and diameters using vanadic acid as the oxidant. *Macromolecules* 40(22): 7890-7894.

Li, G., Yan, S., Zhou, E., and Chen, Y. (2006) Preparation of magnetic and conductive NiZn ferrite-polyaniline nanocomposites with core-shell structure. *Colloids and Surfaces A: Physicochemical and Engineering Aspects* 276(1-3): 40-44.

Li, X., Shen, J.Y., Wan, M.X., Chen, Z.J., and Wei, Y. (2007b) Core-shell structured and electro-magnetic functionalized polyaniline composites. *Synthetic Metals* 157(13-15): 575-579.

Li, Y.G., Cu, Y.T.H., and Luo, D. (2005) Multiplexed detection of pathogen DNA with DNA-based fluorescence nanobarcodes. *Nature Biotechnology* 23(7): 885-889.

Liu, Y.S., Walter, T.M., Chang, W.J., Lim, K.S., Yang, L.J., Lee, S.W. *et al.* (2007) Electrical detection of germination of viable model *Bacillus anthracis* spores in microfluidic biochips. *Lab on A Chip* 7(5): 603-610.

Liu, Y.J., Yao, D.J., Chang, H.Y., Liu, C.M., and Chen, C. (2008) Magnetic bead-based DNA detection with multi-layers quantum dots labeling for rapid detection of *Escherichia coli* O157:H7. *Biosensors and Bioelectronics* 24(4): 558-565.

Lizarraga, L., Andrade, E.M., and Molina, F.V. (2004) Swelling and volume changes of polyaniline upon redox switching. *Journal of Electroanalytical Chemistry* 561(1-2): 127-135.

Ludwig, F., Heim, E., Menzel, D., and Schilling, M. (2006) Investigation of superparamagnetic Fe3O4 nanoparticles by fluxgate magnetorelaxometry for use in magnetic relaxation immunoassays. *Journal of Applied Physics* 99(8).

Luo, X.L., Morrin, A., Killard, A.J., and Smyth, M.R. (2006) Application of nanoparticles in electrochemical sensors and biosensors. *Electroanalysis* 18(4): 319-326.

Lv, R., Zhang, S., Shi, Q., and Kan, J. (2005) Electrochemical synthesis of polyaniline nanoparticles in the presence of magnetic field and erbium chloride. *Synthetic Metals* 150(2): 115-122.

Lyons, M.E.G. (1994) Electroactive Polymer Electrochemistry Plenum Press.

Macdiarmid, A.G., Chiang, J.C., Richter, A.F., and Epstein, A.J. (1987) Polyaniline - A New Concept in Conducting Polymers. *Synthetic Metals* 18(1-3): 285-290.

Mairal, T., Ozalp, V.C., Sanchez, P.L., Mir, M., Katakis, I., and O'Sullivan, C.K. (2008) Aptamers: molecular tools for analytical applications. *Analytical and Bioanalytical Chemistry* 390(4): 989-1007.

Malhotra, B.D., Chaubey, A., and Singh, S.P. (2006) Prospects of conducting polymers in biosensors. *Analytica Chimica Acta* 578(1): 59-74.

Mao, X.L., Yang, L.J., Su, X.L., and Li, Y.B. (2006) A nanoparticle amplification based quartz crystal microbalance DNA sensor for detection of *Escherichia coli* O157:H7. *Biosensors & Bioelectronics* 21(7): 1178-1185.

Marinakos, S.M., Chen, S.H., and Chilkoti, A. (2007) Plasmonic detection of a model analyte in serum by a gold nanorod sensor. *Analytical Chemistry* 79(14): 5278-5283.

Marquette, C.A., and Blum, L.J. (2006) State of the art and recent advances in immunoanalytical systems. *Biosensors & Bioelectronics* 21(8): 1424-1433.

Mason, J.T., Xu, L., Sheng, Z., and O'Leary, T.J. (2006) A lioposome-PCR assay for the ultrasensitive detection of biological toxins. *Nature Biotechnology* 24(5): 555-557

Mathew, F.P., and Alocilja, E.C. (2005) Porous silicon-based biosensor for pathogen detection. *Biosensors and Bioelectronics* 20(8 SPEC. ISS.): 1656-1661.

Mazur, M., Krysinski, P., and Palys, B. (2002) Preparation of ultrathin films of polyaniline and its derivatives by electrochemical deposition on thiol modified gold. *Journal of Electroanalytical Chemistry* 533(1-2): 145-152.

Mehlen, A., Goeldner, M., Ried, S., Stindl, S., Ludwig, W., and Schleifer, K.H. (2004) Development of a fast DNA-DNA hybridization method based on melting profiles in microplates. *Systematic and Applied Microbiology* 27(6): 689-695.

Mishra, N.N., Maki, W.C., Cameron, E., Nelson, R., Winterrowd, P., Rastogi, S.K. *et al.* (2008) Ultra-sensitive detection of bacterial toxin with silicon nanowire transistor. *Lab on A Chip* 8(6): 868-871.

Mock, M., and Fouet, A. (2001) Anthrax. *Annual Review of Microbiology* 55: 647-671.

Mock, M., and Mignot, T. (2003) Anthrax toxins and the host: a story of intimacy. *Cellular Microbiology* 5(1): 15-23.

Moll, N., Pascal, E., Dinh, D.H., Lachaud, J.L., Vellutini, L., Pillot, J.P. *et al.* (2008) Multipurpose Love acoustic wave immunosensor for bacteria, virus or proteins detection. *IRBM* 29(2-3): 155-161.

Moll, N., Pascal, E., Dinh, D.H., Pillot, J.P., Bennetau, B., Rebiere, D. *et al.* (2007) A Love wave immunosensor for whole *E. coli* bacteria detection using an innovative two-step immobilisation approach. *Biosensors & Bioelectronics* 22(9-10): 2145-2150.

Muhammad-Tahir, Z., and Alocilja, E.C. (2003a) A conductometric biosensor for biosecurity. *Biosensors and Bioelectronics* 18(5-6): 813-819.

Muhammad-Tahir, Z., and Alocilja, E.C. (2003b) Fabrication of a disposable biosensor for *Escherichia coli* O157:H7 detection. *IEEE Sensors Journal* 3(4): 345-351.

Muhammad-Tahir, Z., Alocilja, E.C., and Grooms, D.L. (2005) Rapid detection of Bovine viral diarrhea virus as surrogate of bioterrorism agents. *IEEE Sensors Journal* 5(4): 757-762.

Nandakumar, V., La Belle, J.T., Reed, J., Shah, M., Cochran, D., Joshi, L., and Alford, T.L. (2008) A methodology for rapid detection of *Salmonella* Typhimurium using label-free electrochemical impedance spectroscopy. *Biosensors and Bioelectronics* 24(4): 1039-1042.

Nanduri, V., Kim, G., Morgam, M.T., Ess, D., Hahm, B., Kothapalli, A. *et al.* (2006) Antibody immobilization on waveguides using a flow-through system shows improved *Listeria monocytogenes* detection in an automated fiber optic biosensor: RAPTOR^{TM}. *Sensors* 6: 808-822.

O'Sullivan, C.K., and Guilbault, G.G. (1999) Commercial quartz crystal microbalances - theory and applications. *Biosensors & Bioelectronics* 14(8-9): 663-670.

Ohira, M., Sakai, T., Takeuchi, M., Kobayashi, Y., and Tsuji, M. (1987) Raman and infrared spectra of polyaniline. *Synthetic Metals* 18(1-3): 347-352.

Okinaka, R.T., Cloud, K., Hampton, O., Hoffmaster, A.R., Hill, K.K., Keim, P. *et al.* (1999) Sequence and organization of pXO1, the large *Bacillus anthracis* plasmid harboring the anthrax toxin genes. *Journal of Bacteriology* 181(20): 6509-6515.

Pal, S., Alocilja, E.C., and Downes, F.P. (2007) Nanowire labeled direct-charge transfer biosensor for detecting *Bacillus* species. *Biosensors & Bioelectronics* 22(9-10): 2329-2336.

Pal, S., Ying, W., Alocija, E.C., and Downes, F.P. (2008) Sensitivity and specificity performance of a direct-charge transfer biosensor for detecting Bacillus cereus in selected food matrices. *Biosystems Engineering* 99(4): 461-468.

Palchetti, I., and Mascini, M. (2008) Electroanalytical biosensors and their potential for food pathogen and toxin detection. *Analytical and Bioanalytical Chemistry* 391(2): 455-471.

Pan, L.J., Pu, L., Shi, Y., Sun, T., Zhang, R., and Zheng, Y.D. (2006) Hydrothermal synthesis of polyaniline mesostructures. *Advanced Functional Materials* 16(10): 1279-1288.

Panda, B.R., Singh, A.K., Ramesh, A., and Chattopadhyay, A. (2008) Rapid Estimation of Bacteria by a Fluorescent Gold Nanoparticle-Polythiophene Composite. *Langmuir* 24(20): 11995-12000.

Pannifer, A.D., Wong, T.Y., Schwarzenbacher, R., Renatus, M., Petosa, C., Bienkowska, J. et al. (2001) Crystal structure of the anthrax lethal factor. *Nature* 414(6860): 229-233.

Park, M.E., and Chang, J.H. (2007) High throughput human DNA purification with aminosilanes tailored silica-coated magnetic nanoparticles. *Materials Science & Engineering C-Biomimetic and Supramolecular Systems* 27(5-8): 1232-1235.

Patolsky, F., Zheng, G., and Lieber, C.M. (2006) Nanowire-based biosensors. *Analytical Chemistry* 78(13): 4260-4269.

Peruski, A.H., and Peruski, L.F. (2003) Immunological methods for detection and identification of infectious disease and biological warfare agents. *Clinical and Diagnostic Laboratory Immunology* 10(4): 506-513.

Petosa, C., Collier, R.J., Klimpel, K.R., Leppla, S.H., and Liddington, R.C. (1997) Crystal structure of the anthrax toxin protective antigen. *Nature* 385(6619): 833-838.

Pezard, C., Berche, P., and Mock, M. (1991) Contribution of Individual Toxin Components to Virulence of *Bacillus anthracis. Infection and Immunity* 59(10): 3472-3477.

Pileni,M.P. (2001) Semiconductor Nanocrystals. In Nanoscale Materials in Chemistry. Klabunde,K. (ed). John Wiley & Sons, Inc., pp. 85-120.

Piletsky, S.A., Turner, N.W., and Laitenberger, P. (2006) Molecularly imprinted polymers in clinical diagnostics - Future potential and existing problems. *Medical Engineering & Physics* 28(10): 971-977.

Pingarron, J.M., Yβ±ez-Sede±o, P., and Gonzβlez-Cortθs, A. (2008) Gold nanoparticle-based electrochemical biosensors. *Electrochimica Acta* 53(19): 5848-5866.

Poddar, P., Wilson, J.L., Srikanth, H., Morrison, S.A., and Carpenter, E.E. (2004b) Magnetic properties of conducting polymer doped with manganese-zinc ferrite nanoparticles. *Nanotechnology* 15(10): S570-S574.

Poddar, P., Wilson, J.L., Srikanth, H., Morrison, S.A., and Carpenter, E.E. (2004a) Magnetic properties of conducting polymer doped with manganese-zinc ferrite nanoparticles. *Nanotechnology* 15(10): S570-S574.

Pouget, J.P., Jozefowicz, M.E., Epstein, A.J., Tang, X., and Macdiarmid, A.G. (1991) X-Ray Structure of Polyaniline. *Macromolecules* 24(3): 779-789.

Prabhakar, N., Arora, K., Singh, H., and Malhotra, B.D. (2008) Polyaniline based nucleic acid sensor. *Journal of Physical Chemistry B* 112(15): 4808-4816.

Prabhakaran, T., and Hemalatha, J. (2008) Synthesis and characterization of magnetoelectric polymer nanocomposites. *Journal of Polymer Science, Part B: Polymer Physics* 46(22): 2418-2422.

Prakash, R. (2002) Electrochemistry of polyaniline: Study of the pH effect and electrochromism. *Journal of Applied Polymer Science* 83(2): 378-385.

Pumera, M., Castaneda, M.T., Pividori, M.I., Eritja, R., Merkoci, A., and Alegret, S. (2005) Magnetically Trigged Direct Electrochemical Detection of DNA Hybridization Using Au67 Quantum Dot as Electrical Tracer. *Langmuir* 21(21): 9625-9629.

Radke, S.M., and Alocilja, E.C. (2005) A high density microelectrode array biosensor for detection of *E. coli* O157:H7. *Biosensors and Bioelectronics* 20(8): 1662-1667.

Rahman, M.A., Kumar, P., Park, D.S., and Shim, Y.B. (2008) Electrochemical sensors based on organic conjugated polymers. *Sensors* 8(1): 118-141.

Ram, M.K., Salerno, M., Adami, M., Faraci, P., and Nicolini, C. (1999) Physical properties of polyaniline films: Assembled by the layer-by-layer technique. *Langmuir* 15(4): 1252-1259.

Ramanathan, K., Bangar, M.A., Yun, M., Chen, W., Myung, N.V., and Mulchandani, A. (2005) Bioaffinity sensing using biologically functionalized conducting-polymer nanowire. *Journal of the American Chemical Society* 127(2): 496-497.

Ramanavicius, A., Ramanaviciene, A., and Malinauskas, A. (2006) Electrochemical sensors based on conducting polymer- polypyrrole. *Electrochimica Acta* 51(27): 6025-6037.

Ray, A., Asturias, G.E., Kershner, D.L., Richter, A.F., Macdiarmid, A.G., and Epstein, A.J. (1989) Polyaniline - Doping, Structure and Derivatives. *Synthetic Metals* 29(1): E141-E150.

Reddy, K.R., Lee, K.P., Gopalan, A.I., and Showkat, A.M. (2007) Synthesis and properties of magnetite/poly (aniline-co-8-amino-2-naphthalenesulfonic acid) (SPAN) nanocomposites. *Polymers for Advanced Technologies* 18(1): 38-43.

Reif, T.C., Johns, M., Pillai, S.D., and Carl, M. (1994) Identification of Capsule-Forming *Bacillus anthracis* Spores with the PCR and A Novel Dual-Probe Hybridization Format. *Applied and Environmental Microbiology* 60(5): 1622-1625.

Rossi, A.M., Wang, L., Reipa, V., and Murphy, T.E. (2007) Porous silicon biosensor for detection of viruses. *Biosensors & Bioelectronics* 23(5): 741-745.

Rossi, L.M., Shi, L., Rosenzweig, N., and Rosenzweig, Z. (2006) Fluorescent silica nanospheres for digital counting bioassay of the breast cancer marker HER2/nue. *Biosensors and Bioelectronics* 21(10): 1900-1906.

Ruan, C.M., Zeng, K.F., Varghese, O.K., and Grimes, C.A. (2003) Magnetoelastic immunosensors: Amplified mass immunosorbent assay for detection of *Escherichia coli* O157:H7. *Analytical Chemistry* 75(23): 6494-6498.

Ryder, K.S., Morris, D.G., and Cooper, J.M. (1997) Role of conducting polymeric interfaces in promoting biological electron transfer. *Biosensors & Bioelectronics* 12(8): 721-727.

Safina, G., van Lier, M., and Danielsson, B. (2008) Flow-injection assay of the pathogenic bacteria using lectin-based quartz crystal microbalance biosensor. *Talanta* 77(2): 468-472.

Sai, V.V.R., Mahajan, S., Contractor, A.Q., and Mukherji, S. (2006) Immobilization of antibodies on polyaniline films and its application in a piezoelectric immunosensor. *Analytical Chemistry* 78(24): 8368-8373.

Sandhu, A., Kumagai, Y., Lapicki, A., Sakamoto, S., Abe, M., and Handa, H. (2007) High efficiency Hall effect micro-biosensor platform for detection of magnetically labeled biomolecules. *Biosensors and Bioelectronics* 22(9-10): 2115-2120.

Sapsford, K.E., Pons, T., Medintz, I.L., and Mattoussi, H. (2006) Biosensing with luminescent semiconductor quantum dots. *Sensors* 6(8): 925-953.

Sergeeva, T.A., Piletskii, S.A., Rachkov, A.E., and El'skaya, A.V. (1996) Synthesis and Examination of Polyanilines as Labels in Immunosensor Analysis. *Journal of Analytical Chemistry* 51(4): 394.

Shankaran, D.R., Gobi, K.V.A., and Miura, N. (2007) Recent advancements in surface plasmon resonance immunosensors for detection of small molecules of biomedical, food and environmental interest. *Sensors and Actuators B-Chemical* 121(1): 158-177.

Sharma, R., Lamba, S., Annapoorni, S., Sharma, P., and Inoue, A. (2005) Composition dependent magnetic properties of iron oxide-polyaniline nanoclusters. *Journal of Applied Physics* 97(1).

Shen, Z.H., Huang, M.C., Xiao, C.D., Zhang, Y., Zeng, X.Q., and Wang, P.G. (2007) Nonlabeled quartz crystal microbalance biosensor for bacterial detection using carbohydrate and lectin recognitions. *Analytical Chemistry* 79(6): 2312-2319.

Singh, C., Agarwal, G.S., Rai, G.P., Singh, L., and Rao, V.K. (2005) Specific detection of *Salmonella typhi* using renewable amperometric immunosensor. *Electroanalysis* 17(22): 2062-2067.

So, H.M., Park, D.W., Jeon, E.K., Kim, Y.H., Kim, B.S., Lee, C.K. *et al.* (2008) Detection and titer estimation of *Escherichia coli* using aptamer-functionalized single-walled carbon-nanotube field-effect transistors. *Small* 4(2): 197-201.

Song, L.N., Ahn, S., and Walt, D.R. (2005) Detecting biological warfare agents. *Emerging Infectious Diseases* 11(10): 1629-1632.

Song, L.N., Ahn, S., and Walt, D.R. (2006) Fiber-optic microsphere-based arrays for multiplexed biological warfare agent detection. *Analytical Chemistry* 78(4): 1023-1033.

Song, S.P., Wang, L.H., Li, J., Zhao, J.L., and Fan, C.H. (2008) Aptamer-based biosensors. *Trac-Trends in Analytical Chemistry* 27(2): 108-117.

Sorensen, C.M. (2001) Magnetism. In Nanoscale Materials in Chemistry. Klabunde,K. (ed). John Wiley & Sons, Inc., pp. 169-222.

Sotiropoulou, S., Vamvakaki, V., and Chaniotakis, N.A. (2005) Stabilization of enzymes in nanoporous materials for biosensor applications. *Biosensors & Bioelectronics* 20(8): 1674-1679.

Soukka, T., Harma, H., Paukkunen, J., and Lovgren, T. (2001) Utilization of Kinetically Enhanced Monovalent Binding Affinity by Immunoassays Based on Multivalent Nanoparticle-Antibody Bioconjugates. *Analytical Chemistry* 73(10): 2254-2260.

Spanier, J.E. (2006) One-dimensional semiconductor and oxide nanostructures. In Nanomaterials Handbook. Gogotsi,Y. (ed). Taylor and Francis, pp. 283-316.

Spencer, R.C. (2003) *Bacillus anthracis. Journal of Clinical Pathology* 56(3): 182-187.

Stafstrom, S., Bredas, J.L., Epstein, A.J., Woo, H.S., Tanner, D.B., Huang, W.S., and Macdiarmid, A.G. (1987) Polaron Lattice in Highly Conducting Polyaniline - Theoretical and Optical Studies. *Physical Review Letters* 59(13): 1464-1467.

Stejskal, J., and Gilbert, R.G. (2002) Polyaniline. Preparation of a conducting polymer (IUPAC technical report). *Pure and Applied Chemistry* 74(5): 857-867.

Stejskal, J., Kratochvil, P., and Jenkins, A.D. (1996) The formation of polyaniline and the nature of its structures. *Polymer* 37(2): 367-369.

Stringer, R.C., Schommer, S., Hoehn, D., and Grant, S.A. (2008) Development of an optical biosensor using gold nanoparticles and quantum dots for the detection of Porcine Reproductive and Respiratory Syndrome Virus. *Sensors and Actuators B-Chemical* 134(2): 427-431.

Su, X.L., and Li, Y.B. (2004a) A self-assembled monolayer-based piezoelectric immunosensor for rapid detection of *Escherichia coli* O157:H7. *Biosensors & Bioelectronics* 19(6): 563-574.

Su, X.L., and Li, Y.B. (2004b) Quantum dot biolabeling coupled with immunomagnetic separation for detection of *Escherichia coli* O157:H7. *Analytical Chemistry* 76(16): 4806-4810.

Subramanian, A., Irudayaraj, J., and Ryan, T. (2006) A mixed self-assembled monolayer-based surface plasmon immunosensor for detection of *E. coli* O157:H7. *Biosensors & Bioelectronics* 21(7): 998-1006.

Tahir, Z.M., Alocilja, E.C., and Grooms, D.L. (2007) Indium tin oxide-polyaniline biosensor: Fabrication and characterization. *Sensors* 7(7): 1123-1140.

Taitt, C.R., Anderson, G.P., Lingerfelt, B.M., Feldstein, M.J., and Ligler, F.S. (2002) Nine-analyte detection using an array-based biosensor. *Analytical Chemistry* 74(23): 6114-6120.

Tamanaha, C.R., Mulvaney, S.P., Rife, J.C., and Whitman, L.J. (2008) Magnetic labeling, detection, and system integration. *Biosensors and Bioelectronics* 24(1): 1-13.

Tang, D., Yuan, R., and Chai, Y. (2008) Ultrasensitive Electrochemical Immunosensor for Clinical Immunoassay Using Thionine-Doped Magnetic Gold Nanospheres as Labels and Horseradish Peroxidase as Enhancer. *Analytical Chemistry* 80(5): 1582-1588.

Tang, H., Kitani, A., and Shiotani, M. (1996) Cyclic voltammetry of KI at polyaniline-filmed Pt electrodes Part I: formation of polyaniline-iodine charge transfer complexes. *Journal of Applied Electrochemistry* 26(1): 36-44.

Taylor, A.D., Ladd, J., Yu, Q., Chen, S., Homola, J., and Jiang, S. (2006) Quantitative and simultaneous detection of four foodborne bacterial pathogens with a multi-channel SPR sensor. *Biosensors and Bioelectronics* 22(5): 752-758.

Terry, L.A., White, S.F., and Tigwell, L.J. (2005) The application of biosensors to fresh produce and the wider food industry. *Journal of Agricultural and Food Chemistry* 53(5): 1309-1316.

Theegala, C.S., Small, D.D., and Monroe, W.T. (2008) Oxygen electrode-based single antibody amperometric biosensor for qualitative detection of *E. coli* and bacteria in water. *Journal of Environmental Science and Health Part A-Toxic/Hazardous Substances & Environmental Engineering* 43(5): 478-487.

Thurer, R., Vigassy, T., Hirayama, M., Wang, J., Bakker, E., and Pretsch, E. (2007) Potentiometric immunoassay with quantum dot labels. *Analytical Chemistry* 79(13): 5107-5110.

Tims, T.B., and Lim, D.V. (2004) Rapid detection of *Bacillus anthracis* spores directly from powders with an evanescent wave fiber-optic biosensor. *Journal of Microbiological Methods* 59(1): 127-130.

Vaisocherova, H., Mrkvova, K., Piliarik, M., Jinoch, P., Steinbachova, M., and Homola, J. (2007) Surface plasmon resonance biosensor for direct detection of antibody against Epstein-Baff virus. *Biosensors & Bioelectronics* 22(6): 1020-1026.

Varshney, M., and Li, Y. (2007) Interdigitated array microelectrode based impedance biosensor coupled with magnetic nanoparticle-antibody conjugates for detection of *Escherichia coli* O157:H7 in food samples. *Biosensors and Bioelectronics* 22(11): 2408-2414.

Varshney, M., Yang, L., Su, X.L., and Li, Y. (2005) Magnetic Nanoparticle-Antibody Conjugates for the Separation of *Escherichia coli* O157:H7 in Ground Beef. *Journal of Food Protection* 68: 1804-1811.

Vaseashta, A., and mova-Malinovska, D. (2005) Nanostructured and nanoscale devices, sensors and detectors. *Science and Technology of Advanced Materials* 6(3-4): 312-318.

Villamizar, R.A., Maroto, A., Rius, F.X., Inza, I., and Figueras, M.J. (2008) Fast detection of *Salmonella* Infantis with carbon nanotube field effect transistors. *Biosensors & Bioelectronics* 24(2): 279-283.

Waggoner, P.S., and Craighead, H.G. (2007) Micro- and nanomechanical sensors for environmental, chemical, and biological detection. *Lab on A Chip* 7(10): 1238-1255.

Wan, M., and Li, J. (1998) Synthesis and electrical-magnetic properties of polyaniline composites. *Journal of Polymer Science, Part A: Polymer Chemistry* 36(15): 2799-2805.

Wang, J. (2005) Nanomaterial-based electrochemical biosensors. *Analyst* 130(4): 421-426.

Wang, J., Liu, G., and Lin, Y. (2007a) Nanotubes, Nanowires, and Nanocantilevers in Biosensor Development. In Nanomaterials for Biosensors. Kumar,C.S.S.R. (ed). Wiley-VCH, pp. 56-100.

Wang, J. (2002) Electrochemical nucleic acid biosensors. *Analytica Chimica Acta* 469(1): 63-71.

Wang, L., Zhao, W.J., O'Donoghue, M.B., and Tan, W.H. (2007b) Fluorescent nanoparticles for multiplexed bacteria monitoring. *Bioconjugate Chemistry* 18(2): 297-301.

Wang, L.J., Wei, Q.S., Wu, C.S., Hu, Z.Y., Ji, J., and Wang, P. (2008) The *Escherichia coli* O157:H7 DNA detection on a gold nanoparticle-enhanced piezoelectric biosensor. *Chinese Science Bulletin* 53(8): 1175-1184.

Wang, L., Wei, Q., Wu, C., Ji, J., and Wang, P. A QCM biosensor based on gold nanoparticles amplification for real-time bacteria DNA detection. International Conference on Information Acquisition, ICIA 2007, July 09,2007 - July 11,2007. 46-51. 2007c. Jeju City, Korea, Republic of, Inst. of Elec. and Elec. Eng. Computer Society. Proceedings of the 2007 International Conference on Information Acquisition, ICIA.

Wang, S.X., Bae, S.Y., Li, G.X., Sun, S.H., White, R.L., Kemp, J.T., and Webb, C.D. (2005) Towards a magnetic microarray for sensitive diagnostics. *Journal of Magnetism and Magnetic Materials* 293(1): 731-736.

Wang, S.X., and Li, G. (2008) Advances in giant magnetoresistance biosensors with magnetic nanoparticle tags: Review and outlook. *IEEE Transactions on Magnetics* 44(7): 1687-1702.

Waswa, J., Irudayaraj, J., and DebRoy, C. (2007) Direct detection of *E coli* O157:H7 in selected food systems by a surface plasmon resonance biosensor. *Lwt-Food Science and Technology* 40(2): 187-192.

Waswa, J.W., DebRoy, C., and Irudayaraj, J. (2006) Rapid detection of *Salmonella* Enteritidis and *Escherichia coli* using surface plasmon resonance biosensor. *Journal of Food Process Engineering* 29(4): 373-385.

Wei, D., and Ivaska, A. (2006) Electrochemical biosensors based on polyaniline. *Chemia Analityczna* 51(6): 839-852.

Wei, D., Baral, J.K., Osterbacka, R., and Ivaska, A. (2008) Electrochemical fabrication of a nonvolatile memory device based on polyaniline and gold particles. *Journal of Materials Chemistry* 18(16): 1853-1857.

Wu, T.Z., Su, C.C., Chen, L.K., Yang, H.H., Tai, D.F., and Peng, K.C. (2005) Piezoelectric immunochip for the detection of dengue fever in viremia phase. *Biosensors & Bioelectronics* 21(5): 689-695.

Xu, C.J., and Sun, S.H. (2007) Monodisperse magnetic nanoparticles for biomedical applications. *Polymer International* 56(7): 821-826.

Xue, W.Y., Qiu, H., Fang, K., Li, J., Zhao, J.W., and Li, M. (2006) Electrical and magnetic properties of the composite pellets containing DBSA-doped polyaniline and Fe nanoparticles. *Synthetic Metals* 156(11-13): 833-837.

Yang, L.J., and Li, Y.B. (2006) Detection of viable *Salmonella* using microelectrode-based capacitance measurement coupled with immunomagnetic separation. *Journal of Microbiological Methods* 64(1): 9-16.

Yao, C.Y., Zhu, T.Y., Tang, J., Wu, R., Chen, Q.H., Chen, M. *et al.* (2008) Hybridization assay of hepatitis B virus by QCM peptide nucleic acid biosensor. *Biosensors & Bioelectronics* 23(6): 879-885.

Ybarra, G., Moina, C., Florit, M.I., and Posadas, D. (2000) Proton exchange during the redox switching of polyaniline film electrodes. *Electrochemical and Solid-State Letters* 3(7): 330-332.

Ye, L., and Haupt, K. (2004) Molecularly imprinted polymers as antibody and receptor mimics for assays, sensors and drug discovery. *Analytical and Bioanalytical Chemistry* 378(8): 1887-1897.

Yeung, S.W., and Hsing, I.M. (2006) Manipulation and extraction of genomic DNA from cell lysate by functionalized magnetic particles for lab on a chip applications. *Biosensors & Bioelectronics* 21(7): 989-997.

Yoon, H., Kim, J.H., Lee, N., Kim, B.G., and Jang, J. (2008) A novel sensor platform based on aptamer-conjugated polypyrrole nanotubes for label-free electrochemical protein detection. *Chembiochem* 9(4): 634-641.

Yu, C.X., and Irudayaraj, J. (2007) Multiplex biosensor using gold nanorods. *Analytical Chemistry* 79(2): 572-579.

Yun, Y., Bange, A., Heineman, W.R., Halsall, H.B., Shanov, V.N., Dong, Z. *et al.* (2007) A nanotube array immunosensor for direct electrochemical detection of antigen-antibody binding. *Sensors and Actuators B: Chemical* 123(1): 177-182.

Zhang, C.Y., Yeh, H.C., Kuroki, M.T., and Wang, T.H. (2005a) Single-quantum-dot-based DNA nanosensor. *Nature Materials* 4(11): 826-831.

Zhang, D., Carr, D.J., and Alocilja, E.C. (2009a) Fluorescent bio-barcode DNA assay for the detection of *Salmonella enterica* serovar Enteritidis. *Biosensors and Bioelectronics* 24(5): 1377-1381.

Zhang, L., Zhang, J., and Zhang, C. (2009b) Electrochemical synthesis of polyaniline nano-network on α-alanine functionalized glassy carbon electrode and its application for the direct electrochemistry of horse heart cytochrome c. *Biosensors and Bioelectronics* 24(7): 2085-2090.

Zhang, Z.M., Wan, M.X., and Wei, Y. (2005b) Electromagnetic functionalized polyaniline nanostructures. *Nanotechnology* 16(12): 2827-2832.

Zhang, Z., and Wan, M. (2003) Nanostructures of polyaniline composites containing nano-magnet. *Synthetic Metals* 132(2): 205-212.

Zhao, G., Xing, F., and Deng, S. (2007) A disposable amperometric enzyme immunosensor for rapid detection of *Vibrio parahaemolyticus* in food based on agarose/Nano-Au membrane and screen-printed electrode. *Electrochemistry Communications* 9(6): 1263-1268.

Zhao, W., Brook, M.A., and Li, Y.F. (2008) Design of Gold Nanoparticle-Based Colorimetric Biosensing Assays. *Chembiochem* 9(15): 2363-2371.

Zhao, X.J., Hilliard, L.R., Mechery, S.J., Wang, Y.P., Bagwe, R.P., Jin, S.G., and Tan, W.H. (2004) A rapid bioassay for single bacterial cell quantitation using bioconjugated nanoparticles. *Proceedings of the National Academy of Sciences of the United States of America* 101(42): 15027-15032.

Zhou, J., Tsao, H.K., Sheng, Y.J., and Jiang, S.Y. (2004) Monte Carlo simulations of antibody adsorption and orientation on charged surfaces. *Journal of Chemical Physics* 121(2): 1050-1057.

Zhou, R.H., Wang, P., and Chang, H.C. (2006) Bacteria capture, concentration and detection by alternating current dielectrophoresis and self-assembly of dispersed single-wall carbon nanotubes. *Electrophoresis* 27(7): 1376-1385.

Zhu, L., Yang, R., Zhai, J., and Tian, C. (2007) Bienzymatic glucose biosensor based on co-immobilization of peroxidase and glucose oxidase on a carbon nanotubes electrode. *Biosensors and Bioelectronics* 23(4): 528-535.

Zhu, N.N., Chang, Z., He, P.G., and Fang, Y.Z. (2006a) Electrochemically fabricated polyaniline nanowire-modified electrode for voltammetric detection of DNA hybridization. *Electrochimica Acta* 51(18): 3758-3762.

Zhu, N.N., Zhang, A.P., He, P.G., and Fang, Y.Z. (2004) DNA hybridization at magnetic nanoparticles with electrochemical stripping detection. *Electroanalysis* 16(23): 1925-1930.

Zhu, X., Han, K., and Li, G. (2006b) Magnetic Nanoparticles Applied in Electrochemical Detection of Controllable DNA Hybridization. *Analytical Chemistry* 78(7): 2447-2449.